Traveltime approximations for 2D and 3D media and kinematic wavefield attributes

---

Laufzeitapproximationen für 2D und 3D Medien mittels kinematischer Wellenfeldattributen

Zusammenfassung

Die vorliegende Arbeit ist bis auf diese Zusammenfassung in Englisch verfasst. Da auch in der deutschen Sprache einige englische Fachausdrücke gebräuchlich sind, wurde bei diesen Ausdrücken auf eine Übersetzung verzichtet. Sie werden, mit Ausnahme ihrer groß geschriebenen Abkürzungen, *kursiv* dargestellt.

Einleitung

Gegenstand dieser Arbeit ist die Analyse von Wellenfronten und deren Nutzen zur Approximation von Laufzeiten primärer Reflexionseinsätze. In der Anwendung dient eine solche Laufzeitapproximation dazu, aus reflexionsseismischen Messungen kinematische Wellenfeldattribute (Krümmungen und Orientierung von Wellenfronten) abzuleiten.

Wellen und Strahlen

Im Allgemeinen betrachten Geophysiker den Untergrund als elastodynamisches Medium und beschreiben die Wellenpropagation mit Hilfe der elastodynamischen Wellengleichung. Für die kinematischen Untersuchungen in isotropen Medien, wie sie in der vorliegenden Arbeit angestellt werden, ist es jedoch ausreichend akustische Medien mit konstanter Dichte zu betrachten. Diese sind durch die Propagationsgeschwindigkeit $v(x, y, z)$ der Welle definiert. Die Ausbreitungsrichtungen einer Welle können mit Hilfe von Strahlen beschrieben und veranschaulicht werden. Im isotropen Fall verläuft ein Strahl senkrecht zur Wellenfront.

Problemstellung

Der untere Teil der Abbildung 1a zeigt ein einfaches zweidimensionales akustisches Modell des Untergrundes. Das Modell besteht aus drei Schichten, die durch die schwarzen Grenzflächen separiert sind. Innerhalb einer Schicht ist das Medium durch die konstante Geschwindigkeit v_i charakterisiert.

An der Oberfläche ($z = 0$) werden nun zwei voneinander unabhängige idealisierte seismische Messungen durchgeführt. Bei der ersten Messung befinden sich Quelle sowie Empfänger am Punkt

X_0, bei der zweiten Messung sind Quelle und Empfänger getrennt voneinander am Punkt S bzw. G positioniert. Für eine Messung wird nun ein Wellenzug an der Quelle angeregt. Dieser propagiert durch das Medium, wird an der domähnlichen Grenzfläche reflektiert und am Empfänger registriert. Bei einem hier gemessen Reflexionseinsatz handelt es sich um eine sogenannte Primärreflexion, d. h. es fand genau eine Reflexion im Untergrund statt. Die Propagationstrajektorien sind durch die blauen Strahlen gekennzeichnet. Sie lassen sich unabhängig von der Wellenpropagation durch Anwendung des Snell'schen Gesetzes berechnen.
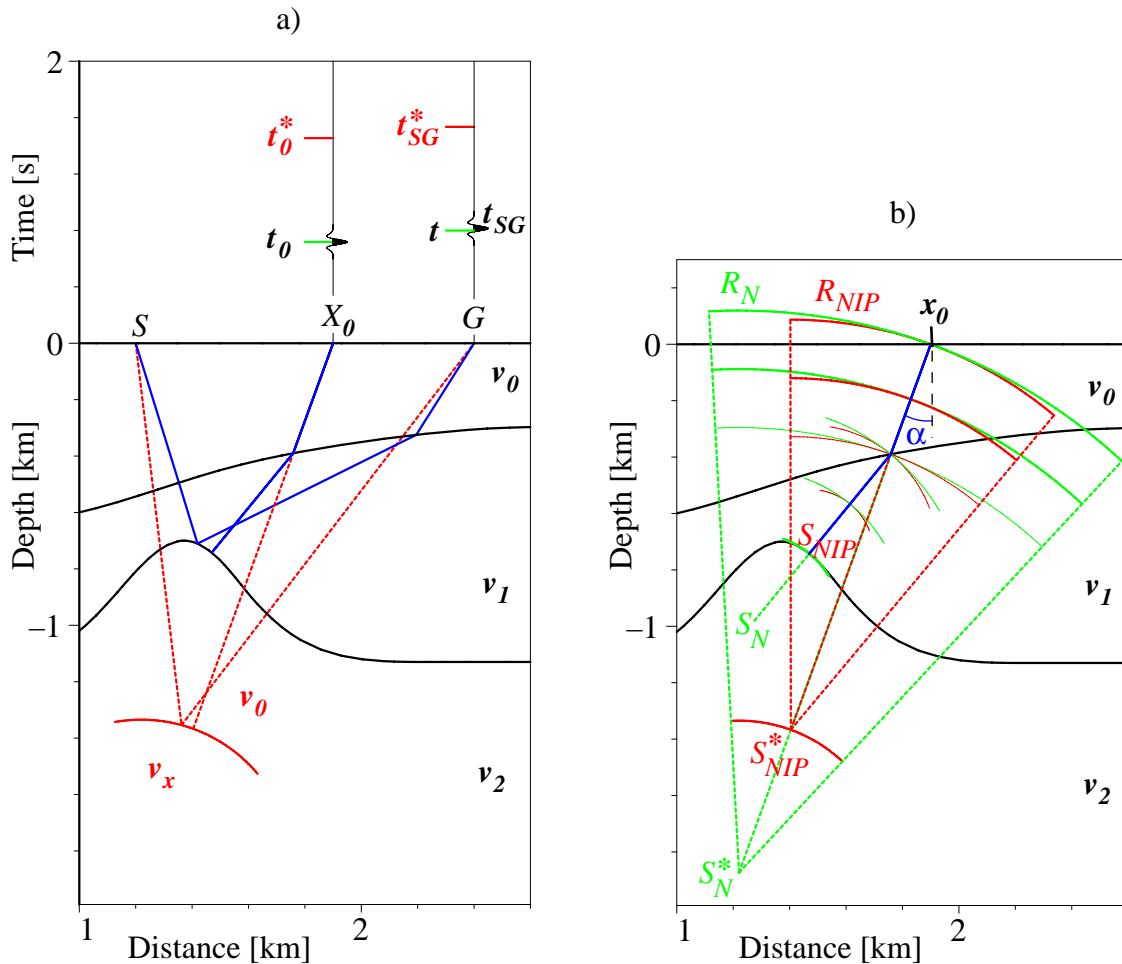

Abbildung 1: a) Wahres Modell und Bildraum. Das wahre Modell ist definiert durch drei Schichten konstanter Geschwindigkeit, die durch die (schwarzen) Grenzflächen getrennt sind. Der Bildraum wird zwischen Oberfläche und dem (roten) Bild als homogenes Medium definiert. b) Konstruktion des Bildes eines Reflektorsegments mittels der Radien der NIP-Wellenfront (rot) und der Normal-Wellenfront (grün) entlang des ZO Strahls (blau).

Bei dem ersten erläuterten Experiment (koinzidentes Quelle/Empfängerpaar bei X_0) handelt es sich um ein sogenanntes *zero-offset* (ZO) Experiment, da Quelle und Empfänger keinen Versatz

(*offset*) zueinander aufweisen. Der zugehörige ZO Strahl trifft hier senkrecht auf den Reflektor (reflektierende Grenzschicht). Eine ZO Messung ist in der Praxis nur möglich, wenn der Empfänger der Anregung der Quelle standhalten kann. Je tiefer man den Untergrund auflösen will, desto stärker muss die Anregung erfolgen. Für reflexionsseismische Zwecke wie der Lokalisierung von Lagerstätten sind dies mehrere Kilometer. Dies schließt eine ZO Akquisition praktisch aus.

Die Registrierung startet unter diesen idealisierten Bedingungen zum Zeitpunkt 0, wenn das Quellsignal an der Quelle seine maximale Amplitude erreicht. Die Zeiten, an denen die registrierten Reflexionseinsätze ihre maximale Amplitude erreichen, beschreiben somit die Laufzeit des Wellenzugs von der Quelle zum Empfänger. Für das erste Experiment erhält man die Laufzeit t_0, für das zweite Experiment ergibt sich die Laufzeit t_{SG}.

Das Problem lässt sich nun wie folgt formulieren: Wie lässt sich ohne Kenntnis des Geschwindigkeitsmodells der Reflexionseinsatz eines ZO Experiments (mit der Laufzeit t_0) durch gemessene Reflexionseinsätze nicht koinzidenter Schuss/Empfänger-Paare (mit den Laufzeiten t_{SG}) simulieren? Dieses Problem wird nur kinematisch betrachtet, d. h., eine korrekte Amplitudensimulation wird nicht berücksichtigt. Es wird im folgenden in zwei Schritten gelöst. In einem ersten Schritt wird ausgehend von t_0 die Laufzeit t_{SG} approximiert. Hier wird auf die in der Laufzeitapproximation auftretenden Parameter eingegangen, dabei aber zunächst die Kenntnis des Geschwindigkeitsmodells vorausgesetzt. Der nächste Schritt beinhaltet, die Parameter der Laufzeitapproximation ohne Kenntnis des Geschwindigkeitsmodells aus reflexionsseismischen Messungen abzuleiten.

Lösungsansatz mit Kenntnis des Geschwindigkeitsmodells

Bei Kenntnis des Geschwindigkeitsmodells werden zwei hypothetische Experimente angesetzt. Im ersten Experiment regt man eine Punktquelle im Reflektorpunkt S_{NIP} an, an dem der ZO Strahl reflektiert wird.[1] Die resultierende Welle wird NIP-Welle genannt. Das zweite Experiment wird durchgeführt, indem man den Reflektor selbst als Quelle nutzt (etwa durch simultane Anregung aller Punkte eines Reflektors). Dies regt die sogenannte Normal-Welle an. In beiden Fällen ist man nur an den Krümmungen der jeweiligen Wellenfronten längs des ZO Strahls interessiert. Daher kann man für das zweite Experiment auch eine Punktquelle im Punkt S_N anregen. Dieser Punkt ist ein Krümmungsmittelpunkt des Reflektors, definiert durch Krümmung und Steigung des Reflektors im Punkt S_{NIP}. In Abbildung 1b sind die Krümmungsradien der NIP- und Normal-Wellenfront entlang des ZO Strahls in rot bzw. grün dargestellt. Für beide Wellenfronten stellt der reflektierte ZO Strahl eine Propagationtrajektorie dar. Daher ist ihre Orientierung längs des ZO Strahls bereits durch diesen festgelegt.

Diese Experimente liefern nun, zusätzlich zur Laufzeit t_0, die erforderlichen Größen zur Laufzeitapproximation. Eine Größe beschreibt den Auftauchwinkel α der Wellenfronten am Punkt $X_0 = (x_0, 0)$. Dieser wird bezüglich der Normalen zur Oberfläche gemessen. Die zwei anderen Größen sind die Krümmungsradien R_{NIP} und R_N der NIP- bzw. Normal-Wellenfront am Punkt X_0.

---

[1]NIP steht für *normal incident point* und beschreibt einen Reflexionspunkt an dem der Strahl senkrecht auf den Reflektor trifft.

Diese Größen stellen kinematische Attribute des NIP- und Normal-Wellenfeldes am Punkt X_0 dar. Sie legen die Krümmungsmittelpunkte S_{NIP}^* und S_N^* der bei X_0 auftauchenden Wellenfronten fest.

Diese Experimente und ihre Bedeutung lassen sich anschaulich mit Hilfe der geometrischen Optik interpretieren. Dazu stelle man sich das Medium als transparent und die Punktquelle bei S_{NIP} bzw. S_N als Lichtquelle vor. Einem Beobachter auf der Oberfläche bei X_0 würde die Lichtquelle am Ort S_{NIP}^* bzw. S_N^* erscheinen. Was passiert nun, wenn sich der Beobachter auf der Oberfläche bewegt? Der allgemeine Fall ist in Abbildung 3.1 dargestellt. In dieser Abbildung befindet sich die Lichtquelle im Punkt S. Je nach Position des Beobachters erscheint diesem die Lichtquelle am konjugierten Punkt (Krümmungsmittelpunkt) der dort auftauchenden Wellenfront. Bewegt sich der Beobachter, so wandert die scheinbare Lichtquelle entlang der Kaustik, die das Ensemble der konjugierten Punkte darstellt. Wäre die auftauchende Wellenfront kreisförmig (wie etwa in einem homogenen Medium), so würde die Kaustik in einem Punkt, dem Bildpunkt, kollabieren.

Für den in Abbildung 1b gezeigten Fall versucht man nun ein Bild des Reflektors um S_{NIP} zu konstruieren. Betrachtet man die auftauchenden NIP- und Normal-Wellenfronten als kreisförmig, erhält man die Bildpunkte S_{NIP}^* und S_N^*. S_{NIP}^* stellt einen Bildpunkt des Reflektors dar, während S_N^* von der Krümmung des Reflektors abgleitet wurde. Daher wertet man die Krümmung der Normal-Wellenfront im Punkt S_{NIP}^* aus und erhält so ein approximatives Bild des Reflektors um S_{NIP}. Dieses Bild ist gegeben durch das Kreissegment mit Radius $R_N - R_{NIP}$ um den Mittelpunkt S_N^*.

Für die Laufzeitapproximation betrachtet man nun dieses Bild als Reflektor in einem Medium, das zwischen der Oberfläche und dem Bild homogen ist und hier durch die oberflächennahe Geschwindigkeit v_0 des wahren Modells charakterisiert wird (Abbildung 1a). Dieses Hilfsmedium wird im folgenden als Bildraum bezeichnet. Die Laufzeiten der Reflexionsereignisse, die von einem kreisförmigen Reflektor in einem homogenen Medium stammen, lassen sich analytisch exakt berechnen. Für die Laufzeit der in Abbildung 1a gezeigten Quelle/Empfänger Paare ergeben sich die Laufzeiten zu $t_0^* = 2R_{NIP}/v_0$ und t_{SG}^*. Um die Laufzeiten der wirklichen Reflexionsereignisse zu approximieren, führt man nun noch die Zeitverschiebung $\Delta t = t_0 - 2R_{NIP}/v_0$ ein. Dies liefert die exakte Laufzeit t_0 für das koinzidente Quelle/Empfänger-Paar bei X_0 und die approximative Laufzeit $t = t_{SG}^* + \Delta t$ für eine Quelle bei S und einen Empfänger bei G.

Die Begründung, warum man diese hypothetischen Experimente zur Laufzeitapproximation benutzen kann, sowie die Herleitung der Formeln findet man in Teil I dieser Arbeit. Hier können nur die zugrunde liegenden Annahmen zusammengefasst werden.

Annahmen

1. Der ZO Strahl trifft senkrecht auf den Reflektor. Dies ist nicht zwangsläufig der Fall. Durch Mehrfachreflexion oder entsprechende Geschwindigkeitsmodelle kann auch ein nicht senkrecht auf den Reflektor treffender ZO Strahl entstehen. Zudem verlaufen die Strahlen senkrecht zu den Wellenfronten. Dies setzt ein isotropes Medium voraus.

2. Es wird davon ausgegangen, dass die zu t_0 und t_{SG} gehörigen Reflexionseinsätze a) Primärreflexionen darstellen und b) von demselben Reflektorsegment stammen.

3. Die auftauchenden Wellenfronten lassen sich in einer gewissen Umgebung von X_0 durch Kreissegmente approximieren. Zudem muss in dieser Umgebung die Propagationsgeschwindigkeit konstant sein.

4. Das approximative Bild des Reflektors wird als Reflektor in einem homogenen Medium benutzt. Dies beeinflusst weniger die Laufzeitapproximation als vielmehr die Position des entsprechenden Quelle/Empfänger Paares.

Annahme 1 sowie die Annahme von Primärreflexionen sind Grundvorrausetzungen. Die Annahmen 2b, 3 und 4 beschränken die Anwendung der Formeln auf die Umgebung von X_0. Das heißt, je weiter Quelle und Empfänger von X_0 entfernt sind, desto ungenauer ist die Laufzeitapproximation.

Laufzeitapproximation ohne Kenntnis des Geschwindigkeitsmodells

Kennt man das Geschwindigkeitsmodell sind Laufzeitapproximationen eigentlich nicht erforderlich. Das ist jedoch in der Praxis selten der Fall. Vielmehr stellt die Bestimmung eines Geschwindigkeitsmodells die größte Hürde dar. Im Folgenden wird auf die gegebenen Daten eingegangen, die den Ausgangspunkt darstellen.

Reflexionsseismische Datenakquisition

Bei einer üblichen 2D Datenakquisition liegen Quelle und Empfänger entlang einer Geraden (seismischen Linie) auf der Oberfläche. Abbildung 1.1 zeigt einen 2D Schnitt längs einer seismischen Linie. Die Quelle ist durch einen Blitz, die Empfänger sind durch Dreiecke symbolisiert. Jeder der Empfänger registriert eine sogenannte Spur, die das Wellenfeld am Empfänger als Funktion der Zeit wiedergibt. In Abbildung 1.1 beinhaltet das aufgezeichnete Wellenfeld Primärreflexionen, die vom ersten und zweiten Reflektor stammen. In der Praxis würden u. a. noch die direkte Welle (die entlang der Oberfläche propagiert), multiple Reflexionen sowie Rauschen aufgezeichnet werden. Eine Messung mit einer solchen Anordnung von Quelle und Empfänger nennt man eine *common-shot* (CS) Akquisition, die zugehörige Aufzeichnung CS Sektion. Um nun mehr Information aus dem Untergrund zu erhalten, wird die gesamte CS Anordnung längs der seismischen Linie verschoben. Reiht man die resultierenden CS Sektionen aneinander, so erhält man einen dreidimensionalen Datensatz.

Datengeometrie

Meist werden die Daten für die Bearbeitung umsortiert. Dazu berechnet man den *midpoint* x_m und den *half-offset* h aus den Quelle und Empfänger Koordinaten x_s und x_g:

$$x_m = \frac{1}{2}(x_g + x_s), \quad h = \frac{1}{2}(x_g - x_s).$$

Die Spur eines Empfängers wird ausgehend von diesen Gleichungen bei (x_n, h) über die Zeit aufgetragen. Abbildung 1.2 zeigt einen solchen Datenraum. Zur Illustration sind hier allerdings keine Spuren aufgetragen, sondern die Laufzeiten der Reflexionseinsätze des zweiten Reflektors (in Abbildung 1.1). Die durch A gekennzeichnete Laufzeitkurve in Abbildung 1.1 ist ebenfalls im Datenraum gekennzeichnet. Die Laufzeiten der Reflexionseinsätze eines Reflektors bilden eine Laufzeitfläche, die hier durch *common-offset* (CO) Kurven dargestellt ist. Der Term CO fasst Quelle/Empfänger-Paare zusammen, die einen konstanten Abstand von der Quelle zum Empfänger aufweisen (siehe Abbildung 1.2). Eine CO Kurve liegt in einer CO Sektion, die im Datenraum durch eine Ebene $h = $ const gegeben ist. Die vorderste Ebene $h = 0$ ist die in der Regel nicht direkt messbare ZO Sektion.

Bestimmung der kinematischen Wellenfrontattribute

Das Problem der Laufzeitapproximation wurde ausgehend von x_0, t_0 und den Attributen α, R_{NIP} und R_N gelöst. Sei nun zunächst die Lokation $P_0 = (x_0, t_0)$ einer Primärreflexion in der ZO Sektion bekannt, für die die drei Attribute zu bestimmen sind. Dieser Schritt ist nur von praktischer Natur. Man variiert die Attribute der analytischen Laufzeitfläche und passt sie damit an die gemessene an. Da die Laufzeitfläche in den Daten durch kohärente Reflexionsereignisse bestimmt ist, benutzt man hierzu Kohärenzanalysen. Schließlich summiert man die Amplitudenwerte im Datenraum entlang der bestmöglichst angepassten Laufzeitfläche auf und weist diesen Wert P_0 zu. Dies wird als *stack* (Stapelung) bezeichnet. Der Punkt P_0 trägt nun folgende Information: Den Summenwert, einen Kohärenzwert und den Wert der drei Attribute.

Um nun das Problem vollständig zu lösen, muss man auch die ZO Lokation (x_0, t_0) einer Primärreflexion bestimmen. Dies wird jedoch umgangen, indem man auf die ZO Sektion ein Gitter legt und das oben erwähnte Verfahren für jeden Gitterpunkt durchführt. Man erhält auf diese Weise eine simulierte ZO Sektion (durch die Stapelung), eine Kohärenzsektion und drei Attributsektionen. Gitterpunkte, die nicht mit einem Reflexionseinsatz in der ZO Sektion assoziiert sind, liefern in der Regel einen niedrigen Kohärenzwert und Summenwert.

Laufzeitformeln

In den vorhergehenden Abschnitten wurden der Datenraum und das Verfahren zur Bestimmung der Attribute erklärt. Diese stellen anwendungsbedingte Anforderungen an die analytischen Laufzeitflächen. Die exakte Lösung der Laufzeitberechnung für einen kreisförmigen Reflektor in einem homogenen Medium, die zur Laufzeitapproximation dient, ist parametrischer Natur und kann nicht in expliziter Form dargestellt werden. Ihre Darstellung zur Laufzeitapproximation bei inhomogenen Medien (die sich durch die erwähnte zusätzliche Zeitverschiebung unterscheidet) ist in den Gleichungen (3.6) und (3.5) wiedergegeben. Wie man an den Gleichungen erkennen kann, ist sie streng genommen teilparamterisch. Der *half-offset* h kann explizit gegeben werden, während der *midpoint* x_m eine Funktion von h und dem Parameter $\tilde{\alpha}$ ist. Soll nun die Laufzeit bei gegebenen Initialwerten $(x_0, t_0, \alpha, R_{NIP}, R_N)$ für eine im Datenraum vorhandene Spur bei (x_m, h) berechnet werden, so müsste man zuerst zu dem gewünschten *midpoint* x_m iterieren, um die Laufzeit für die

Spur zu berechnen. Zudem ist nicht sichergestellt, dass sich der gewünschten *midpoint x_n* überhaupt berechnen lässt, wie die Beispiele in Anhang C zeigen. Zwar ist dies durchaus sinnvoll, führt aber in der Praxis dazu, dass eine unterschiedliche Anzahl von Spuren zur Kohärenzanalyse beitragen und reduziert damit die Stabilität des Verfahrens.

In Abschnitt 4 werden drei Taylor-Reihen der parametrischen Laufzeitformel bis zur vierten Ordnung präsentiert. Für die Praxis spielen jedoch nur die Taylor-Reihen bis zur zweiten Ordnung eine Rolle, da diese besser handhabbar sind. Die Taylor-Reihen zerstören jedoch die anschauliche Interpretation der Laufzeitapproximation die anhand von Abbildung 1 erläutert wurde. Allerdings stellt ja bereits die parametrische Laufzeitformel für inhomogene Medien eine Approximation dar. Daher kann man hier nicht grundsätzlich davon ausgehen, das eine Taylor-Reihe eine schlechtere Näherung darstellt.

Das Hauptaugenmerk gilt in dieser Arbeit der sogenannten hyperbolischen Laufzeitformel (Gleichung (4.1b) bis zur 2. Ordnung). Diese wird in der Praxis von der *common-reflection-surface* (CRS) Methode verwendet. Diese Terminologie basiert auf der hier erklärten Idee, die Reflexionseinsätze eines Reflektors lokal zu approximieren. Für reflexionsseismische Daten aus 2D Akquisitionen wurde der CRS *stack* bereits erfolgreich angewendet. Ein Ziel in Teil II der vorliegenden Arbeit ist es, die hyperbolische Laufzeitformel für Daten von 3D Akquisitionen zu erweitern.

Von 2D zu 3D Medien

Lassen Sie mich an dieser Stelle klären, warum ich es bisher vermieden habe, von Laufzeitapproximationen für 2D Medien zu sprechen und sie stattdessen auf 2D Akquisitionen bezog. Unabhängig von der Art der Akquisition ist der Untergrund in der realen Welt de facto dreidimensional. Abbildung 7.1 zeigt eine Wellenfront die an der Oberfläche auftaucht. Wenn man nun entlang der schwarzen Linie diese Wellenfront direkt messen würde, so würde man nur ihre Auswirkungen in einer Ebene registrieren. Diese Beobachtungsebene ist definiert durch die Propagationsrichtung und die seismische Linie (siehe Abbildung 7.1 und 7.2). Genau solch eine Messung macht aber der CRS *stack* für eine 2D Akquisition, dabei nimmt er aber diese Information aus den reflexionsseismischen Daten. Daher ist die bisher erklärte CRS Methode auch für 3D Medien gültig. Allerdings reicht die dabei gewonnene Information nicht aus, um die auftauchenden Wellenfronten in einem 3D Medium vollständig zu beschreiben. Selbst die (stark einschränkende) Annahme einer kugelförmigen Wellenfront kann nur die Krümmung, nicht aber die vollständige Propagationsrichtung beschreiben.

Das 3D Problem

Die Problemstellung für den 3D Fall ist dieselbe wie für den erläuterten 2D Fall. Auch der Ansatz, die Laufzeitapproximation mit Hilfe der hypothetischen Wellenfronten zu lösen, bleibt erhalten. Diese werden, analog zum 2D Fall, durch dieselben hypothetischen Experimente angeregt, nur stellen die Grenzflächen sowie die Wellenfronten Flächen in 3D Medien dar.

Der Ausgangspunkt ist durch reflexionsseismische Daten einer 3D Akquisition gegeben. Diese unterscheiden sich von den Daten einer 2D Akquisition dadurch, dass zwei weitere Dimensionen einbezogen sind: die Lokationen von Quelle ($\mathbf{x_s}$) sowie Empfänger ($\mathbf{x_g}$) sind durch 2D Vektoren auf der Oberfläche charakterisiert. Der *midpoint* $\mathbf{m}$ und der *half-offset* $\mathbf{h}$ sind nun gegeben durch

$$\mathbf{m} = \frac{1}{2}(\mathbf{x_g} + \mathbf{x_s}) \quad \text{und} \quad \mathbf{h} = \frac{1}{2}(\mathbf{x_g} - \mathbf{x_s}).$$

Somit bilden etwa eine CS, CO oder ZO Sektion ein dreidimensionales Volumen. Der Datenraum einer 3D Akquisition mit mehreren Quelle Empfänger-Paaren ist somit fünfdimensional.

Das Ziel ist also wieder aus den Daten einer reflexionsseismischen 3D Akquisition eine lokale Approximation der NIP- und Normal-Wellenfronten an einem Punkt X_0 auf der Oberfläche zu erhalten und dabei eine simulierte ZO Sektion zu erstellen. Dies erfordert aber zuerst eine adäquate Beschreibung der Wellenfront, um unter anderem die Frage nach der Anzahl der Parameter zu klären.

Notation

Für den 3D Fall werden Vektoren und Matrizen unterschiedlicher Dimension benötigt, die hier exemplarisch für die Größe a durch folgende Notation gekennzeichnet sind:

	Symbol	Element			Symbol	Element
2D Vektor	$\mathbf{a}$	a_i $(i = 0, 1)$		3D Vektor	$\underline{\mathbf{a}}$	a_i $(i = 0, 1, 2)$
2×2 Matrix	$\mathbf{A}$	a_{ij} $(i, j = 0, 1)$		3×3 Matrix	$\underline{\mathbf{A}}$	a_{ij} $(i, j = 0, 1, 2)$

Besondere Vektoren und Matrizen sind

$$\underline{\mathbf{e_x}} = \begin{pmatrix} 1 \\ 0 \\ 0 \end{pmatrix}, \quad \underline{\mathbf{e_y}} = \begin{pmatrix} 0 \\ 1 \\ 0 \end{pmatrix}, \quad \underline{\mathbf{e_z}} = \begin{pmatrix} 0 \\ 0 \\ 1 \end{pmatrix} \quad \text{und} \quad \underline{\mathbf{I}} = \begin{pmatrix} \underline{\mathbf{e_x}} & \underline{\mathbf{e_y}} & \underline{\mathbf{e_z}} \end{pmatrix}.$$

Wird ein Vektor oder eine Matrix sowohl in 2D als auch in 3D verwendet, so gilt folgender Zusammenhang:

$$\underline{\mathbf{a}} = \begin{pmatrix} \mathbf{a} \\ a_2 \end{pmatrix} \quad \underline{\mathbf{A}} = \begin{pmatrix} \mathbf{A} & \begin{matrix} a_{02} \\ a_{12} \end{matrix} \\ a_{20} \; a_{21} \; a_{22} \end{pmatrix}$$

Ein 2D Vektor oder eine 2×2 Matrix ist somit, falls vorhanden, durch seine 3D Darstellung bzw. die 3×3 Matrix definiert.

Zudem werden ein lokales und ein strahlzentriertes Koordinatensystem eingeführt und wie folgt beschrieben:

	Achsen ausgedrückt im globalen und lokalen System	auf das jeweilige System bezogene Variablen, Vektoren, Matrizen
Lokales System	$[\underline{\mathbf{e_x}}, \underline{\mathbf{e_y}}, \underline{\mathbf{e_z}}]$	$a, \underline{\mathbf{a}}, \underline{\mathbf{A}}$
Strahlzentriertes System	$[\underline{\mathbf{w_x}}, \underline{\mathbf{w_y}}, \underline{\mathbf{w_z}}]$	$\hat{a}, \hat{\underline{\mathbf{a}}}, \hat{\underline{\mathbf{A}}}$

Ausgenommen von letzterer Regel, die Variablen systembezogen zu kennzeichnen, sind Winkel, Krümmungen, sowie Radien.

Lokale Beschreibung einer Wellenfront in 3D

Analog zum 2D Fall wird in 3D eine lokale Approximation der Wellenfront zweiter Ordnung angesetzt. Diese liefert die Orientierung und Krümmung der Wellenfront an einer betrachteten Position. Abbildung 5.1 zeigt eine Wellenfront und zwei Koordinatensysteme. Die **Orientierung** der Wellenfront wird nun durch ihre Propagationsrichtung festgelegt. Dazu werden der Azimuthwinkel φ_0 und der Polarwinkel φ_1 benutzt. Man betrachte nun ein kartesisches Koordinatensystem, dessen z-Achse durch die Propagationsrichtung definiert ist. Die x- bzw. y-Achse seien frei wählbar; den Ursprung legt man in den Punkt, an dem die Wellenfront beschrieben werden soll. In diesem strahlzentrierten Koordinatensystem lassen sich die **Krümmungen** der Wellenfront durch die symmetrische Krümmungsmatrix $\hat{\mathbf{A}}$ beschreiben:

$$\hat{z} = -\frac{1}{2}\hat{\mathbf{x}}^\mathbf{T}\hat{\mathbf{A}}\hat{\mathbf{x}} \quad \text{mit} \quad \hat{\mathbf{x}} = \begin{pmatrix} \hat{x} \\ \hat{y} \end{pmatrix}, \quad \hat{\mathbf{A}} = \begin{pmatrix} \hat{a}_{00} & \hat{a}_{01} \\ \hat{a}_{10} & \hat{a}_{11} \end{pmatrix}, \quad \hat{a}_{10} = \hat{a}_{01}. \tag{1a}$$

Die Krümmung der Wellenfront in einem Normalschnitt[2] wird durch die zweite Richtungsableitung $D^2_{\hat{\mathbf{u}}}\{\hat{z}(\hat{x},\hat{y})\}$ definiert:

$$k = -D^2_{\hat{\mathbf{u}}}\{\hat{z}(\hat{x},\hat{y})\}(0,0) = \hat{\mathbf{u}}^\mathbf{T}\hat{\mathbf{A}}\hat{\mathbf{u}} \quad \text{mit} \quad \|\hat{\mathbf{u}}\| = 1, \tag{1b}$$

wobei $\underline{\mathbf{u}}$ einen 2D (Richtungs-) Vektor in der x-y-Ebene des strahlzentrierten Koordinatensystems darstellt.[3] Die erläuterte Beobachtungsebene stellt einen Normalschnitt der Wellenfront am betrachteten Punkt dar. Daher verknüpft Gleichung (1b) die Krümmung der Wellenfront in der Beobachtungsebene mit der Krümmungsmatrix.

Koordinatensysteme

Zusätzlich zu dem oben schon erwähnten strahlzentrierten Koordinatensystem wird ein lokales Koordinatensystem konstruiert. Lassen Sie mich die notwendigen Bedingungen der zwei involvierten Koordinaten zusammenfassen:

- **Beide** Koordinatensysteme sind rechtshändige kartesische Koordinatensysteme und besitzen denselben Ursprung $X_0 = (x_0, y_0, 0)$. Der Ursprung liegt daher auf der Oberfläche.

---

[2]Ein Normalschnitt einer Fläche enthält den Normalen- und einen Tangentenvektor der Fläche im betrachten Punkt. Für die Wellenfront ist die Normale gegeben durch die Propagationsrichtung, ein Tangentenvektor liegt in der x-y-Ebene des strahlzentrierten Koordinatensystems.

[3]Dies entspricht bis auf das Minuszeichen der mathematischen Definition der Krümmung in einem Normalschnitt.

- Die x-y-Ebene des **lokalen** Koordinatensystems ist durch die planare Oberfläche definiert. Zudem kann es durch Translation des globalen Koordinatensystems erhalten werden.[4]

- Die z-Achse des **strahlzentrierten** Koordinatensystems ist definiert durch die Propagationsrichtung (Normale) der Wellenfront im betrachten Punkt X_0.

Da das lokale System durch eine reine Translation gewonnen wurde, bleiben Richtungsvektoren (wie etwa die Richtung der seismischen Linie) aus dem globalen System erhalten. Ein Ortsvektor $\underline{\mathbf{r}}$ im globalen System wird einfach durch $\underline{\mathbf{r}} - \underline{\mathbf{x_0}}$ im lokalen System ausgedrückt, wobei $\underline{\mathbf{x_0^T}} = (x_0, y_0, 0)$ die Translation beschreibt.

Der Vorteil des lokalen Systems liegt darin, dass die Transformation vom lokalen in das strahlzentrierte System keine Translation mehr enthält. Die Orientierung des lokalen Koordinatensystems (ausgedrückt im lokalen System) ist durch die Vektoren $[\underline{\mathbf{e_x}}, \underline{\mathbf{e_y}}, \underline{\mathbf{e_z}}]$ gegeben. Die Basis bildet die Einheitsmatrix $\underline{\mathbf{I}} = (\underline{\mathbf{e_x}}\, \underline{\mathbf{e_y}}\, \underline{\mathbf{e_z}})$.

Ein strahlzentriertes Koordinatensystem $[\underline{\mathbf{v_x}}, \underline{\mathbf{v_y}}, \underline{\mathbf{w_z}}]$ ist unmittelbar durch Drehungen mit den Winkeln φ_0 und φ_1 um die y- bzw. z-Achse des lokalen Systems gegeben:

$$\underline{\mathbf{v_x}} = \underline{\mathbf{T_{IV}}}\,\underline{\mathbf{e_x}} \quad \underline{\mathbf{v_y}} = \underline{\mathbf{T_{IV}}}\,\underline{\mathbf{e_y}} \quad \underline{\mathbf{w_z}} = \underline{\mathbf{T_{IV}}}\,\underline{\mathbf{e_z}} \quad \text{mit} \quad \underline{\mathbf{T_{IV}}} = \underline{\mathbf{D_z}}(\varphi_0)\,\underline{\mathbf{D_y}}(\varphi_1). \tag{2}$$

Die Drehmatrizen $\underline{\mathbf{D_z}}(\varphi)$ und $\underline{\mathbf{D_y}}(\varphi)$ sind in Gleichungen (5.1) definiert. Der Vektor $\underline{\mathbf{w_z}}$ beschreibt die Propagationsrichtung der Wellenfront. Ein Nachteil dieser Transformation ist, dass sich die x- oder y-Achse des strahlzentrierten Koordinatensystems nicht frei wählen lassen.

Eine Möglichkeit, die x-Achse des strahlzentrierten Koordinatensystem zu wählen, besteht darin, zuerst eine zusätzliche Drehung um die z-Achse auszuführen. Das dadurch erhaltene strahlzentrierte Koordinatensystem $[\underline{\mathbf{w_x}}, \underline{\mathbf{w_y}}, \underline{\mathbf{w_z}}]$ genügt den Gleichungen

$$\underline{\mathbf{w_i}} = \underline{\mathbf{T_{IW}}}\,\underline{\mathbf{e_i}} \quad \text{mit} \quad i = \text{x,y,z} \quad \text{und} \quad \underline{\mathbf{T_{IW}}} = \underline{\mathbf{D_z}}(\varphi_0)\,\underline{\mathbf{D_y}}(\varphi_1)\,\underline{\mathbf{D_z}}(\varphi_F). \tag{3}$$

Der Winkel φ_F wird entweder frei gewählt oder berechnet, indem man verlangt, dass die x-Achse in einem Normalschnitt liegt, der z.B. mit Hilfe eines gewählten Richtungsvektor $\underline{\mathbf{s_F}}$ auf der Oberfläche festgelegt wird (siehe Gleichung (6.10b)).

Da beide hier vorgestellten strahlzentrierten Koordinatensysteme benutzt werden können, wird im Folgenden die Transformationsmatrix vom lokalen zum strahlzentrierten Koordinatensystem als $\underline{\mathbf{T}}$ bezeichnet. Hierbei muss jedoch beachtet werden, dass die Transformationsmatrix das Koordinatensystem definiert, in dem die Krümmungsmatrix der Wellenfront definiert ist.

Beziehungen in der Beobachtungsebene

Mit Hilfe der durch $\underline{\mathbf{w_z}}$ und $\mathbf{A}$ beschriebenen Wellenfront und der Transformationsmatrix $\underline{\mathbf{T}}$ lassen sich nun die Beziehungen zu den längs einer seismischen Linie gemessenen Größen (Auftauchwinkel α und Radius R der Wellenfront) mathematisch formulieren. Wie schon erwähnt wurde,

---

[4]Dies erfordert ein globales rechtshändiges kartesisches System dessen x-y-Ebene parallel zur planaren Oberfläche ist. Diese Bedingung wird im allgemeinen angetroffen und vereinfacht die Darstellung globaler Größen im lokalen Koordinatensystem. Sollte jedoch das globale Koordinatensystem nicht dieser Anforderung entsprechen, zeigt Abschnitt 5.2.1 die grundlegende Theorie für Transformationen im allgemeinen Fall.

stellt eine Beobachtungsebene (definiert durch die Richtung der seismischen Linie und die Propagationsrichtung der Wellenfront am betrachteten Punkt) einen Normalschnitt der Wellenfront dar. Die Richtung der seismischen Linie wird im Folgendem durch den Einheitsvektor $\underline{\mathbf{s_i}}$ ausgedrückt:

$$\underline{\mathbf{s_i}} = \begin{pmatrix} \cos\beta_i \\ \sin\beta_i \\ 0 \end{pmatrix} \qquad \mathbf{s_i} = \begin{pmatrix} \cos\beta_i \\ \sin\beta_i \end{pmatrix} \qquad (-\pi < \beta_i \leq \pi). \tag{4}$$

In der Beobachtungsebene ist der Winkel zwischen dem Vektor $\underline{\mathbf{w_z}}$ (der die Propagationsrichtung beschreibt) und der Normalen zur seismischen Linie gegeben durch:

$$\sin\alpha_i = \mathbf{w_z} \cdot \mathbf{s_i} \quad \text{bzw.} \quad \cos\alpha_i = \sqrt{1 - \left(\mathbf{w_z} \cdot \mathbf{s_i}\right)^2} \qquad (-\pi/2 < \alpha_i \leq \pi/2). \tag{5}$$

Die Krümmung der Wellenfront in der Beobachtungsebene kann mit Gleichung (1b) berechnet werden. Allerdings muss zuvor der Richtungsvektor $\hat{\mathbf{u}}$ bestimmt werden. Dieser beschreibt die Beobachtungsebene im strahlzentrierten Koordinatensystem und liegt in dessen x-y-Ebene. Um ihn zu berechnen, wird der Richtungsvektor der seismischen Linie $\underline{\mathbf{s}}$ mit Hilfe der Transformation $\underline{\mathbf{T}}$ (vom lokalen System zum strahlzentrierten System) im strahlzentrierten System ausgedrückt. Dies liefert $\underline{\mathbf{T}}^{\mathbf{T}} \underline{\mathbf{s_i}}$. Dieser Vektor wird nun auf die x-y-Ebene projiziert und schließlich normalisiert, um $\hat{\mathbf{u}}$ zu erhalten. Zusammengefasst lässt sich dies durch

$$\hat{\mathbf{u}}_\mathbf{i} = \begin{pmatrix} \cos\gamma_i \\ \sin\gamma_i \end{pmatrix} = \frac{\mathbf{T}^{\mathbf{T}} \mathbf{s_i}}{\sqrt{1 - \left(\mathbf{w_z} \cdot \mathbf{s_i}\right)^2}} \tag{6}$$

ausdrücken, wobei sich zeigen lässt, dass $\|\mathbf{T}^{\mathbf{T}} \mathbf{s_i}\| = \sqrt{1 - \left(\mathbf{w_z} \cdot \mathbf{s_i}\right)^2}$ (Anhang D).

Laufzeitapproximation

Nutzt man die im vorherigen Abschnitt erhaltenen Beziehungen und setzt sie in die hyperbolische Laufzeitgleichung für Daten einer 2D Akquisition ein, so ergibt sich eine "hyperbolische" Laufzeitgleichung für Daten einer 3D Akquisitionen:

$$t_{hyp}^2 = \left(t_0 + \frac{2}{v}\, \mathbf{w_z} \cdot \mathbf{m}\right)^2 + \frac{2t_0}{v}\, \mathbf{m}^{\mathbf{T}}\, \mathbf{T}\, \hat{\mathbf{N}}\, \mathbf{T}^{\mathbf{T}}\, \mathbf{m} + \frac{2t_0}{v}\, \mathbf{h}^{\mathbf{T}}\, \mathbf{T}\, \hat{\mathbf{M}}\, \mathbf{T}^{\mathbf{T}}\, \mathbf{h} \tag{7}$$

wobei v die oberflächennahe Geschwindigkeit darstellt und $\hat{\mathbf{M}}$ bzw. $\hat{\mathbf{N}}$ die Krümmungsmatrix der NIP bzw. Normal-Wellenfront kennzeichnet. Streng genommen gilt diese Herleitung nur für parallele *midpoint* $\mathbf{m}$ und *half-offset* $\mathbf{h}$ Vektoren. Daher wurde in Anhang G eine alternative Herleitung mit Hilfe der Hamilton-Gleichung durchgeführt. Diese liefert dasselbe Resultat.

Bestimmung der kinematischen Wellenfrontattribute für 3D Medien

Um die Wellenfrontattribute zu bestimmen, wird analog zum 2D Fall vorgegangen. Allerdings erhöht sich die Anzahl der Parameter von drei (α, R_{NIP}, R_N) im 2D Fall auf acht (φ_0, φ_1 und die

sechs unabhängigen Elemente der symmetrischen Krümmungsmatrizen $\hat{\mathbf{M}}$ und $\hat{\mathbf{N}}$). Gleichung (7) lässt sich auch schreiben als

$$t_{hyp}^2 = \left(t_0 + \frac{2}{v}\, \mathbf{w_z} \cdot \mathbf{m} \right)^2 + \frac{2t_0}{v}\, \mathbf{m^T}\, \mathbf{A}\, \mathbf{m} + \frac{2t_0}{v}\, \mathbf{h^T}\, \mathbf{B}\, \mathbf{h}\,. \qquad (8)$$

Für jeden Punkt im ZO Volumen wird diese Hyperfläche mittels Variation der Elemente von $\mathbf{w_z}$, $\mathbf{A}$, $\mathbf{B}$ an die Daten angepasst. Anschließend werden zunächst die Winkel φ_0, φ_1 aus den Elementen von $\mathbf{w_z}$ bestimmt:

$$\cos\varphi_0 = \frac{w_{z0}}{\sigma}\,, \quad \sin\varphi_0 = \frac{w_{z1}}{\sigma}\,, \quad \cos\varphi_1 = w_{z2}\,, \quad \sin\varphi_1 = \sigma \quad \text{mit} \quad \sigma = \sqrt[+]{w_{z0}^2 + w_{z1}^2}\,. \qquad (9)$$

Die Winkel φ_0, φ_1 erlauben es nun die Transformationsmatrix $\underline{\mathbf{T}}$ zu bestimmen (siehe Gleichung (2) oder (3)). Die Krümmungsmatrizen der NIP- und Normal-Wellenfront ergeben sich dann aus

$$\hat{\mathbf{N}} = \mathbf{T^T A T} \qquad (10)$$

$$\text{und} \quad \hat{\mathbf{M}} = \mathbf{T^T B T}\,. \qquad (11)$$

Alternativ kann man sich auch des CRS *stack* für 2D Akquisitionen bedienen. Allerdings erfordert dies für eine zu simulierende ZO Spur mindestens drei sich kreuzende seismische Linien. Die genaue Vorgehensweise ist in Teil II, Abschnitt 9.3 beschrieben.

Vergleiche

Im Rahmen meiner Arbeit habe ich ein Programm entwickelt, das für 3D Modelle mit mehreren Schichten konstanter Propagationsgeschwindigkeit der Wellen die Krümmungsmatrizen längs eines Strahls berechnet und visualisiert. Die zugrundeliegenden Formeln für die Implementierung sind in Kapitel 10 beschrieben. Quantitative Vergleiche der Laufzeitapproximation mit den wahren Laufzeiten sind in Kapitel 11 dargestellt. Sie bestätigen die geforderte Approximation der Laufzeiten bis zur zweiten Ordnung.

Schlussfolgerungen

Die Parameter der hergeleiteten Laufzeitformeln stellen wichtige kinematische Wellenfrontattribute dar, die ohne explizite Kenntnisse eines Geschwindigkeitsmodells aus reflexionsseismischen Daten gewonnen werden können. Die Laufzeitformeln dienen dazu, die wahren Reflexionslaufzeiten in der Umgebung einer ZO Primärreflexion zu approximieren. Sie lassen sich somit als Stapeloperator zur Simulation einer ZO Sektion verwenden.

Die hyperbolische Laufzeitformel stellt einen guten Kompromiss zwischen erforderter Genauigkeit und anwendungsbedingten Anforderungen dar. Ihre attributbasierte Formulierung, die bislang

nur im dreidimensionalen Datenraum von 2D Akquisitionen angewendet wurde, wurde auf den fünfdimensionalen Datenraum von 3D Akquisitionen erweitert. Diese Verallgemeinerung erhöht die Anzahl der Parameter von drei auf acht.

Eine wichtige Erkenntnis der Arbeit ist, dass die ursprünglich für 2D Medien entwickelte Laufzeitformeln auch für 3D Medien ihre Gültigkeit behalten. Sie stellen daher einen Spezialfall der 3D Laufzeitformeln dar. Dies unterstreicht den modellunabhängigen Charakter der vorgestellten CRS Theorie und der daraus abgeleiteten Laufzeitapproximationen.

Abstract

The topic of this thesis is to present analytic formulae for the model-independent zero-offset (ZO) simulation for 2D as well as for 3D seismic reflection imaging. One main interest in this respect is to express these formulae by means of parameters that provide a local second-order approximation of specific wavefronts at the measurement surface. These kinematic wavefield attributes serve for a variety of seismic reflection imaging topics such as the determination of a velocity model, the computation of geometrical spreading factors and minimum aperture for stacking and migration.

In 3D, a local second-order description of a wavefront determines its orientation and curvatures. The orientation is defined by the polar and azimuth angles of the propagation direction (assumed to be orthogonal to the wavefront). The curvatures are described by means of a symmetric 2×2 curvature matrix. In 2D these parameters reduce to one angle and a scalar curvature. Two hypothetical wavefronts considered along the same ray (propagation trajectory) are involved in the derivation of formulae that approximate the traveltime of the reflection events for a ZO sample (point in the ZO section). This yields three parameters for the ZO simulation from seismic reflection data of 2D acquisitions and eight parameters in the 3D case. In practice, the parameters for a ZO sample are determined by fitting the operator to the reflection events. Therefore, no model information is required.

The theory presented here forms the basis for the common-reflection-surface (CRS) stack. This terminolgy states the idea to locally gather the information that stem from a curved reflector segment in the subsurface and that is distributed in a multicoverage data set.

This work is divided into two parts. In the first part I present the CRS formulae for 2D acquisitions and derive them by means of geometrical optics. My main concern, however, is the generalization of the theory to the 3D case presented in the second part. Essentially, this requires the extension of a wavefront description as mentioned above. Of fundamental importance is the introduction of a ray-centered coordinate system and the associated transformation matrix that are explained in detail. I also present formulae and a scheme to compute the wavefront curvatures along a ray for a model with iso-velocity layers. This is used for illustration and traveltime comparisons.

One interesting result that makes the CRS stack even more attractive is that the three parametric CRS stack for 2D acquisitions accounts for 3D models. As a consequence, the 2D CRS stack determines a subset of the parameters required for 3D. The relationships are shown and used to formulate a strategy to determine the eight parameters of a 3D CRS stack by means of 2D CRS stacks.

Contents

Contents

Chapter 1

Introduction

The intention of exploration geophysics is to provide an image of the subsurface that shows its structure and composition. Three successive processes are involved to achieve this aim:

- acquisition of data

- processing of data

- interpretation

My aim is to give a theoretical contribution to the second step in seismic reflection imaging for 2D and 3D acquisitions. But let me start with a quick introduction to the considered media, the general acquisition geometry, the nature of recorded data, and the common processing steps for seismic reflection exploration.

Seismic waves and rays

In general, geophysicists use the elastodynamic wave equation to describe wave propagation in the subsurface. However, for the investigated case of isotropic media and because I am only interested in kinematic attributes of the wavefield it is sufficient to consider acoustic media. The considered wavefield attributes describe the directions of propagation and curvatures of wavefronts. The propagation directions can be determined by means of rays which are defined by the trajectories along which a wavefront propagates. Paraxial ray theory (Červený, 2001), in addition, gives a local description (including the wavefront curvature) of the wavefield along a ray. An acoustic medium is fully described by the spatial distribution of the bulk modulus $\kappa(x, y, z)$ and the density $\rho(x, y, z)$. These parameters define the wave propagation velocity $v(x, y, z) = \sqrt{\kappa/\rho}$. The traveltime between two points of the medium that are connected by a ray is defined by the integration of $1/v(x, y, z)$ along the ray. For the sake of simplicity but again without the loss of generality I use models that are composed of constant velocity layers. For this purpose, the layers are separated by interfaces which are piecewise analytically defined by a cubic spline interpolation of interface points. Therefore, the considered interfaces are continuous up to the second order.

Acquisition

Figure 1.1 shows a common 2D acquisition, where shot and receivers are placed along a straight line (seismic line) on the measurement surface. Shown is the 2D slice along the seismic line. The bolt and triangles on the measurement surface ($z = 0$) indicate the shot and receivers, respectively. The model in the lower part of Figure 1.1 is composed of three iso-velocity layers that are limited by the black interfaces. A "point" source at the shot emits a wave that is partly absorbed within the medium, and partly transmitted and reflected at the interfaces. The reflected part of the wave is recorded at the receivers. Therefore, each receiver records a so-called (seismic) trace that describes the particle velocity as a function of time. The entire set of traces for this acquisition geometry provides a common shot (CS) section shown in the time domain of Figure 1.1. Only primary reflection events are displayed; all other events are omitted. In this context, an event is defined as the location of a recorded reflection in the time domain. Also shown is a traveltime curve in blue that is associated with the reflection events of the dome-like interface. In the lower part of Figure 1.1, the primary wave that is reflected at the dome-like interface is indicated by the green wavefront; its reflection at the first interface is not displayed. Also shown are the associated rays that, as mentioned above, describe the trajectories along which the wavefront propagates.

In Figure 1.1 the 2D model serves only for illustration purposes. A real registration records of course a part of a three-dimensional wavefield, i. e. is the result of waves propagating in a 3D model. Unfortunately, common processing schemes for 2D acquisitions rely on a 2D model what causes out-of-plane reflections to be uncorrectly imaged. In any case, it is true that a 2D acquisition can hardly resolve a 3D model.

For a 3D CS acquisition the situation is, of course, the same. However, the wavefield is recorded by an array of receivers distributed on the whole measurement surface. Here, a single CS experiment provides a data volume.

Data geometry

To explain the geometry of the data let me firstly consider the 2D case. In general, a single CS configuration is shifted along the same seismic line such that different CS sections are acquired. These records provide a multicoverage data set that can be visualized in a x_m-h-t volume, where t denotes the time, h the half-offset, and x_m the midpoint. The latter two coordinates are connected to the shot and receiver locations, x_s and x_g, by

$$x_m = \frac{1}{2}(x_s + x_g) \quad \text{and} \quad h = \frac{1}{2}(x_g - x_s) . \tag{1.1}$$

This means that a trace recorded at the receiver location $(x_g, 0)$ for a shot positioned at $(x_s, 0)$ is located at the respective (x_m, h) position in the volume. This positioning of the traces provide common-offset (CO) sections and common-midpoint (CMP) gathers and can be conceived as a sorting process. A CMP gather provides the recorded data of shot/receiver pairs that have the same midpoint x_m. A CO section provides the recorded data of a single shot/receiver pair that
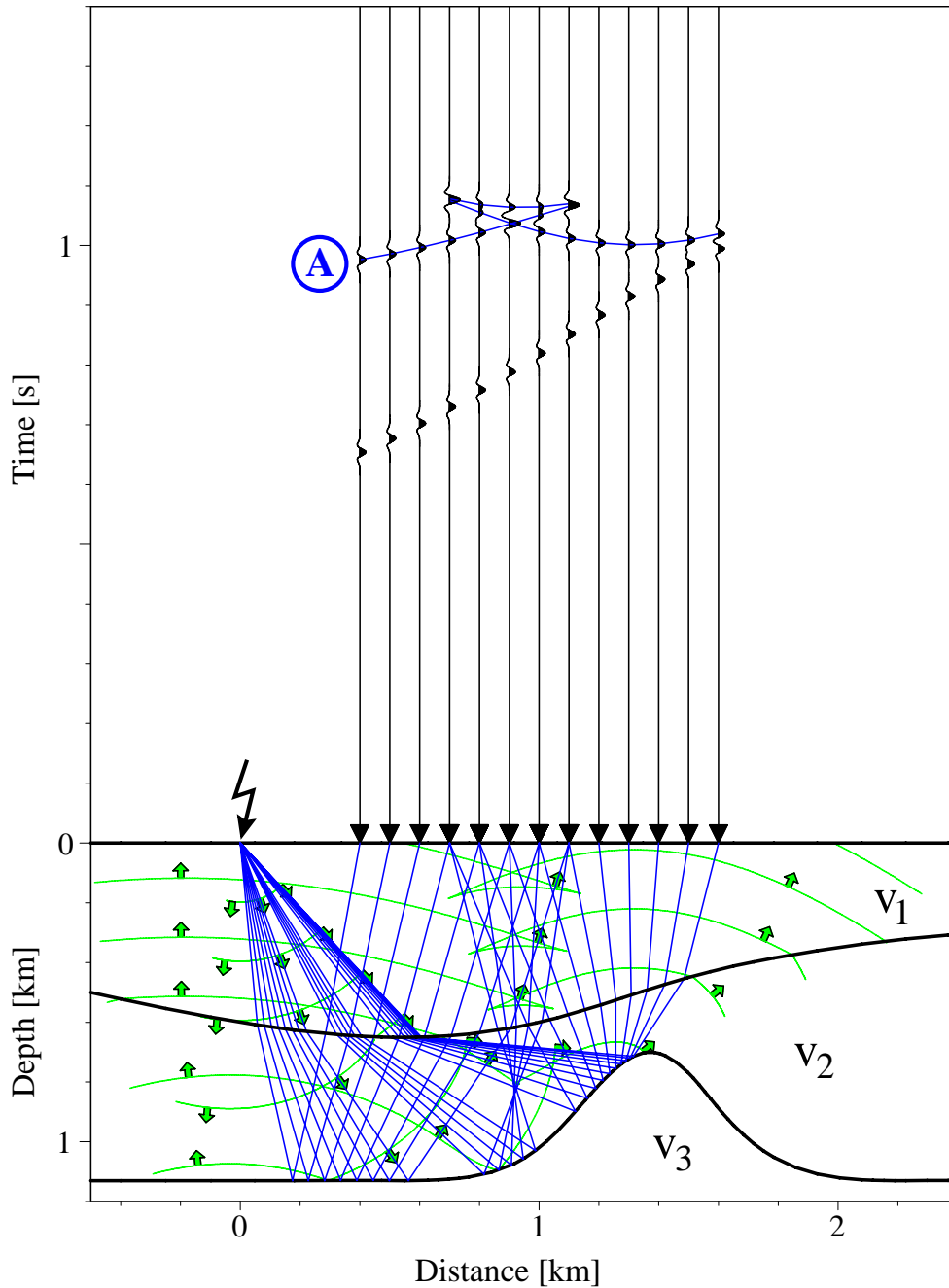
Figure 1.1: Common Shot acquisition: the bolt and the triangles indicate the source and the receivers, respectively. The lower part shows a wave that is reflected at the second interface (dome-like structure) by the green wavefronts. The associated rays are displayed in blue. The upper part shows the traces that are recorded at the receivers, where among other things the direct wave, multiple reflections and noise are omitted. The traveltime curve associated with the reflection events from the second interface is shown in blue.

is shifted along the seismic line (measurement surface) with a constant offset between shot and receiver.

Figure 1.2 shows the different source/receiver geometries for CS, CMP, and CO configurations. Also shown are the rays that are associated with the primary wave that is reflected at the dome-like structure. The traveltimes of these reflection events form a traveltime surface in the multicoverage data volume. In Figure 1.2 this traveltime surface is constructed by means of the different CO traveltime curves. Of course, it could also be made up of CS or CMP traveltime curves. Not shown is the reflection traveltime surface that pertains to the reflection events of the first interface. However, a real registration provides such a data volume filled with amplitudes from all kinds of events (including noise), where due to the filled volume the traveltime surfaces can hardly be identified by simple visualization.

One important process in exploration geophysics is the simulation of a zero-offset (ZO) section. Such a simulation provides the data that would be recorded by coincident shot/receiver pairs along the seismic line (see Figure 1.2). The advantages of this procedure are mentioned below. To obtain the traveltimes of the reflection events in the ZO section one has to extrapolate, for instance, the traveltime curves of the CS or CMP records to the ZO section. This is indicated by the dotted curves in the volume of Figure 1.2.

In the 3D case the data dimension increases by two dimensions: a shot and a receiver position is defined by a 2D vector on a plane. The consequence is that each section or gather represents a volume and that a multicoverage data set is five-dimensional.

Common processing schemes

In reflection seismics one can distinguish, in principle, between two different processing schemes to obtain a depth image of the subsurface:

  i pre-stack depth migration (model-dependent)

  ii ZO simulation (model-dependent or model-independent) and subsequent post-stack depth migration (model-dependent).

The term stack means summing up amplitudes along curves, surfaces or hyper-surfaces in the data set and putting the result into a target of the output section. The term depth migration is used for the transformation of the reflection events from the time to the depth domain. Model-dependent/independent means whether a-priori information about the subsurface is required or not. In this context model-dependent states that a velocity model of the subsurface has to be available. A velocity model is a model where the velocity is a function of the depth: $v(x, y)$ in 2D or $v(x, y, z)$ in 3D. Often a velocity model is a discrete model of the subsurface where a velocity value is assigned to each grid point. Other velocity models split the subsurface into layers or blocks, where inside of each layer (or block) an analytic velocity function is used. For instance, I use for traveltime investigations layered velocity models where the ith layer defines the constant

4
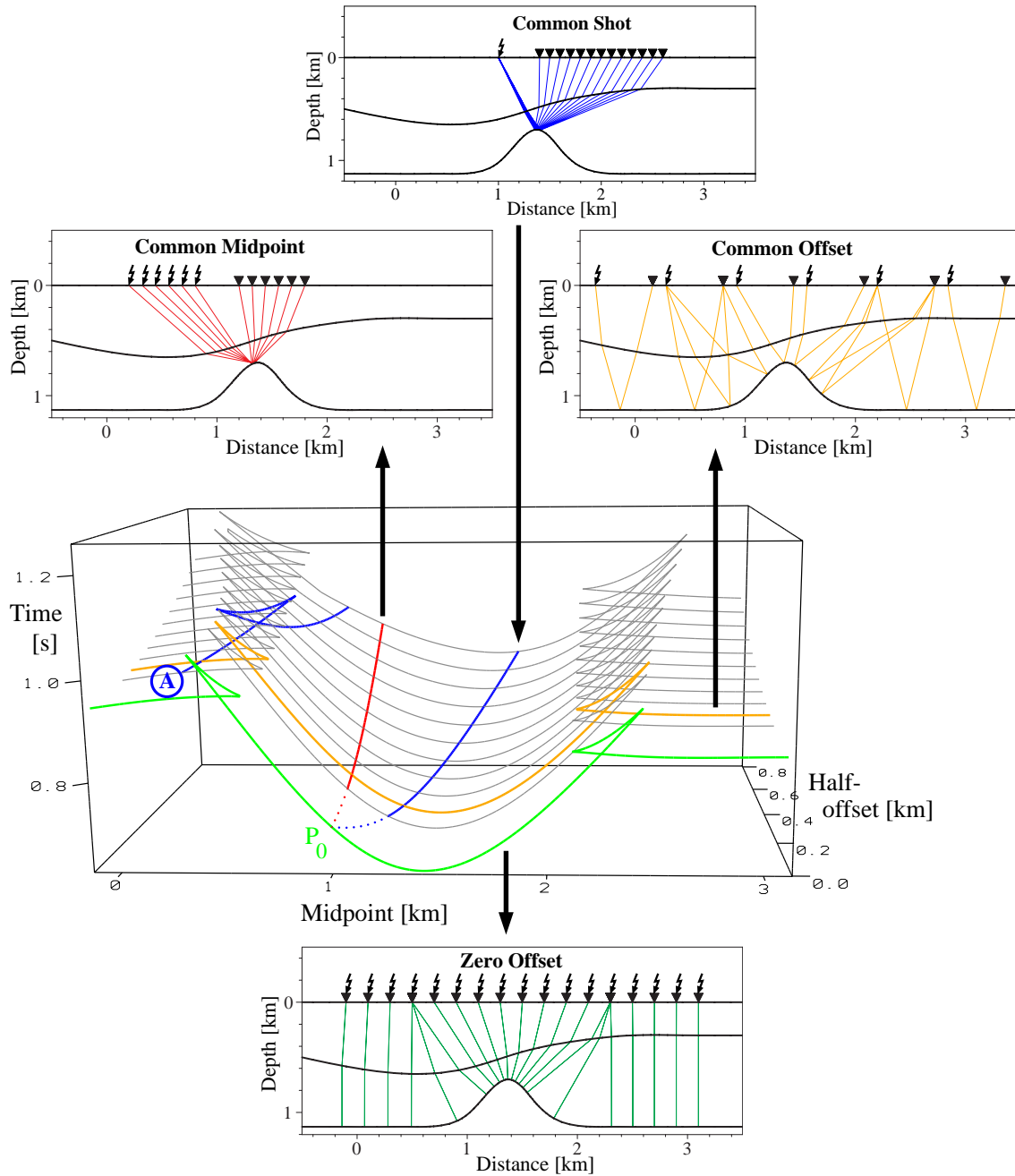
Figure 1.2: Data geometry: the CS data are resorted in midpoint/half-offset coordinates. This sorting provides the CO sections and CMP gathers. A CO section is defined by h=const; a CMP gather is given by x_m=const. The different traveltime curves in the data volume define the traveltimes of the reflection events that stem from the dome-like structure. Also shown is the searched-for ZO traveltime curve that is associated with coincident shot/receiver pairs.

velocity v_i. Method i) is a one step process where the data are directly transformed into the depth. Strategy ii) is separated into two steps: firstly, a ZO stack is performed which is subsequently transformed to the depth.

Motivation and application

In general, no information about the subsurface is available. My main concern is to provide analytic traveltime formulae for the model-independent ZO simulation. The aim of this processing step is to reduce the amount of data, to increase the signal to noise ratio and to determine parameters that provide information about the recorded wavefield.

The formulae that I present describe curves, surfaces or hyper-surfaces (subsequently summarized as operator) that approximate the traveltime of the reflection events in a data set. They are model-independent in the sense that they depend upon parameters that give a local second-order description of specific hypothetical wavefronts at the measurement surface. By variation of the parameters the operator is fit to the reflection events in the vicinity of a sample $P_0 = (x_0, y_0, t_0)$ in the ZO section. An accompanying coherence analysis determines the parameters that yield the best fit of the operator. Note that P_0 is the only point which is fixed upon variation of the parameters. To simulate the amplitude at P_0 the amplitudes along the operator are summed up and assigned to P_0. The result of this procedure is that P_0 carries the following information: a stack value (summed amplitude), the parameter values and a coherency value. Of course, the location of actual reflection events in the ZO section is unknown. Therefore, the procedure described above is applied to a grid of ZO samples. This yields a simulated ZO section, a coherence section, and parameter sections. To identify actual reflection events one can consider the coherence and stack sections as well as the in general met continuity of the parameters along these events.

History

In the past, model-independent seismic reflection imaging was mainly investigated for 2D media. Here, I give a brief summary of related studies about the 2D case.

The idea of model-independent seismic reflection imaging goes back to de Bazelaire (1986) and Gelchinsky (1988). de Bazelaire (1986) investigated hyperbolic moveouts in the CMP gather by means of geometrical optics. Gelchinsky (1988) considered common-reflection-point (CRP) trajectories in the multicoverage data volume. de Bazelaire and Thore (1987) then analyzed hyperbolic moveouts in the ZO section. Similar investigations for the ZO section were performed by Keydar et al. (1990) under the name of common-evolute element and for the CS gather by Keydar et al. (1993). Berkovitch et al. (1994) then presented a theory for traveltime surfaces called multifocusing.

The common-reflection-surface (CRS) method is based upon these ideas and relies on hypothetical wavefronts described by Hubral (1983). The related formulae can be obtained by either using CRP trajectories (Höcht et al., 1997; Perroud et al., 1997) and a hyperbola in the ZO section (Höcht,

1998; Höcht et al., 1999) or by paraxial traveltime formulae (Jäger, 1999; Müller, 1999). Paraxial traveltime are already available for the 3D case (Bortfeld, 1989; Schleicher et al., 1993) but have here not been related to the hypothetical wavefronts. In this respect, a first approach is given by Jäger (1999).

Applications of the CRS method

The CRS method was successfully applied for 2D acquisitions of synthetic and real data (Jäger, 1999; Müller, 1999; Mann et al., 1999). The application of the parameters with respect to geometrical spreading and Fresnel zones for 2D was shown by Vieth (2001). Majer (2000) investigated the determination of a 2D velocity model by means of the parameters.

Restrictions and remarks

As stated above, the aim of the CRS method is to fit an operator to the reflection events in the pre-stack data. The operator itself is a smooth surface (or hypersurface in the 3D case). Therefore, a successful application requires reflection events that locally can be approximated by the CRS operator. In this context, the definition of "locally" strongly depends on the character of the data. For instance, noisy data require a larger range of contributing events. Reflection events that are associated with shattered wavefronts in complex media can of course hardly be approximated by a smooth operator. Note that this operator is based on a second-order approximation of specific hypothetical wavefronts.

With respect to the topography of the measurement surface I restrict myself to the planar case. Co-workers are currently working on the extension of the formulae for smoothly varying and rugged topography.

Finally, the reader will observe that the near surface velocity enters in the model-independent formulae. However, an estimation of it is sufficient since it may be corrected together with the parameters afterwards. Since this correction is part of the inversion, it is not mentioned here. For the 2D case, it is formulated by Majer (2000).

Structure of the thesis

This thesis is divided into two parts: the first part deals with reflection times from 2D measurements and is published in a similar form by Höcht et al. (1999), the second part is the extension to the 3D problem. In principle the two parts can be read independently of each other. However, for a deeper understanding of the involved hypothetical wavefronts and their use for traveltime approximations I refer to part I.

Part I

The 2D case

Chapter 2

Introduction

In this part I derive various model-independent moveout formulae with the help of which multi-coverage reflection data from a 2D acquisition can be stacked into a simulated zero-offset (ZO) section. Based on concepts of geometrical optics I derive a parametric moveout surface that approximates the traveltimes of the reflection events in the multicoverage data set. Various Taylor series expansions of this surface are presented up to the fourth order in midpoint–half-offset coordinates. The second-order representations of these formulae are the so-called parabolic and hyperbolic approximation (Schleicher et al., 1993) and, restricted to the CMP gather, the normal moveout hyperbola (Hubral and Krey, 1980) and the delayed hyperbola (de Bazelaire, 1988). An application of the hyperbolic approximation to a real data set is shown by Mann et al. (1999). I also present and generalize the practically very useful delayed hyperbolae (de Bazelaire, 1988; de Bazelaire and Thore, 1987) in such form that they can be better related to and compared with the other model-independent ZO simulation formulae described here.

Let me quickly summarize the content of this part with the help of the first two figures. Figure 2.1 shows a 2D depth model with three constant velocity layers. The measurement surface in Figure 2.1 coincides with the midpoint axis of Figure 2.2, where the seismic multi-coverage data are found in the x_m-h-t space. The parameter h denotes the half-offset and t denotes time. Figure 2.2 shows the common-offset (CO) traveltime curves in the CO sections that define the traveltimes of the reflections from the dome-like interface. You can also observe a macro-model-independent stacking surface—subsequently called the common-reflection-surface (CRS) surface—parameterized by common-reflection-point (CRP) trajectories (Gelchinsky, 1988; Perroud et al., 1997, 1999). Such a CRP trajectory is an approximation of a "true" CRP trajectory that defines the locations of all primary reflection events in the x_m-h-t space that pertain to the same reflection point on a reflector. Therefore, the CRS surface is an approximation of the kinematic multicoverage reflection response of the reflector segment around a point S_{NIP}, where S_{NIP} is the normal-incidence point (NIP) of a ZO ray. This states that this ZO ray, also referred to as central ray, is normal incident on the reflector and connects the midpoint x_0 with point S_{NIP}. The CRS surface is tangent to the surface defined by all CO traveltime curves at $P_0 = (x_0, t_0)$, where t_0 denotes the recorded traveltime provided by a ZO experiment at x_0, i.e., the two-way traveltime along the central ray. A CRS surface is constructed for a point P_0 in the ZO section and depends

11

upon the three parameters α, R_{NIP} and R_N. The parameter α is the emergence angle of the central ray at x_0 on the measurement surface. R_{NIP} is the radius of curvature of a hypothetical wavefront that would be observed at x_0 on the measurement surface if one places a point source at S_{NIP} on the reflector. R_N is the radius of curvature of a hypothetical wavefront that would be observed at x_0 on the measurement surface if one considers an exploding reflector segment around S_{NIP}. Therefore, the CRS surface is model independent in the sense that it only depends upon parameters that locally describe specific wavefronts at the measurement surface.

This part is structured as follows: in chapter 3 I derive a CRS surface by means of CRP trajectories (section 3.2) and a hyperbola in the ZO section (section 3.3). Based on this parameterization of the CRS surface I present in chapter 4 three different fourth-order Taylor expansions of the CRS surface.
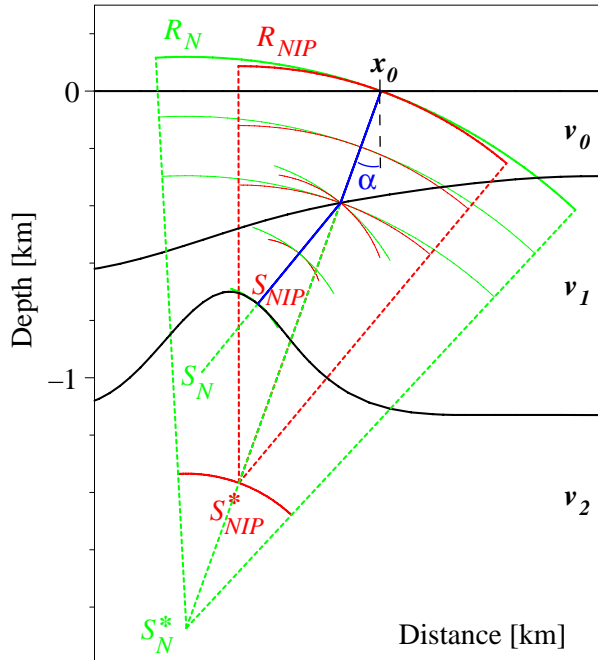
Figure 2.1: Model with object points S_{NIP} and S_N and their image points S^*_{NIP} and S^*_N provided by the radii of curvature of the NIP wave and the normal wave at x_0 on the surface. The radii of curvature of the NIP wave and the normal wave along the central ray (blue) are plotted in red and green, respectively.
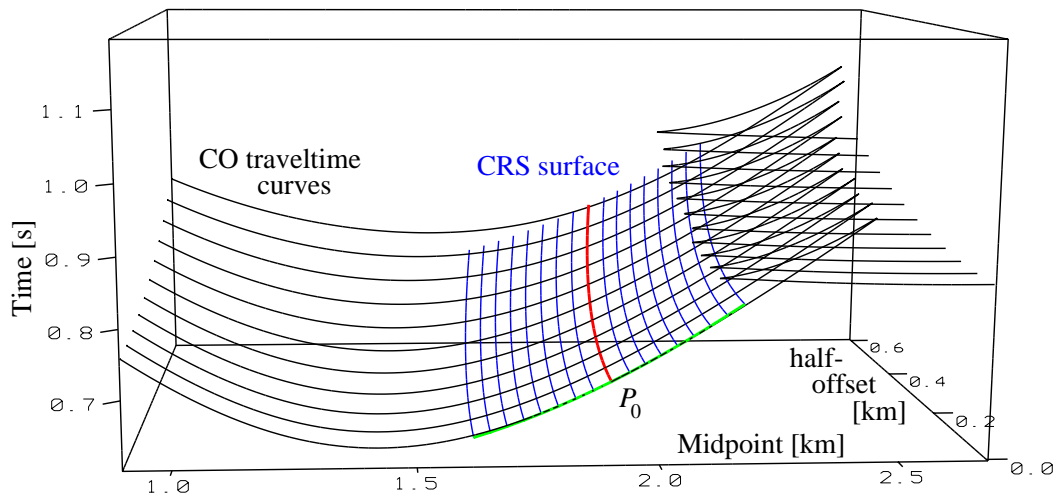
Figure 2.2: Multicoverage data set: The reflection events align along the CO traveltime curves in the x_m-h-t space. These curves build the traveltime surface that is approximated in the vicinity of $P_0 = (x_0, 0, t_0)$ by a CRS surface. The CRS surface is constructed by means of the (green) hyperbola in the ZO section and (red and blue) CRP trajectories.

13

Chapter 3

Traveltime response of curved interfaces

In this chapter, I derive an analytical approximation of the traveltime of reflection events. In order to obtain formulae that do not require any knowledge about the velocity model I use concepts of geometrical optics that relate object points in the model to image points in the image space.

3.1   General case and basic assumptions

Let me consider a point source S in an inhomogeneous medium illustrated here by the model shown in Figure 3.1 that consists of two constant velocity layers. The so-called object point is defined by the location of the point source. Imagine this point source to emit light that could be observed on the measurement surface ($z = 0$). For an observer standing at the observation point x_0 on the measurement surface the light appears to stem from a point source at the so-called conjugate point S^* of S. The conjugate point S^* is defined by the emergence angle α and the radius of curvature R of the wave observed at x_0 that stems from the point source at S: $S^* = (x_0 - R\sin\alpha, R\cos\alpha)$. In general, all conjugate points observed along the measurement surface form a caustic[1] (Figure 3.1). The so-called object point is the point source at S in the true model, which defines the object space.

To approximate the wavefront analytically in the vicinity of x_0 on the measurement surface I make the following assumptions: i) the emerging wave is circular, defined by the emergence angle α and the radius of curvature R of the true wave observed at x_0 and ii) it propagates with a constant velocity near to the surface. Under these assumptions the caustic collapses into the so-called image point S^*. The image point is thought to be located in an image space, which I define to be an auxiliary homogeneous medium with the constant near-surface velocity v_0 of the model.

For the derivation of a moveout formulae and the interpretation of the involved parameters let me consider the reflection event located at P_0 in the ZO section (Figure 2.2). The corresponding observation point is given by the emergence location of the associated ZO ray, i. e., by x_0 on the measurement surface (Figure 2.1).

---

[1]More about this subject can be found in Born and Wolf (1959), de Bazelaire (1988), Thore and de Bazelaire (1991).
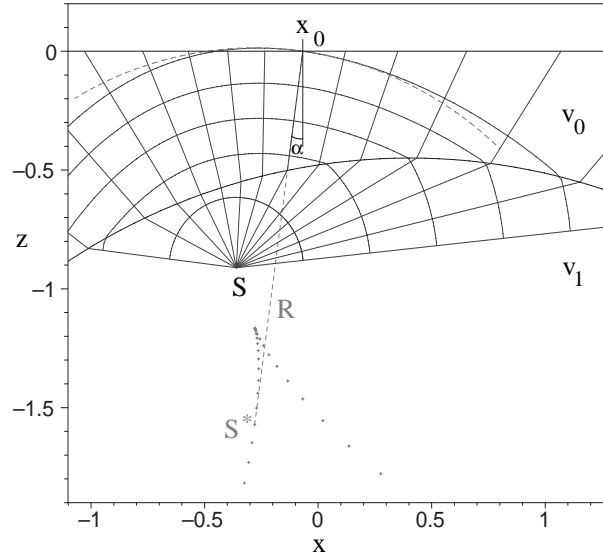
Figure 3.1: Model and image space: A point source at the object point S provides a wave shown in dark gray at different instants of time. The conjugate point S^* would be observed at x_0 on the measurement surface. All conjugate points observed on the measurement surface form a caustic (light gray points).

In the following I make use of two hypothetical experiments (Figure 2.1). A point source at S_{NIP} provides the so-called *NIP wave* (Hubral, 1983) emerging at x_0 on the measurement surface with the radius of curvature R_{NIP}. Object point and image point are located at S_{NIP} and S^*_{NIP}, respectively. An exploding reflector segment around S_{NIP} provides the so called *normal wave* (Hubral, 1983) emerging at x_0 on the measurement surface with the radius of curvature R_N. To determine the image point S^*_N I consider the center of curvature S_N of the interface at S_{NIP} as object point. Both waves emerge at x_0 with the angle α of the ZO ray and arrive at time $t_0/2$ if both waves are initiated at S_{NIP} at time $t = 0$.

3.2 Moveout trajectory for a reflection point

To determine the multicoverage traveltime response of the reflection point S_{NIP} associated with the reflection event at P_0 I make use of the NIP wave originating at S_{NIP}. The motivation for introducing this hypothetical wave is the following: the traveltime of any ray that is reflected at S_{NIP} can be computed by placing a point source at S_{NIP}. The resulting NIP wave emerges at time $t_0/2$ at x_0 on the measurement surface. Let me denote by Δt the traveltime difference between the traveltime t_0 for the coincident shot/receiver pair at x_0 and the traveltime t for an arbitrary shot/receiver pair associated with a ray that passes through S_{NIP}. It can be determined by means of the instants of time t_1 and t_2 when the NIP wave emerges at source and receiver coordinates, respectively: $\Delta t = t - t_0 = t_1 - t_0/2 + t_2 - t_0/2$ (Figure 3.2). Observe that this traveltime difference

depends only on the medium through which the NIP wave passes in the time interval between $\min(t_1, t_0/2, t_2)$ and $\max(t_1, t_0/2, t_2)$.
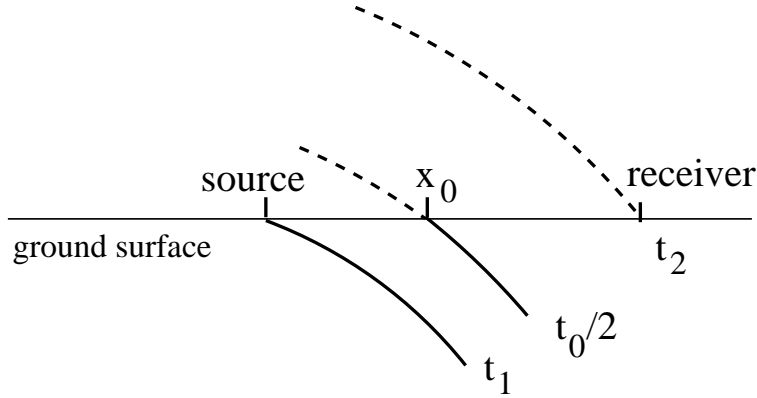

Figure 3.2: NIP wave at different instants of time.

A point source at S^*_{NIP} in the image space would provide the same NIP wavefront at x_0 on the measurement surface as a point source at S_{NIP} in the actual model. However, the traveltime $t_0/2$ of the NIP wave from S_{NIP} to $(x_0, 0)$ in the model will in general differ from the traveltime R_{NIP}/v_0 from S^*_{NIP} to $(x_0, 0)$ in the image space.

Denoting again t to be the traveltime for an arbitrary shot/receiver pair associated with a ray passing through S_{NIP} in the model and t_I to be the traveltime for the same shot/receiver pair with a ray passing through S^*_{NIP} in the image space, the traveltime difference $t - t_0$ occurring in the true model is equal to the traveltime difference $t_I - \frac{2}{v_0}R_{NIP}$ occurring in the image space. Hence, the traveltime for a shot/receiver pair is given by

$$t = t_I - \frac{2}{v_0}R_{NIP} + t_0. \tag{3.1}$$

Evaluating the traveltimes by means of this formula for arbitrary shot/receiver pairs would provide the traveltime response of a diffractor at S_{NIP}, which is a surface in the x_m-h-t space. Into this surface falls the common-reflection-point (CRP) trajectory of S_{NIP} that describes the locations of all reflection events in the x_m-h-t space that pertain to rays that are reflected on the interface at S_{NIP}. To determine the CRP trajectory of S_{NIP}, I consider its image point S^*_{NIP} as a reflection point defining its dip by the emergence angle α of the ZO ray. This enters into the derivation as an additional assumption.

For constant velocity media the CRP trajectory is given by an analytical formula (see appendix A). I make use of this result for inhomogeneous media approximating the true CRP trajectory of the object point S_{NIP} with a time-delayed CRP trajectory of its image point S^*_{NIP}. To describe the CRP trajectory of S^*_{NIP} in the image space one only has to substitute $\frac{2}{v_0}R_{NIP}$ for t_0 in eqs. (A.4). This provides the midpoints x_m and time t_I for source/receiver pairs separated by the half offset h. Taking into account the time delay given by eq. (3.1) the true CRP trajectory for S_{NIP} is approximated

17

by:

$$x_m(h) = x_0 + r_T \left(\sqrt{\frac{h^2}{r_T^2} + 1} - 1 \right), \tag{3.2a}$$

$$\left[t(h) - \left(t_0 - \frac{2}{v_0} R_{NIP} \right) \right]^2 = 4 \frac{h^2}{v_0^2} + \frac{2}{v_0^2} R_{NIP}^2 \left(\sqrt{\frac{h^2}{r_T^2} + 1} + 1 \right), \tag{3.2b}$$

$$\text{where} \quad r_T = \frac{1}{2} \frac{R_{NIP}}{\sin \alpha}.$$

The CRP trajectory for point P_0 is shown in red in Figure 2.2. As shown in section 3.4 eqs. (3.2) serve to determine a fundamental moveout surface (see Figure 2.2) from which all other moveout surfaces and trajectories presented in this part are derived.

3.3 Moveout hyperbola for a reflector segment in the ZO section

For the zero-offset (ZO) acquisition geometry it is sufficient to consider the normal wave provided by an exploding segment of the interface around S_{NIP}. The above motivation in connection with the NIP wave applies in a similar way to the normal wave: the exploding reflector segment around S_{NIP} defines half the traveltimes of ZO rays with normal incidence on this reflector segment. Now, the object point is located at S_N whereas the image observed at x_0 stems from S_N^*.

However, the formulation is now much simpler since a ZO acquisition geometry is defined by coincident shot/receiver pairs. Therefore, one does not have to determine the locations of the shot/receiver pairs as were required for the derivation of the CRP trajectory (eqs. (3.2)). The kinematic reflection response of a coincident shot/receiver pair located at $\tilde{x}_0$ in the vicinity of x_0 on the measurement surface is approximated by the following hyperbola (Appendix B):

$$\left[\tilde{t}_0(\tilde{x}_0) - \left(t_0 - \frac{2}{v_0} R_N \right) \right]^2 = \left(\frac{2}{v_0} \right)^2 \left[(\tilde{x}_0 - x_0)^2 + 2 R_N \sin \alpha \, (\tilde{x}_0 - x_0) + R_N^2 \right]. \tag{3.3}$$

The hyperbola for point P_0 is shown in green in Figure 2.2. In the following section formulae (3.2) and (3.3) are combined to construct the moveout surface indicated in Figure 2.2.

3.4 Moveout surface for a reflector segment

In section 3.2 I considered the traveltime of rays that had the object point S_{NIP} as a common reflection point, whereas in section 3.3 I approximated the traveltime of rays with normal incidence on a reflector segment around S_{NIP}. My aim now is to extend this description by considering all rays that are reflected on the segment of the interface around S_{NIP}. I call such a reflector segment a common-reflection-surface (CRS) and its traveltime response in the x_m-h-t space a CRS surface. However, to determine the CRS surface for P_0 I confine myself to the information available from

18

the NIP and normal wave at x_0 on the measurement surface, i.e. the three attributes α, R_{NIP}, and R_N.

I now make use of the CRP trajectories for points $\tilde{x}_0$ on the measurement surface located in the vicinity of x_0. The CRP trajectory for P_0 depends on the attributes α and R_{NIP}. To construct the CRP trajectory for a point $\tilde{x}_0$ one has to determine the respective initial values $\tilde{\alpha}(\tilde{x}_0)$, $\tilde{R}_{NIP}(\tilde{x}_0)$, and, in addition the traveltime $\tilde{t}_0(\tilde{x}_0)$ in the ZO section. This can be done with help of the normal wave. Therefore, $\tilde{t}_0(\tilde{x}_0)$ is given by eq. (3.3) and $\tilde{\alpha}(\tilde{x}_0)$ is determined by the emergence angle of the normal wave available from $\sin\tilde{\alpha} = d\tilde{t}_0/d\tilde{x}_0$. To determine $\tilde{R}_{NIP}(\tilde{x}_0)$ I assume that R_{NIP} is, similar as the traveltime $t_0/2$, constant on the normal wavefront emerging at x_0. These assumptions provide the following initial values:

$$\sin\tilde{\alpha}(\tilde{x}_0) = \frac{\tilde{x}_0 - x_0 + R_N \sin\alpha}{R_N A\left(\tilde{x}_0\right)}, \tag{3.4a}$$

$$\tilde{t}_0(\tilde{x}_0) = \frac{2}{v_0} R_N \left[A\left(\tilde{x}_0\right) - 1\right] + t_0, \tag{3.4b}$$

$$\tilde{R}_{NIP}(\tilde{x}_0) = R_N \left[A\left(\tilde{x}_0\right) - 1\right] + R_{NIP}, \tag{3.4c}$$

$$\text{where} \quad A(\tilde{x}_0) = \sqrt{\frac{\left(\tilde{x}_0 - x_0\right)^2}{R_N^2} + 2\frac{\left(\tilde{x}_0 - x_0\right)\sin\alpha}{R_N} + 1}.$$

Please note that these formulae cannot handle the case of a normal wave focusing at x_0. A simpler representation is given by using the emergence angle $\tilde{\alpha}$ as variable instead of $\tilde{x}_0$ (Appendix B):

$$\tilde{x}_0(\tilde{\alpha}) = x_0 + R_N \left(\cos\alpha \tan\tilde{\alpha} - \sin\alpha\right), \tag{3.5a}$$

$$\tilde{t}_0(\tilde{\alpha}) = \frac{2}{v_0} R_N \left(\frac{\cos\alpha}{\cos\tilde{\alpha}} - 1\right) + t_0, \tag{3.5b}$$

$$\tilde{R}_{NIP}(\tilde{\alpha}) = R_N \left(\frac{\cos\alpha}{\cos\tilde{\alpha}} - 1\right) + R_{NIP}. \tag{3.5c}$$

The latter parameterization can account for a focusing normal wave but fails for a planar normal wave ($\tilde{\alpha} = \alpha \wedge R_N = \infty$) at x_0. With the initial values given by eqs. (3.5) one can construct the CRS surface by means of the associated CRP trajectories. Since $\tilde{t}_0 - 2\tilde{R}_{NIP}/v_0 = t_0 - 2R_{NIP}/v_0$, the time delay is constant for all involved CRP trajectories and equation (3.5b) is not required. Using $\tilde{\alpha}$ and h as parameters to construct the CRS surface it is given by[2]

$$x_m(\tilde{\alpha}, h) = \tilde{x}_0(\tilde{\alpha}) + \tilde{r}_T(\tilde{\alpha})\left(\sqrt{\frac{h^2}{\tilde{r}_T^2(\tilde{\alpha})} + 1} - 1\right), \tag{3.6a}$$

$$\left[t(\tilde{\alpha}, h) - \left(t_0 - \frac{2}{v_0} R_{NIP}\right)\right]^2 = 4\frac{h^2}{v_0^2} + \frac{2}{v_0^2}\tilde{R}_{NIP}^2(\tilde{\alpha})\left(\sqrt{\frac{h^2}{\tilde{r}_T^2(\tilde{\alpha})} + 1} + 1\right), \tag{3.6b}$$

$$\text{where} \quad \tilde{r}_T(\tilde{\alpha}) = \frac{1}{2}\frac{\tilde{R}_{NIP}(\tilde{\alpha})}{\sin\tilde{\alpha}}.$$

---

[2]By using $\tilde{x}_0$ as parameter to construct the CRS surface one has to set in eqs. (3.6) $\tilde{x}_0(\tilde{\alpha}) = \tilde{x}_0$, $R_{NIP}(\tilde{\alpha}) = R_{NIP}(\tilde{x}_0)$, $\sin\tilde{\alpha} = \sin\tilde{\alpha}(\tilde{x}_0)$, and $\tilde{r}_T(\tilde{\alpha}) = \tilde{r}_T(\tilde{x}_0)$. The initial values are then given by eqs. (3.4).

In Figure 2.2 the CRS surface for point P_0 represents the ensemble of CRP trajectories shown in red and blue. The involved assumptions allow a simple geometrical interpretation of the CRS surface: without the time delay on the left-hand side of eq. (3.6b) it describes the traveltime surface of a circular reflector segment located at S_{NIP}^* in the image space, oriented by the emergence angle α and with radius of curvature $R_N - R_{NIP}$ (Figure 2.1). Therefore, equations (3.6) provide an exact description for the multicoverage reflection time surface of a circular reflector segment in a constant velocity medium, where $R_{NIP} = v_0 t_0 / 2$. For inhomogeneous media one can conceive the reflector segment around S_{NIP} to be the object and the circular reflector at S_{NIP}^* to be the image: each point on the reflector segment around S_{NIP} is thought to be imaged to a point on the circular reflector at S_{NIP}^*.

Chapter 4

Taylor-series expansions of the CRS surface

In order to get an explicit expression of the CRS surface I derive various Taylor expansions of eqs. (3.6). However, note that such representations cannot handle all cases as, for instance, those two examples shown in appendix C. In the following I provide three different Taylor expansions of the CRS surface in the x_m-h-t space: firstly for t, secondly for t^2, and finally for $(t - t_0 + \frac{2}{v_0}R_{NIP})^2$. The latter expansion implies that the time delay is introduced after the expansion.[1] Up to the second order, the Taylor expansions for t and t^2 reduce to the formulae obtained by paraxial ray theory (Schleicher et al., 1993).

Taylor expansion for t

$$t(x_m, h) =$$
$$t_0 + \frac{2\sin\alpha}{v_0}(x_m - x_0)$$
$$+ \frac{\cos^2\alpha}{v_0 R_N}(x_m - x_0)^2 + \frac{\cos^2\alpha}{v_0 R_{NIP}}h^2$$
$$- \frac{\sin\alpha\cos^2\alpha}{v_0 R_N^2}(x_m - x_0)^3 - \frac{\sin\alpha\cos^2\alpha(2R_{NIP} + R_N)}{v_0 R_{NIP}^2 R_N}(x_m - x_0)h^2$$
$$- \frac{\cos^2\alpha}{2v_0 R_{NIP}^3 R_N^2}\left[R_{NIP}^2\left(8\cos^2\alpha - 6\right) + R_{NIP}R_N\left(5\cos^2\alpha - 4\right) - 2R_N^2\sin^2\alpha\right](x_m - x_0)^2 h^2$$
$$- \frac{\cos^2\alpha\left(5\cos^2\alpha - 4\right)}{4v_0 R_N^3}(x_m - x_0)^4 + \frac{\cos^2\alpha\left(4R_{NIP}\sin^2\alpha - R_N\cos^2\alpha\right)}{4v_0 R_{NIP}^3 R_N}h^4$$

(4.1a)

---

[1]A Taylor expansion of $t - t_0 + \frac{2}{v_0}R_{NIP}$ is, of course, equivalent to a Taylor expansion of t.

Taylor expansion for t^2

$$t^2(x_m, h) = t_0^2 + \frac{4t_0 \sin \alpha}{v_0}(x_m - x_0) + 2\frac{v_0 t_0 \cos^2 \alpha + 2R_N \sin^2 \alpha}{v_0^2 R_N}(x_m - x_0)^2 + \frac{2t_0 \cos^2 \alpha}{v_0 R_{NIP}}h^2$$

$$+ \frac{2\sin \alpha \cos^2 \alpha (2R_N - v_0 t_0)}{v_0^2 R_N^2}(x_m - x_0)^3$$

$$+ \frac{2\sin \alpha \cos^2 \alpha (2R_{NIP}R_N - 2v_0 t_0 R_{NIP} - v_0 t_0 R_N)}{v_0^2 R_{NIP}^2 R_N}(x_m - x_0)h^2$$

$$+ \frac{\cos^2 \alpha \left[R_N (10 \cos^2 \alpha - 8) + v_0 t_0 (4 - 5 \cos^2 \alpha)\right]}{2v_0^2 R_N^3}(x_m - x_0)^4$$

$$+ \frac{\cos^2 \alpha}{v_0^2 R_{NIP}^3 R_N^2}\left[v_0 t_0 R_{NIP}^2 (6 - 8 \cos^2 \alpha) + v_0 t_0 R_{NIP} R_N (4 - 5 \cos^2 \alpha)\right.$$

$$\left. + 2v_0 t_0 R_N^2 \sin^2 \alpha - 4R_{NIP}R_N^2 \sin^2 \alpha + R_{NIP}^2 R_N (10 \cos^2 \alpha - 8)\right](x_m - x_0)^2 h^2$$

$$+ \frac{\cos^2 \alpha (4v_0 t_0 R_{NIP} \sin^2 \alpha - v_0 t_0 R_N \cos^2 \alpha + 2R_{NIP}R_N \cos^2 \alpha)}{2v_0^2 R_{NIP}^3 R_N}h^4$$

$$\tag{4.1b}$$

Taylor expansion for $(t - t_0 + \frac{2}{v_0}R_{NIP})^2$

$$\left(t(x_m, h) - t_0 + \frac{2}{v_0}R_{NIP}\right)^2 = \left(\frac{2}{v_0}R_{NIP}\right)^2 + \frac{8R_{NIP} \sin \alpha}{v_0^2}(x_m - x_0)$$

$$+ 4\frac{R_{NIP} \cos^2 \alpha + R_N \sin^2 \alpha}{v_0^2 R_N}(x_m - x_0)^2 + 4\frac{\cos^2 \alpha}{v_0^2}h^2$$

$$+ \frac{4\sin \alpha \cos^2 \alpha (R_N - R_{NIP})}{v_0^2 R_N^2}(x_m - x_0)^3$$

$$- \frac{8\sin \alpha \cos^2 \alpha}{v_0^2 R_N}(x_m - x_0)h^2$$

$$+ \frac{\cos^2 \alpha \left[R_N (5 \cos^2 \alpha - 4) + R_{NIP} (4 - 5 \cos^2 \alpha)\right]}{v_0^2 R_N^3}(x_m - x_0)^4$$

$$+ \frac{4\cos^2 \alpha (3 - 4 \cos^2 \alpha)}{v_0^2 R_N^2}(x_m - x_0)^2 h^2$$

$$+ \frac{4\cos^2 \alpha \sin^2 \alpha}{v_0^2 R_{NIP} R_N}h^4.$$

$$\tag{4.1c}$$

Such explicit representations of the CRS surface are of course better suited to handle the discrete seismic reflection data than the parametric description given by (3.6). Let me now investigate these Taylor expansions in order to get a better insight and to make a choice. In this respect it is important to keep in mind that a second-order description of the hypothetical wavefronts is used. This description is already involved in the second-order expansions of eqs. (4.1). Therefore, it would be sufficient to consider the second-order representations. This is mostly done in practice. The second-order expansion of t and t^2 are the so called parabolic and hyperbolic traveltime approximations. Comparisons performed by forward modeling showed that the parabolic approximation has a smaller range where it fits to the reflection events than the hyperbolic approximation because the reflection traveltimes are often of hyperbolic nature (Jäger, 1999; Höcht, 1998). Therefore, the Taylor expansion of t will not be further investigated.

4.1 CMP gather

The CMP gather for the midpoint x_0 is defined by $x_m = x_0$. Here, eqs. (4.1b) and (4.1c) reduce to

$$t^2(h) = t_0^2 + \frac{2t_0 \cos^2 \alpha}{v_0 R_{NIP}} h^2$$
$$+ \frac{\cos^2 \alpha \left[4v_0 t_0 R_{NIP} \sin^2 \alpha - v_0 t_0 R_N \cos^2 \alpha + 2R_{NIP} R_N \cos^2 \alpha \right]}{2 v_0^2 R_{NIP}^3 R_N} h^4,$$

(4.2a)

$$\left(t(x_m, h) - t_0 + \frac{2}{v_0} R_{NIP} \right)^2 = \left(\frac{2}{v_0} R_{NIP} \right)^2 + 4 \frac{\cos^2 \alpha}{v_0^2} h^2 + \frac{4 \cos^2 \alpha \sin^2 \alpha}{v_0^2 R_{NIP} R_N} h^4.$$

(4.2b)

For constant velocity, i.e. $R_{NIP} = v_0 t_0 / 2$, formulae (4.2a) and (4.2b) can be obtained from the fourth-order model-dependent moveout expression given by Fomel and Grechka (1998), who showed that the dependency of the CMP moveout on the change of the reflector's curvature is of the sixth order in h. One can observe that the fourth-order term of formula (4.2b) vanishes for planar normal waves as for instance in 2D models with constant layer velocity and planar layer boundaries. In such cases the second-order expansion is as accurate as the fourth-order expansion. The dependency of equations (4.2) upon R_N is due to what is commonly called the "reflection point dispersal" of the rays that are associated with the symmetric shot/receiver pairs of the CMP gather. However, the dependency on R_N comes only into play for terms higher than the second order.

The second-order representation of eq. (4.2a) is commonly formulated with v_{st} that combines the parameters R_{NIP} and α:

$$t^2(h) = t_0^2 + \frac{4}{v_{st}^2} h^2 \quad \text{with} \quad v_{st}^2 = 2v_0 \frac{R_{NIP}}{t_0 \cos^2 \alpha}$$

(4.3)

The second-order representation of eq. (4.2b) is used by de Bazelaire (1988). For further details see Höcht et al. (1999).

4.2   ZO section

The ZO section is defined by $h = 0$. Here, the parametric CRS formula is given explicitly by eq. (3.3) which is used in a different representation by de Bazelaire and Thore (1987). For comparisons I refer to Höcht et al. (1999). Note that none of the hyperbolic Taylor expansions recover eq. (3.3):

$$t^2(x_m) = t_0^2 + \frac{4 t_0 \sin \alpha}{v_0} (x_m - x_0) + 2 \frac{v_0 t_0 \cos^2 \alpha + 2 R_N \sin^2 \alpha}{v_0^2 R_N} (x_m - x_0)^2$$

(4.4a)

$$\left(t(x_m) - t_0 + \frac{2}{v_0} R_{NIP} \right)^2 = \left(\frac{2}{v_0} R_{NIP} \right)^2 + \frac{8 R_{NIP} \sin \alpha}{v_0^2} (x_m - x_0)$$
$$+ 4 \frac{R_{NIP} \cos^2 \alpha + R_N \sin^2 \alpha}{v_0^2 R_N} (x_m - x_0)^2$$

(4.4b)

Equation (4.4b) seems rather strange because R_{NIP} appears in this ZO formula. Investigations showed that, as expected, the higher the order of a Taylor expansion of $\left(t(x_m) - t_0 + 2 R_{NIP}/v_0 \right)^2$ in the ZO section, the less influences R_{NIP} the result. This is, however, a first reason that makes it unattractive for practical purposes. A second disadvantage is that the slope $dt(x_m, 0)/dx_m\big|_{x_m = x_0}$ of the Taylor expansion of $\left(t(x_m) - t_0 + 2 R_{NIP}/v_0 \right)^2$ in the ZO section depends on the order of the Taylor expansion.

4.3   Remarks

The presented Taylor expansions have, of course, the advantage to be explicit formulae. However, none of them recover the explicit ZO hyperbola given by eq. (3.3). An opportunity would be to attach CMP trajectories given by eqs. (4.2) to the original ZO hyperbola. Thereby, t_0, α, and R_{NIP} can be determined by eqs. (3.4a) and eqs. (3.4c), respectively. For the in practice mostly involved second-order expansions of $t(x_m, h)^2$ and $(t(x_m) - t_0 + 2 R_{NIP}/v_0)^2$ the formulation is:

$$t^2(x_m, h) = \tilde{t}_0^2(x_m) + \frac{2 \tilde{t}_0(x_m) \cos^2 \tilde{\alpha}(x_m)}{v_0 \tilde{R}_{NIP}(x_m)} h^2 ,$$

(4.5a)

$$\left(t(x_m, h) - t_0 + \frac{2}{v_0} R_{NIP} \right)^2 = \left(\frac{2}{v_0} \tilde{R}_{NIP}(x_m) \right)^2 + 4 \frac{\cos^2 \tilde{\alpha}(x_m)}{v_0^2} h^2 ,$$

(4.5b)

with

$$\sin\tilde{\alpha}(x_m) = \frac{x_m - x_0 + R_N \sin\alpha}{R_N A(x_m)},$$

$$\tilde{t}_0(x_m) = \frac{2}{v_0} R_N [A(x_m) - 1] + t_0,$$

$$\tilde{R}_{NIP}(x_m) = R_N [A(x_m) - 1] + R_{NIP},$$

$$A(x_m) = \sqrt{\frac{(x_m - x_0)^2}{R_N^2} + 2\frac{(x_m - x_0)\sin\alpha}{R_N} + 1}.$$

4.4   Summary

Using a surface to approximate the traveltimes of the reflection events, the best choice from the presented Taylor expansions is to use the hyperbolic approximation (second-order expansion of t^2) in order to satisfy accuracy and practical requirements. This formula is used be the CRS method (Mann et al., 1999). Useful alternatives are given by eqs. (4.5) which include the original hyperbola of the parametric CRS surface in the ZO section.

The parameters can also be determined by means of the traveltime curves in the CMP gather and in the ZO section. Here, the CRS method is based upon the hyperbolic approximation in the CMP gather (eq. (4.3)) and in the ZO section (eq. (4.4a)). An alternative is given by the delayed hyperbolae approach in the CMP gather (eq. (4.2b) restricted to the second-order; de Bazelaire (1988)) and in the ZO section (eq. (3.3); de Bazelaire and Thore (1987)).

Chapter 5

Conclusions

I showed that different model-independent moveout trajectories and surfaces can be obtained from
a particular parametric CRS surface which approximates the traveltime surface of a reflector seg-
ment in the multicoverage data set. The involved assumptions imply that the parametric CRS
surface coincides with the exact traveltime surface of a circular reflector segment in a constant
velocity medium. However, for inhomogeneous media a time delay is required. This time de-
lay accounts for the hypothetical NIP wave that can be interpreted together with the hypothetical
normal wave by means of geometrical optics. All moveout formulae represent different Taylor
expansions of the parametric CRS surface. In order to minimize the computational expense in
the implementation it helps to determine the attributes (α, R_{NIP}, R_N) in two steps. Such an ef-
ficient strategy is, for instance, given by the delayed-hyperbolae approach (de Bazelaire, 1986;
de Bazelaire and Thore, 1987) or by Mann et al. (1999). The data-derived attributes detected in
this manner can serve as initial values for an optimization procedure that uses moveout surfaces
(Mann et al., 1999). The three attributes assigned to an actual primary reflection located at (x_0, t_0)
in the simulated ZO section can be interpreted by means of geometrical optics. They finally allow
to perform a subsequent inversion (Majer, 2000; Hubral and Krey, 1980; Thore and de Bazelaire,
1989).

Appendix A

Common-reflection-point trajectory

My goal is to establish a relationship between the traveltimes of primary reflection events in different CO sections that stem from the same reflection point on the reflector. To do so, I assume a medium with the known constant velocity v_0. Let me consider the isochron of a shot/receiver pair defined by the half-offset h, the midpoint x_m, and the corresponding traveltime $t(x_m, h)$ (Figure A.1). As a result of Snell's law or Fermat's principle this isochron is an ellipse:

$$F(x, z; x_m, h) = \frac{(x - x_m)^2}{\left(\frac{1}{2}v_0 t\right)^2} + \frac{z^2}{\left(\frac{1}{2}v_0 t\right)^2 - h^2} - 1 = 0 \tag{A.1a}$$

$$\text{with} \quad t = t(x_m, h).$$

In the depth domain, either x or z can be used as variable to describe the ellipse. Using x_m and h as parameters eq. (A.1a) represents a family of ellipses. The envelope can already be determined from a subset of this family provided by a CO section (eq. (A.1a) with $h = $ const.). Then, the parameter is midpoint x_m and the envelope is defined by the condition

$$\frac{dF}{dx_m} = \frac{\partial F}{\partial x_m} + \frac{\partial F}{\partial t}\frac{\partial t}{\partial x_m} = 0. \tag{A.1b}$$

Solving eqs. (A.1) provides the envelope in the depth domain as a function of midpoint x_m:

$$x = x_m + \frac{1}{2h^2}\frac{t}{t'}\left[\left(\frac{v_0}{2}t\right)^2 - h^2\right]\left[1 - \sqrt{1 + 4h^2\left(\frac{t t'}{t^2 - \left(\frac{2}{v_0}h\right)^2}\right)^2}\right], \tag{A.2a}$$

$$z = \sqrt{\left[\left(\frac{v_0}{2}t\right)^2 - h^2\right]\left[1 - \frac{(x - x_m)^2}{\left(\frac{1}{2}v_0 t\right)^2}\right]}, \tag{A.2b}$$

$$\text{with} \quad t = t(x_m, h)$$

$$\text{and} \quad t' = \frac{\partial t(x_m, h)}{\partial x_m}.$$

29

Actually, the envelope is the searched-for reflector since both have to be tangent to at least one of the ellipses in each point. Now, let me choose the traveltime $\hat{t} = t(\hat{x}_m, \hat{h})$ of an event in a CO section specified by the half-offset $\hat{h}$ (Figure A.1). Furthermore, I assume to know the slope $\hat{t}' = \frac{\partial t}{\partial x_m}\big|_{x_m = \hat{x}_m, h = \hat{h}}$ of the associated CO traveltime curve at $\hat{t}$. The associated reflection point $R = (\hat{x}, \hat{z})$ is then given by eqs. (A.2), i.e. $\hat{x} = x(\hat{x}_m, \hat{h}, \hat{t})$ and $\hat{z} = z(\hat{x}_m, \hat{h}, \hat{t})$. Now, one can compute the intersections of the tangent and the normal of the reflector at R with the x-axis at $z = 0$, denoted with x_T and x_0, respectively (Figure A.1). This is done by means of the associated ellipse, which is tangent to the reflector at R. The distance between these intersections is given by

$$2\,r_T = x_0 - x_T = \frac{\hat{t}^2 - \left(\frac{2}{v_0}\hat{h}\right)^2}{\hat{t}\,\hat{t}'} \tag{A.3a}$$

and has to be constant for all traveltime events associated with R since the normal and the tangent are constant quantities of the reflector at R. Therefore, r_T turns out to be (similar to the reflector dip at R) a "characteristic quantity" of point R. All reflection events that stem from the same reflection point on the reflector $R = (\hat{x}, \hat{z})$ have to satisfy eqs. (A.2) for $x = \hat{x}$ and $z = \hat{z}$. The normal of the ellipse at R determines the searched-for normal incident ZO ray. Computing its intersection with the measurement surface I obtain the location $(x_0, 0)$ of the coincident shot-receiver pair for the corresponding ZO experiment:

$$x_0 = \hat{x}_m - r_T\left(\sqrt{\frac{\hat{h}^2}{r_T^2} + 1} - 1\right). \tag{A.3b}$$

The length of the normal between R and $(x_0, 0)$ equals $v_0 t_0/2$, where t_0 denotes the associated ZO reflection time:

$$t_0^2 = 2\frac{\hat{t}^2 - \left(\frac{2}{v_0}\hat{h}\right)^2}{\left(\sqrt{\left(\frac{\hat{h}}{r_T}\right)^2 + 1} + 1\right)}. \tag{A.3c}$$

With these equations I establish the following general relationship between point $(\hat{x}_m, \hat{h}, \hat{t})$ and the locations of the reflection events in other CO sections that pertain to R:

$$x_m(h) - r_T\sqrt{\left(\frac{h}{r_T}\right)^2 + 1} = \hat{x}_m - r_T\sqrt{\left(\frac{\hat{h}}{r_T}\right)^2 + 1}, \tag{A.3d}$$

$$\frac{t(h)^2 - \left(\frac{2h}{v_0}\right)^2}{1 + \sqrt{\left(\frac{h}{r_T}\right)^2 + 1}} = \frac{\hat{t}^2 - \left(\frac{2\hat{h}}{v_0}\right)^2}{1 + \sqrt{\left(\frac{\hat{h}}{r_T}\right)^2 + 1}}. \tag{A.3e}$$

Here, r_T can be determined by the known reflection event and the dip of the corresponding CO reflection time curve at this reflection event (eq. (A.3a)). Choosing the ZO section by setting the

initial values to $\hat{x}_m = x_0$, $\hat{h} = 0$ and $\hat{t} = t_0$ provides

$$x_m(h) = x_0 + r_T \left(\sqrt{\frac{h^2}{r_T^2} + 1} - 1 \right) , \tag{A.4a}$$

$$t^2(h) = 4\frac{h^2}{v_0^2} + \frac{1}{2}t_0^2 \left(\sqrt{\frac{h^2}{r_T^2} + 1} + 1 \right) , \tag{A.4b}$$

with $\quad 2r_T = \dfrac{t_0}{t_0'}. \tag{A.4c}$

By either using the well known relationship of the ray parameter p to the respective ZO traveltime $p = t_0'/2 = \sin\alpha/v_0$ or evaluating the distance $2r_T$ by means of the dip of the reflector, eq. (A.4c) becomes

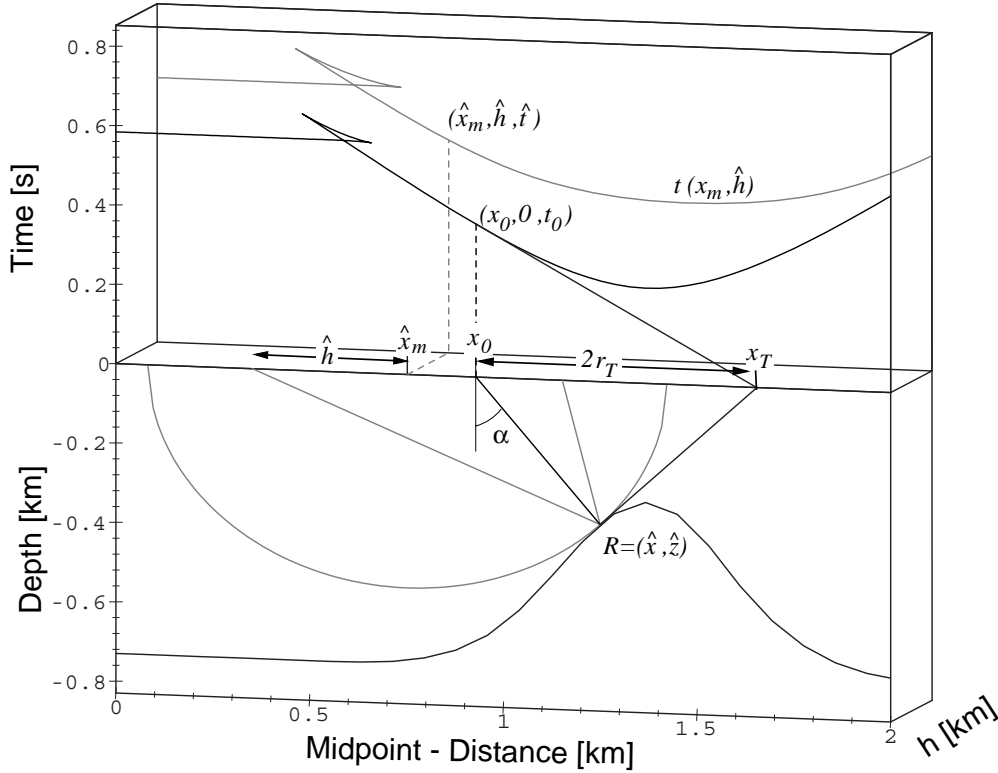$$2r_T = \frac{v_0}{2}\frac{t_0}{\sin\alpha}. \tag{A.4d}$$

Figure A.1: Constant velocity model and two CO traveltime curves in the (x_m, h, t)-space: the isochron of point $(\hat{x}_m, \hat{h}, \hat{t})$ is the dark gray ellipse that is tangent to the reflector at point R. The isochron of point $(x_0, 0, t_0)$ is a circle (not plotted) that is also tangent to the reflector at point R.

Appendix B

Zero-offset hyperbola

To determine the traveltimes $\tilde{t}_0(\tilde{x}_0)$ of a reflector segment in the ZO section I assume a circular normal wavefront emerging at time t_0 at x_0 on the surface. By means of the image point $S_N^* = (x_c, z_c)$ one can easily calculate $\tilde{t}_0$ with respect to $\tilde{x}_0$ (Figure B.1):

$$
\begin{aligned}
\left[\frac{v_0}{2}\Delta t + R_N\right]^2 = \left[\frac{v_0}{2}\left(\tilde{t}_0 - t_0\right) + R_N\right]^2 &= \left(\tilde{x}_0 - x_c\right)^2 + z_c^2 \\
&= \left(\tilde{x}_0 - x_0 + x_0 - x_c\right)^2 + z_c^2 \\
&= \left(\tilde{x}_0 - x_0 + R_N \sin \alpha\right)^2 + \left(R_N \cos \alpha\right)^2 \\
&= \left(\tilde{x}_0 - x_0\right)^2 + 2 R_N \left(\tilde{x}_0 - x_0\right) \sin \alpha + R_N^2 .
\end{aligned}
\tag{B.1}
$$

Equation (B.1) provides an explicit formula for the ZO traveltimes. The derivative of $\tilde{t}_0$ with respect to $\tilde{x}_0$ determines the emergence angle of a ZO ray emerging at $\tilde{x}_0$:

$$
\sin \tilde{\alpha}(\tilde{x}_0) = \frac{v_0}{2}\frac{d\tilde{t}_0}{d\tilde{x}_0} = \frac{\tilde{x}_0 - x_0 + R_N \sin \alpha}{R_N \sqrt{\frac{\left(\tilde{x}_0 - x_0\right)^2}{R_N^2} + 2\frac{\left(\tilde{x}_0 - x_0\right) \sin \alpha}{R_N} + 1}} .
\tag{B.2}
$$

Considering circular wavefronts, it is more suitable to use the emergence angle $\tilde{\alpha}$ of a ZO ray instead of $\tilde{x}_0$ as variable. In this respect one has to determine $\tilde{x}_0(\tilde{\alpha})$ and $\tilde{t}_0(\tilde{\alpha})$ instead of $\tilde{t}_0(\tilde{x}_0)$ and $\tilde{\alpha}(\tilde{x}_0)$.

To determine $\tilde{x}_0(\tilde{\alpha})$ I use the following relationships (Figure B.1):

$$
x_c = x_0 - R_N \sin \alpha, \qquad z_c = R_N \cos \alpha,
\tag{B.3a}
$$

$$
\tan \tilde{\alpha} = \frac{\tilde{x}_0 - x_c}{z_c} .
\tag{B.3b}
$$

Solving equation (B.3b) for $\tilde{x}_0$ and inserting the values of x_c and z_c provided by eqs. (B.3a) yields

$$
\tilde{x}_0(\tilde{\alpha}) = x_0 + R_N \left(\cos \alpha \tan \tilde{\alpha} - \sin \alpha\right) .
\tag{B.4}
$$

Figure B.1: Circular normal wavefront and its corresponding image point $S_N^* = (x_c, z_c)$.

To determine $\tilde{t}_0(\tilde{\alpha})$ I use (Figure B.1):

$$\tilde{R}_N \cos\tilde{\alpha} = R_N \cos\alpha \quad \Rightarrow \quad \tilde{R}_N = R_N \frac{\cos\alpha}{\cos\tilde{\alpha}}, \tag{B.5a}$$

$$\frac{v_0}{2}\Delta t = \frac{v_0}{2}\left(\tilde{t}_0 - t_0\right) = \tilde{R}_N - R_N. \tag{B.5b}$$

Using these equations $\tilde{t}_0(\tilde{\alpha})$ evaluates to

$$\tilde{t}_0(\tilde{\alpha}) = \frac{2}{v_0}R_N\left(\frac{\cos\alpha}{\cos\tilde{\alpha}} - 1\right) + t_0. \tag{B.6}$$

Appendix C

Special cases of the CRS surface

In this section, I display two cases for two particular values of R_N that the parametric CRS surface (eqs. (3.6)) can acount for but none of its Taylor expansions. In Figures C.1 and C.2 the CRS surface is plotted in gray; the CRP trajectory for $x_0 = 0\,\text{km}$, $t_0 = 1\,\text{s}$, $\alpha = 13°$ and $R_{NIP} = 1\,\text{km}$ is shown in black. Observe the restricted range in the x_m-h plane, where the description of the CRS surface is valid in these cases.

- In the first case $R_N = 0$ (Figure C.1) a Taylor expansion is not valid due to the non-existence of the derivative $\partial t / \partial x_m$ in the ZO section. In this case the parametric CRS formula (eqs. (3.6)) reduces to the explicit formula

$$\left[t\left(x_m, h\right) - \left(t_0 - \frac{2}{v_0} R_{NIP} \right) \right]^2 = 4 \frac{h^2}{v_0^2} + \frac{2}{v_0^2} R_{NIP}^2 \left[\frac{h^2 + \left(x_m - x_0\right)^2}{h^2 - \left(x_m - x_0\right)^2} + 1 \right] \quad \text{with} \quad \left| x_m - x_0 \right| < \left| h \right|.$$

(C.1)
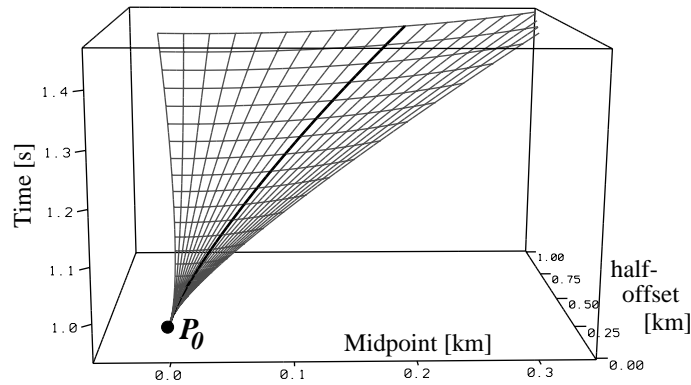
Figure C.1: The case of a normal wave focusing at x_0 on the measurement surface ($R_N = 0$).

- The second case $R_N < 0$ (Figure C.2) can provide triplications of the CRS surface in the considered range. The larger the value of $|R_N|$ the further the triplications are apart from the ZO section. Such triplications cannot be handled by the explicit Taylor expansions. However, they remain valid in the vicinity of P_0.
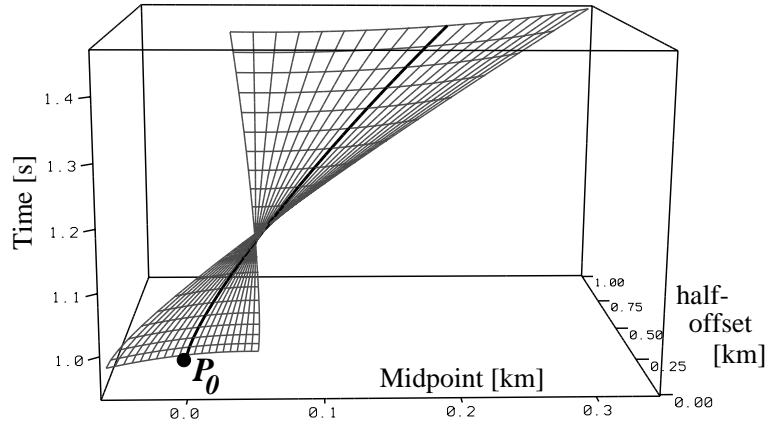

Figure C.2: The case of a normal wave focusing slightly above the measurement surface ($R_N = -0.2\,\text{km}$).

Part II

The 3D case

Chapter 4

Introduction

In the previous part, I derived various formulae that serve to simulate a ZO section along the seismic line of a 2D acquisition. I will now extend this theory to 3D acquisitions where the ZO section becomes a volume. In practice the CRS procedure for 2D acquisitions uses the hyperbolic formulae and, therefore, I restrict myself to the generalization of the latter. Additionally, the parabolic equation for 3D acquisition is obtained.

The lower half of Figure 4.1 shows two emerging hypothetical wavefronts seen from above the measurement surface. Figure 4.2 illustrates the same scene viewed from below the measurement surface. In these Figures the red and the green wavefronts indicate the NIP and normal wavefront, respectively. The upper half of Figure 4.1 illustrates the ZO traveltimes. The two hypothetical wavefronts are associated with a point $P_0=(x_0,y_0,t_0)$ in the ZO section by the observation point $X_0=(x_0,y_0,0)$ and the corresponding ZO traveltime t_0. The associated central ray (blue curve in Figure 4.2) defines the propagation direction of the wavefronts from a normal-incident point in the subsurface to the observation point X_0. The ZO traveltime t_0 is, as in the 2D case, twice the traveltime of the hypothetical wavefronts along the central (ZO) ray. The central ray is assumed to be normal to the wavefronts. As in the 2D case, one can approximate the true reflection traveltimes in the vicinity of P_0 by means of a second-order approximation of the hypothetical wavefronts. Note that Figures 4.1 and 4.2 are the three-dimensional counterparts to the two-dimensional Figures 2.1 and 2.2 with the difference that Figure 4.1 does not illustrate the whole multicoverage data set but only the ZO volume. As mentioned in the introduction at the beginning of this thesis, the multicoverage data set for a 3D acquisition is five-dimensional.

The hypothetical experiments that form the basics of the CRS theory are the same for 2D and 3D media. A description for 3D media can be found in Hubral (1983). The justification why these hypothetical wavefronts can be used for the traveltime approximation is the same than in the 2D case and has been explained in part I. In addition, I will show that the 2D CRS method even accounts for 3D media. Therefore, the extension to the 3D case concerns mainly the description of the wavefronts. However, the relationships between points on the measurement surface in the vicinity of X_0 and the emerging wavefronts, in order to determine paraxial traveltimes, becomes more complex. A suitable representation of the wavefronts in 3D requires the introduction of a

ray-centered coordinate system. Important in this respect are the transformations between different coordinate systems and their properties.

This part covers the following topics:

- **coordinate transformation** (section 5.2):
  explains fundamental properties of coordinate transformation for the general case and for the considered case.

- **description of a wavefront** (section 5.3):
  a suited description for the wavefront is its representation by a 2×2 curvature matrix in a ray-centered coordinate system.

- **coordinate systems for traveltime formulae** (chapter 6):
  explains two ray-centered coordinate systems in which the curvature matrices of the NIP and normal wavefronts can be expressed. Unlike in forward modeling (chapter 10), here, a ray-centered system is defined by means of two parameters (the polar and the azimuth angle) of the traveltime formulae. I also define a local observation system and determine the transformation from the latter to a ray-centered system.

- **relationships of the 2D and the 3D case** (chapter 7):
  the fundamental relationships between parameters (wavefront attributes) of the 2D and the 3D case are derived. These relationships form the basics to determine the attributes in subsequent steps and can also be used to derive second-order approximations of the traveltime.

- **traveltime formulae** (chapter 8):
  I derive the second-order approximations for 3D acquisitions by means of the second-order approximations for 2D media and the relationships established in chapter 7. A more stringent derivation by means of Hamilton's equation is given in appendix G.

- **determination of wavefront parameters** (chapter 9):
  the CRS procedure determines, in general, combinations of the parameters. This chapter describes how to obtain the searched-for attributes of the wavefronts by means of such combined parameters. I also show that the CRS stack for 2D acquisition can serve to obtain the searched-for parameters. Note that this chapter does not focus on search strategies but how the obtained parameters are related to the searched-for wavefront attributes.

- **wavefront curvatures in layered media** (chapter 10):
  the wavefront curvatures along a ray in a medium with iso-velocity layers can be computed by means of analytic formulae (Hubral and Krey, 1980). The interfaces have to be continuous up to the second order. I explain the involved coordinate systems and how to obtain the transformations and curvature matrices in the respective systems. Although I used this procedure for forward modeling, it would also be required for an inversion that provides a velocity model.

- **model-derived traveltime comparisons** (chapter 11):
  the second-order approximations of the traveltime determined by forward calculated wavefront attributes are compared to the traveltimes computed by ray-tracing.
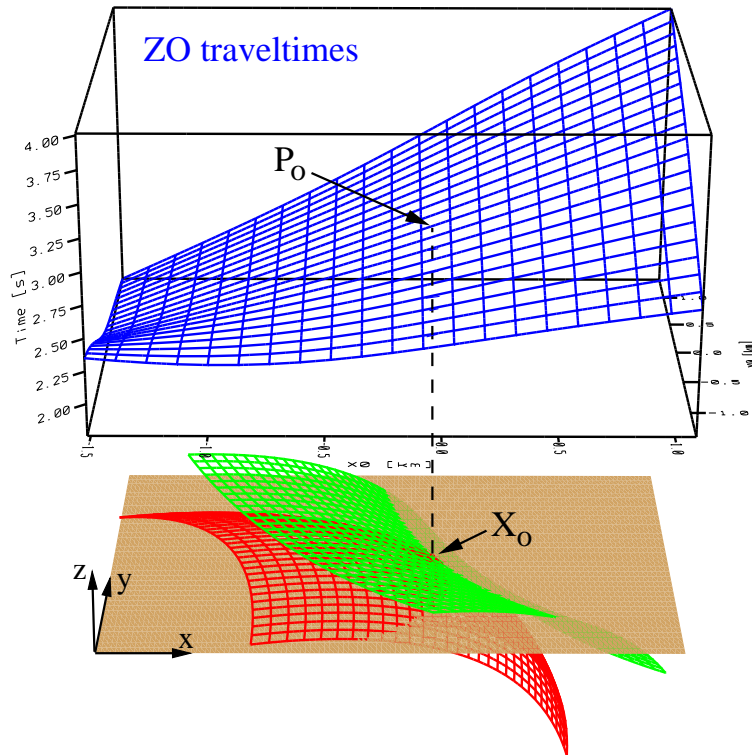
Figure 4.1: lower part: NIP wavefront (red surface) and normal wavefront (green surface) emerging at X_0 on the measurement surface (brown plane). Upper Part: ZO traveltimes (blue surface) in a distance-distance-time volume. Point P_0 indicates the ZO traveltime that would be observed at X_0 on the measurement surface.
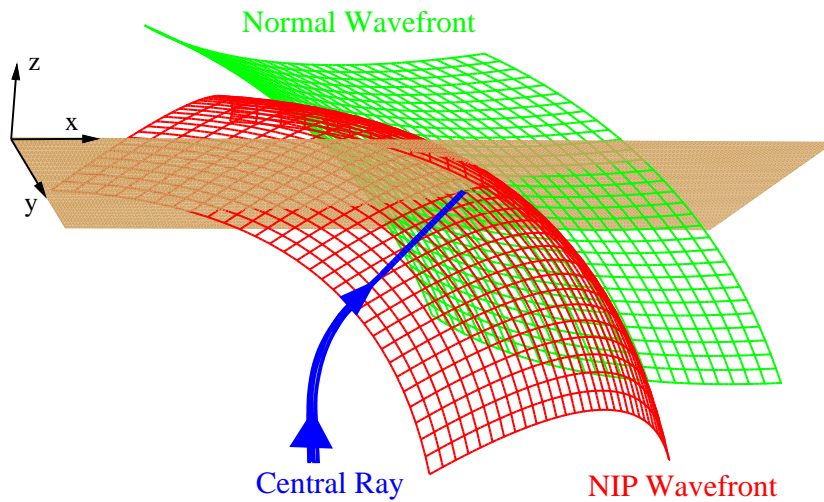
Figure 4.2: same scene as in the upper Figure viewed from below the measurement surface. The central ray (blue curve) emerges at X_0 on the surface.

41

4.1   Notation

Vectors and matrices

Vectors and matrices are denoted bold, vectors are written in lowercase, and matrices with capital letters. 3D vectors and matrices are underlined. Examples for letter *a*:

	Symbol	Element
2D vector	$\mathbf{a}$	$a_i\ (i = 0, 1)$
3D vector	$\underline{\mathbf{a}}$	$a_i\ (i = 0, 1, 2)$

	Symbol	Element
2×2 matrix	$\mathbf{A}$	$a_{ij}\ (i, j = 0, 1)$
3×3 matrix	$\underline{\mathbf{A}}$	$a_{ij}\ (i, j = 0, 1, 2)$

Vector operations

Operator	meaning
·	inner product
×	cross product
$\mathbf{a}^{\mathrm{T}}$	transpose of $\mathbf{a}$

Matrix operations

Operation	meaning
$\mathbf{A}^{\mathrm{T}}$	transpose of $\mathbf{A}$
$\mathbf{A}^{-1}$	inverse of $\mathbf{A}$

Special vectors and matrices are

$$\underline{\mathbf{e}}_{\mathbf{x}} = \begin{pmatrix} 1 \\ 0 \\ 0 \end{pmatrix}, \quad \underline{\mathbf{e}}_{\mathbf{y}} = \begin{pmatrix} 0 \\ 1 \\ 0 \end{pmatrix}, \quad \underline{\mathbf{e}}_{\mathbf{z}} = \begin{pmatrix} 0 \\ 0 \\ 1 \end{pmatrix} \quad \text{and} \quad \underline{\mathbf{I}} = \begin{pmatrix} \underline{\mathbf{e}}_{\mathbf{x}} & \underline{\mathbf{e}}_{\mathbf{y}} & \underline{\mathbf{e}}_{\mathbf{z}} \end{pmatrix} . \tag{4.1}$$

Coordinate systems

	axes	variable, vector, matrix that refer to the system
Local system	$[\underline{\mathbf{e}}_{\mathbf{x}}, \underline{\mathbf{e}}_{\mathbf{y}}, \underline{\mathbf{e}}_{\mathbf{z}}]$	$x, \underline{\mathbf{x}}, \underline{\mathbf{A}}$
Ray-centered system	$[\underline{\mathbf{w}}_{\mathbf{x}}, \underline{\mathbf{w}}_{\mathbf{y}}, \underline{\mathbf{w}}_{\mathbf{z}}]$	$\hat{x}, \underline{\hat{\mathbf{x}}}, \underline{\hat{\mathbf{A}}}$
Interface system	$[\underline{\mathbf{q}}_{\mathbf{x}}, \underline{\mathbf{q}}_{\mathbf{y}}, \underline{\mathbf{q}}_{\mathbf{z}}]$	$\tilde{x}, \underline{\tilde{\mathbf{x}}}, \underline{\tilde{\mathbf{A}}}$

However, angles, curvatures and radii of curvature are not labeled with respect to a system.

Transformations

If not indicated differently, the transformation from a system X to a system Y is denoted by $\underline{\mathbf{T}}_{\mathbf{XY}}$

Chapter 5

Basics

5.1 Rotation matrices

Often required are the rotation matrices around the *z*- and the *y*-axis

$$\underline{\mathbf{D}}_{\mathbf{z}}(\varphi) = \begin{pmatrix} \cos\varphi & -\sin\varphi & 0 \\ \sin\varphi & \cos\varphi & 0 \\ 0 & 0 & 1 \end{pmatrix} \quad \text{and} \quad \underline{\mathbf{D}}_{\mathbf{y}}(\varphi) = \begin{pmatrix} \cos\varphi & 0 & \sin\varphi \\ 0 & 1 & 0 \\ -\sin\varphi & 0 & \cos\varphi \end{pmatrix} \tag{5.1}$$

as well as its upper left 2×2 submatrices

$$\mathbf{D}_{\mathbf{z}}(\varphi) = \begin{pmatrix} \cos\varphi & -\sin\varphi \\ \sin\varphi & \cos\varphi \end{pmatrix} \quad \text{and} \quad \mathbf{D}_{\mathbf{y}}(\varphi) = \begin{pmatrix} \cos\varphi & 0 \\ 0 & 1 \end{pmatrix}. \tag{5.2}$$

Note also that the combinations

$$\underline{\mathbf{D}}_{\mathbf{z}}(\varphi_0)\,\underline{\mathbf{D}}_{\mathbf{y}}(\varphi_1) \quad \text{and} \quad \underline{\mathbf{D}}_{\mathbf{z}}(\varphi_0)\,\underline{\mathbf{D}}_{\mathbf{y}}(\varphi_1)\,\underline{\mathbf{D}}_{\mathbf{z}}(\varphi_2) \tag{5.3}$$

have the upper left 2×2 submatrices

$$\mathbf{D}_{\mathbf{z}}(\varphi_0)\,\mathbf{D}_{\mathbf{y}}(\varphi_1) \quad \text{and} \quad \mathbf{D}_{\mathbf{z}}(\varphi_0)\,\mathbf{D}_{\mathbf{y}}(\varphi_1)\,\mathbf{D}_{\mathbf{z}}(\varphi_2), \tag{5.4}$$

which can be easily verified by comparing the elements of these matrices.

5.2 Properties of coordinate transformations

Because I read some articles that improperly handle the behavior of vectors and matrices upon transformation, let me point out this topic. I start with the general case and simplify the obtained formulae to the considered case, which (with one exception in chapter 10) are used throughout this part. The reader may however skip the general case.

43

5.2.1 General case

Let me consider two coordinate systems in the 3D space that systems are represented in the global system:

- the X-system $[\underline{\mathbf{x}}_x, \underline{\mathbf{x}}_y, \underline{\mathbf{x}}_z]$ with the base matrix $\underline{\mathbf{X}} = (\underline{\mathbf{x}}_x\, \underline{\mathbf{x}}_y\, \underline{\mathbf{x}}_z)$ and

- the Y-system $[\underline{\mathbf{y}}_x, \underline{\mathbf{y}}_y, \underline{\mathbf{y}}_z]$ with the base matrix $\underline{\mathbf{Y}} = (\underline{\mathbf{y}}_x\, \underline{\mathbf{y}}_y\, \underline{\mathbf{y}}_z)$.

A vector or matrix is denoted by

- $\underline{\mathbf{a}}$ or $\underline{\mathbf{A}}$ if expressed in the global system,

- $\bar{\underline{\mathbf{a}}}$ or $\bar{\underline{\mathbf{A}}}$ if expressed in the X-system,

- $\hat{\underline{\mathbf{a}}}$ or $\hat{\underline{\mathbf{A}}}$ if expressed in the Y-system,

except for the vectors $\underline{\mathbf{e}}_i$ (i=x,y,z) that are defined by eqs. (4.1).

The transformations $\underline{\mathbf{T}}_{XY}$ and $\bar{\underline{\mathbf{T}}}_{XY}$ from the X- to the Y-system are given by:

$$\underline{\mathbf{y}}_i = \underline{\mathbf{T}}_{XY}\, \underline{\mathbf{x}}_i \quad \text{in the global system,} \tag{5.5a}$$

$$\bar{\underline{\mathbf{y}}}_i = \bar{\underline{\mathbf{T}}}_{XY}\, \bar{\underline{\mathbf{x}}}_i \quad \Rightarrow \quad \bar{\underline{\mathbf{y}}}_i = \bar{\underline{\mathbf{T}}}_{XY}\, \underline{\mathbf{e}}_i \quad \text{in the X-system,} \tag{5.5b}$$

where i=x,y,z. It should be clear that $\bar{\underline{\mathbf{x}}}_i = \underline{\mathbf{e}}_i$ since these are the bases of the X-system expressed in the X-system.

The transformations $\underline{\mathbf{T}}_{YX}$ and $\hat{\underline{\mathbf{T}}}_{YX}$ from the Y- to the X-system are given by:

$$\underline{\mathbf{x}}_i = \underline{\mathbf{T}}_{YX}\, \underline{\mathbf{y}}_i \quad \text{in the global system,} \tag{5.5c}$$

$$\hat{\underline{\mathbf{x}}}_i = \hat{\underline{\mathbf{T}}}_{YX}\, \hat{\underline{\mathbf{y}}}_i \quad \Rightarrow \quad \hat{\underline{\mathbf{x}}}_i = \hat{\underline{\mathbf{T}}}_{YX}\, \underline{\mathbf{e}}_i \quad \text{in the Y-system,} \tag{5.5d}$$

where again i=x,y,z. The bases of the Y-system represented in the Y-system yield $\hat{\underline{\mathbf{y}}}_i = \underline{\mathbf{e}}_i$. Note that eqs. (5.5) cannot be used for translations and therefore account for direction vectors[1]. This should be clear since the bases of the coordinate systems defines only the orientation of the system. A translation can always be easily considered separately.

Transformation matrices

Let me first analyze these transformation matrices. Therefore, consider the bases represented in the different systems:

$$\underline{\mathbf{x}}_i = \underline{\mathbf{X}}\, \underline{\mathbf{e}}_i = \underline{\mathbf{Y}}\, \hat{\underline{\mathbf{x}}}_i \tag{5.6a}$$

$$\underline{\mathbf{y}}_i = \underline{\mathbf{X}}\, \bar{\underline{\mathbf{y}}}_i = \underline{\mathbf{Y}}\, \underline{\mathbf{e}}_i \tag{5.6b}$$

---

[1] A trick to apply a translation in 3D by a matrix is to use 4×4 matrices and 4D vectors. However, this may remove important properties of the transformation matrix and is not required in this work.

The different transformation matrices can be expressed by the base matrices:

$$\underline{\mathbf{y}}_i = \begin{cases} \underline{\mathbf{T}}_{XY}\underline{\mathbf{x}}_i = \underline{\mathbf{T}}_{XY}\underline{\mathbf{X}}\underline{\mathbf{e}}_i & \text{(eqs. (5.5a) and (5.6a))} \\ \underline{\mathbf{Y}}\underline{\mathbf{e}}_i & \text{(eq. (5.6b))} \end{cases} \quad \Rightarrow \quad \underline{\mathbf{T}}_{XY} = \underline{\mathbf{Y}}\underline{\mathbf{X}}^{-1}, \quad (5.7)$$

$$\underline{\bar{\mathbf{y}}}_i = \begin{cases} \underline{\bar{\mathbf{T}}}_{XY}\underline{\mathbf{e}}_i & \text{(eq. (5.5b))} \\ \underline{\mathbf{X}}^{-1}\underline{\mathbf{Y}}\underline{\mathbf{e}}_i & \text{(eq. (5.6b))} \end{cases} \quad \Rightarrow \quad \underline{\bar{\mathbf{T}}}_{XY} = \underline{\mathbf{X}}^{-1}\underline{\mathbf{Y}}, \quad (5.8)$$

$$\underline{\mathbf{x}}_i = \begin{cases} \underline{\mathbf{T}}_{YX}\underline{\mathbf{y}}_i = \underline{\mathbf{T}}_{XY}\underline{\mathbf{Y}}\underline{\mathbf{e}}_i & \text{(eqs. (5.5c) and (5.6b))} \\ \underline{\mathbf{X}}\underline{\mathbf{e}}_i & \text{(eq. (5.6a))} \end{cases} \quad \Rightarrow \quad \underline{\mathbf{T}}_{YX} = \underline{\mathbf{X}}\underline{\mathbf{Y}}^{-1}, \quad (5.9)$$

$$\underline{\hat{\mathbf{x}}}_i = \begin{cases} \underline{\hat{\mathbf{T}}}_{YX}\underline{\mathbf{e}}_i & \text{(eq. (5.5d))} \\ \underline{\mathbf{Y}}^{-1}\underline{\mathbf{X}}\underline{\mathbf{e}}_i & \text{(eq. (5.6a))} \end{cases} \quad \Rightarrow \quad \underline{\hat{\mathbf{T}}}_{YX} = \underline{\mathbf{Y}}^{-1}\underline{\mathbf{X}}. \quad (5.10)$$

Observe that $\underline{\mathbf{T}}_{YX} = \underline{\mathbf{T}}_{XY}^{-1}$ and $\underline{\hat{\mathbf{T}}}_{YX} = \underline{\bar{\mathbf{T}}}_{XY}^{-1}$ as expected, but in general $\underline{\mathbf{T}}_{XY} \neq \underline{\bar{\mathbf{T}}}_{XY}$ and $\underline{\mathbf{T}}_{YX} \neq \underline{\hat{\mathbf{T}}}_{YX}$.

Now let me focus on the transformations $\underline{\bar{\mathbf{T}}}_{XY}$ and $\underline{\hat{\mathbf{T}}}_{YX}$. By means of the base matrices expressed in the X- and Y-systems:

$$\underline{\bar{\mathbf{X}}} = \underline{\mathbf{I}}, \quad \underline{\bar{\mathbf{Y}}} = (\underline{\bar{\mathbf{y}}}_x \; \underline{\bar{\mathbf{y}}}_y \; \underline{\bar{\mathbf{y}}}_z) \quad \text{and} \quad \underline{\hat{\mathbf{X}}} = (\underline{\hat{\mathbf{x}}}_x \; \underline{\hat{\mathbf{x}}}_y \; \underline{\hat{\mathbf{x}}}_z), \quad \underline{\hat{\mathbf{Y}}} = \underline{\mathbf{I}}.$$

one obtains:

$$\underline{\bar{\mathbf{y}}}_i = \begin{cases} \underline{\bar{\mathbf{T}}}_{XY}\underline{\bar{\mathbf{e}}}_i \\ \underline{\bar{\mathbf{Y}}}\underline{\bar{\mathbf{e}}}_i \end{cases} \quad \Rightarrow \quad \underline{\bar{\mathbf{T}}}_{XY} = \underline{\bar{\mathbf{Y}}}, \qquad \underline{\hat{\mathbf{x}}}_i = \begin{cases} \underline{\hat{\mathbf{T}}}_{YX}\underline{\hat{\mathbf{e}}}_i \\ \underline{\hat{\mathbf{X}}}\underline{\hat{\mathbf{e}}}_i \end{cases} \quad \Rightarrow \quad \underline{\hat{\mathbf{T}}}_{YX} = \underline{\hat{\mathbf{X}}}.$$

From $\underline{\hat{\mathbf{T}}}_{YX} = \underline{\bar{\mathbf{T}}}_{XY}^{-1}$ follows that $\underline{\hat{\mathbf{X}}}^{-1} = \underline{\bar{\mathbf{Y}}}$. To summarize, the transformations $\underline{\bar{\mathbf{T}}}_{XY}$ and $\underline{\hat{\mathbf{T}}}_{YX}$ can be determined from the base matrices expressed in the different systems as follows:

$$\boxed{\underline{\bar{\mathbf{T}}}_{XY} = \underline{\mathbf{X}}^{-1}\underline{\mathbf{Y}} = \underline{\bar{\mathbf{Y}}} = \underline{\hat{\mathbf{X}}}^{-1}},$$

$$\underline{\hat{\mathbf{T}}}_{YX} = \underline{\bar{\mathbf{T}}}_{XY}^{-1} = \underline{\mathbf{Y}}^{-1}\underline{\mathbf{X}} = \underline{\bar{\mathbf{Y}}}^{-1} = \underline{\hat{\mathbf{X}}}.$$

Transformations of vectors and matrices

Now let us assume the X-system to be the "current" system. The aim is to represent quantities (vectors or matrices) in the "new" Y-system. In general it is stated that

$$\underline{\bar{\mathbf{y}}} = \underline{\bar{\mathbf{T}}}_{XY}\underline{\bar{\mathbf{x}}} \quad (5.11)$$

transforms the vector $\underline{\bar{\mathbf{x}}}$ to the Y-system. A common mistake is that these equations are used to express a vector $\underline{\bar{\mathbf{x}}}$ (represented in the X-system) in the Y-system. However, as I will show a vector $\underline{\bar{\mathbf{x}}}$ that refers to the X-system is represented by $\underline{\bar{\mathbf{T}}}_{XY}^{-1}\underline{\bar{\mathbf{x}}}$ in the Y-system. One should be aware that eq. (5.11) expresses both vectors in the X-system.

Therefore, consider the representation of an arbitrary vector $\underline{\mathbf{x}}$ in the X- and in the Y-system:

$$\underline{\mathbf{x}} = \underline{\mathbf{X}}\,\bar{\underline{\mathbf{x}}} = \underline{\mathbf{Y}}\,\hat{\underline{\mathbf{x}}}. \tag{5.12}$$

This yields

$$\bar{\underline{\mathbf{x}}} = \underline{\mathbf{X}}^{-1}\underline{\mathbf{Y}}\,\hat{\underline{\mathbf{x}}}, \tag{5.13}$$

and with eq. (5.8) the fundamental relationships

$$\boxed{\hat{\underline{\mathbf{x}}} = \bar{\underline{\mathbf{T}}}_{\mathbf{XY}}^{-1}\,\bar{\underline{\mathbf{x}}}}, \tag{5.14}$$

$$\boxed{\bar{\underline{\mathbf{x}}} = \bar{\underline{\mathbf{T}}}_{\mathbf{XY}}\,\hat{\underline{\mathbf{x}}}}. \tag{5.15}$$

To transform a matrix $\bar{\underline{\mathbf{A}}}$ from the X- to the Y-system observe its application in the X-system:

$$\bar{\underline{\mathbf{y}}} = \bar{\underline{\mathbf{A}}}\,\bar{\underline{\mathbf{x}}}. \tag{5.16}$$

With eq. (5.15) this yields

$$\bar{\underline{\mathbf{T}}}_{\mathbf{XY}}\,\hat{\underline{\mathbf{y}}} = \bar{\underline{\mathbf{A}}}\,\bar{\underline{\mathbf{T}}}_{\mathbf{XY}}\,\hat{\underline{\mathbf{x}}}, \tag{5.17}$$

and, therefore:

$$\boxed{\hat{\underline{\mathbf{A}}} = \bar{\underline{\mathbf{T}}}_{\mathbf{XY}}^{-1}\,\bar{\underline{\mathbf{A}}}\,\bar{\underline{\mathbf{T}}}_{\mathbf{XY}}}, \tag{5.18}$$

$$\boxed{\bar{\underline{\mathbf{A}}} = \bar{\underline{\mathbf{T}}}_{\mathbf{XY}}\,\hat{\underline{\mathbf{A}}}\,\bar{\underline{\mathbf{T}}}_{\mathbf{XY}}^{-1}}. \tag{5.19}$$

Special case – Transformations between Cartesian coordinate systems

In a Cartesian coordinate system the base vectors are orthogonal, e. g. for the X system: $\underline{\mathbf{x}}_i \cdot \underline{\mathbf{x}}_j = 0$ (i,j=x,y,z $\wedge$ i$\neq$ j). In order to build an orthogonal transformation matrix from the base matrices, the base vectors have to be normalized:

$$\underline{\mathbf{X}} = \left(\frac{\underline{\mathbf{x}}_x}{\|\underline{\mathbf{x}}_x\|}, \frac{\underline{\mathbf{x}}_y}{\|\underline{\mathbf{x}}_y\|}, \frac{\underline{\mathbf{x}}_z}{\|\underline{\mathbf{x}}_z\|}, \right), \quad \underline{\mathbf{x}}_i \cdot \underline{\mathbf{x}}_j = 0 \ \ (\text{i,j=x,y,z} \wedge \text{i}\neq \text{j}) \quad \Rightarrow \quad \underline{\mathbf{X}}^{-1} = \underline{\mathbf{X}}^{\mathbf{T}} \tag{5.20}$$

$$\underline{\mathbf{Y}} = \left(\frac{\underline{\mathbf{y}}_x}{\|\underline{\mathbf{y}}_x\|}, \frac{\underline{\mathbf{y}}_y}{\|\underline{\mathbf{y}}_y\|}, \frac{\underline{\mathbf{y}}_z}{\|\underline{\mathbf{y}}_z\|}, \right), \quad \underline{\mathbf{y}}_i \cdot \underline{\mathbf{y}}_j = 0 \ \ (\text{i,j=x,y,z} \wedge \text{i}\neq \text{j}) \quad \Rightarrow \quad \underline{\mathbf{Y}}^{-1} = \underline{\mathbf{Y}}^{\mathbf{T}} \tag{5.21}$$

Further can the transformations $\underline{\mathbf{T}}_{\mathbf{XY}}$ between Cartesian coordinate systems be set up by combinations of the orthogonal rotation matrices defined in section 5.1. The transformation between right-handed orthogonal systems with unit base vectors imply that $\det \underline{\mathbf{T}}_{\mathbf{XY}} = +1$.

5.2.2 Considered case

I consider the transformation between Cartesian coordinate systems in the 3D space. One of the systems is a local system that is obtained by translating the global system. Therefore, it has the same orientation (base) than the global system. The translation can be easily considered by whether expressing global quantities in this local system or by applying it afterwards.

Let me denote the two coordinate systems between which the transformation occur by:

- the local system $[\underline{\mathbf{e}}_x, \underline{\mathbf{e}}_y, \underline{\mathbf{e}}_z]$ with the base matrix $\underline{\mathbf{I}} = (\underline{\mathbf{e}}_x\, \underline{\mathbf{e}}_y\, \underline{\mathbf{e}}_z)$ and

- the Y-system $[\underline{\mathbf{y}}_x, \underline{\mathbf{y}}_y, \underline{\mathbf{y}}_z]$ with the base matrix $\underline{\mathbf{Y}} = (\underline{\mathbf{y}}_x\, \underline{\mathbf{y}}_y\, \underline{\mathbf{y}}_z)$.

The bases of the Y-system fulfills the conditions:

- $\underline{\mathbf{y}}_i \cdot \underline{\mathbf{y}}_j = 0$ (i,j=x,y,z $\wedge$ i$\neq$ j) to be Cartesian, and,

- $\|\underline{\mathbf{y}}_i\| = 1$ to build an orthogonal transformation matrix.

A vector or matrix is denoted by

- $\underline{\mathbf{a}}$ or $\underline{\mathbf{A}}$ if expressed in the local system,

- $\underline{\hat{\mathbf{a}}}$ or $\underline{\hat{\mathbf{A}}}$ if expressed in the Y-system.

Let me give a quick summary of important properties established in section 5.2.1.[2] The transformation from the local to the Y-system is given by:

$$\underline{\mathbf{y}}_i = \underline{\mathbf{T}}_{IY}\, \underline{\mathbf{e}}_i \quad (i = \text{x,y,z}) \quad \text{where} \quad \underline{\mathbf{T}}_{IY}^{-1} = \underline{\mathbf{T}}_{IY}^{\mathrm{T}}. \tag{5.22}$$

- The transformation from the local to the Y-system is given by the base vectors of the Y-system, or the Y-system is given by the transformation:

$$\boxed{\underline{\mathbf{T}}_{IY} = \underline{\mathbf{Y}}} \tag{5.23}$$

- A vector $\underline{\mathbf{x}}$ of the local system is represented in the Y-system by

$$\boxed{\underline{\hat{\mathbf{x}}} = \underline{\mathbf{T}}_{IY}^{\mathrm{T}}\, \underline{\mathbf{x}}}. \tag{5.24}$$

- A vector $\underline{\hat{\mathbf{x}}}$ of the Y-system is represented in the local system by

$$\boxed{\underline{\mathbf{x}} = \underline{\mathbf{T}}_{IY}\, \underline{\hat{\mathbf{x}}}}. \tag{5.25}$$

---

[2]The reader who struggled through section 5.2.1 should notice that the X-system in that section coincides for the considered case with the global system (the local system here). The equations presented in section 5.2.1 considerably simplify for $\underline{\mathbf{X}} = \underline{\mathbf{I}}$, among other things, is $\underline{\bar{\mathbf{T}}}_{XY} = \underline{\mathbf{T}}_{XY}$.

- A matrix $\underline{\mathbf{A}}$ of the local system is represented in the Y-system by

$$\boxed{\hat{\underline{\mathbf{A}}} = \underline{\mathbf{T}}_{\mathbf{IY}}^{\mathbf{T}} \underline{\mathbf{A}} \, \underline{\mathbf{T}}_{\mathbf{IY}}} \, . \tag{5.26}$$

- A matrix $\hat{\underline{\mathbf{A}}}$ of the Y-system is represented in the local system by

$$\boxed{\underline{\mathbf{A}} = \underline{\mathbf{T}}_{\mathbf{IY}} \hat{\underline{\mathbf{A}}} \, \underline{\mathbf{T}}_{\mathbf{IY}}^{\mathbf{T}}} \, . \tag{5.27}$$

Note that the common mistake mentioned in section 5.2.1 is in this case more obvious: a vector $\underline{\mathbf{x}}$ is represented by eq. (5.24) in the Y-system and not by $\underline{\mathbf{y}} = \underline{\mathbf{T}}_{\mathbf{IY}} \underline{\mathbf{x}}$.

5.3 Local description of a wavefront

Required throughout this part of the thesis is a local second-order description of a wavefront along a ray. In general such a description involves the position, orientation and curvatures of the wavefront. The **position** can be omitted if one considers a local system that is obtained by a translation of the global system to a point of the ray where the wavefront has to be described. The **orientation** of the wavefront is given by the propagation direction of the wavefront, i. e. the ray direction. The latter can for instance be described by the azimuth and polar angle, φ_0 and φ_1. By means of the ray direction I can construct an orthogonal ray-centered coordinate system. A necessary condition for the ray-centered system is that its z-axis is defined by the ray direction vector $\underline{\mathbf{w}}_{\mathbf{z}}$ and that its origin coincides with the local system (see Figure 5.1). Its x- and y-axes are orthogonal but can be arbitrarily chosen. The ray direction vector $\underline{\mathbf{w}}_{\mathbf{z}}$ is assumed to be perpendicular to the wavefront surface. Therefore, the $x - y$ plane of the ray-centered system is the tangent plane of the wavefront surface at the considered point $(\hat{x}, \hat{y}, \hat{z}) = (0, 0, 0)$. Suitable ray-centered coordinate systems for the traveltime formulae and modeling are described in chapter 6 and 10, respectively. A suitable local second-order description of the wavefront is given in ray-centered coordinates (where the first-order terms vanish) by means of the symmetric curvature matrix $\hat{\mathbf{A}}$:

$$\hat{z} = -\frac{1}{2} \hat{\mathbf{x}}^{\mathbf{T}} \hat{\mathbf{A}} \hat{\mathbf{x}} \quad \text{with} \quad \hat{\mathbf{x}} = \begin{pmatrix} \hat{x} \\ \hat{y} \end{pmatrix}, \quad \hat{\mathbf{A}} = \begin{pmatrix} \hat{a}_{00} & \hat{a}_{01} \\ \hat{a}_{10} & \hat{a}_{11} \end{pmatrix}, \quad \hat{a}_{10} = \hat{a}_{01} \, . \tag{5.28a}$$

Although eq. (5.28a) defines a paraboloid, this description only serves to determine the curvatures of the wavefront. This means that the true wavefront could be of any shape with curvatures defined by eq. (5.28a). The minus sign in eq. (5.28a) will be explained below; I follow the definition used by Hubral and Krey (1980). I define the **curvature** k of the wavefront in a direction given by a unit vector $\hat{\mathbf{u}}$ in the $x - y$ plane of the ray-centered coordinate system by minus the second directional derivative at $(\hat{x}, \hat{y}) = (0, 0)$:

$$k = -D_{\hat{\mathbf{u}}}^2 \{ \hat{z}(\hat{x}, \hat{y}) \} (0, 0) = \hat{\mathbf{u}}^{\mathbf{T}} \hat{\mathbf{A}} \, \hat{\mathbf{u}} \quad \text{with} \quad \| \hat{\mathbf{u}} \| = 1 \, . \tag{5.28b}$$

Let me shortly investigate the sign of the curvature k. Therefore, consider a plane that is spanned by $\underline{\mathbf{w}}_{\mathbf{z}}$ and $\hat{\mathbf{u}}$. This plane is a normal section plane of the surface because it contains the surface

normal at the considered point. The intersection of a normal section plane with the wavefront yields a curve that, considered in the normal section plane, has the curvature k at $(\hat{x}, \hat{y}) = (0,0)$. The curvature k is referred to as normal curvature. This means that k determines the curvature of the wavefront in propagation direction for an azimuth defined by $\hat{\mathbf{u}}$ in the ray-centered $x - y$ plane. The minus signs used in definitions (5.28) have the following consequences if considering the wavefront in ray direction in the normal section plane defined by $\mathbf{w_z}$ and $\hat{\mathbf{u}}$: if $k > 0$ the wavefront curve appears concave; if $k < 0$ it appears convex. Of course, this sign convention also applies to a radius of curvature $R = 1/k$.
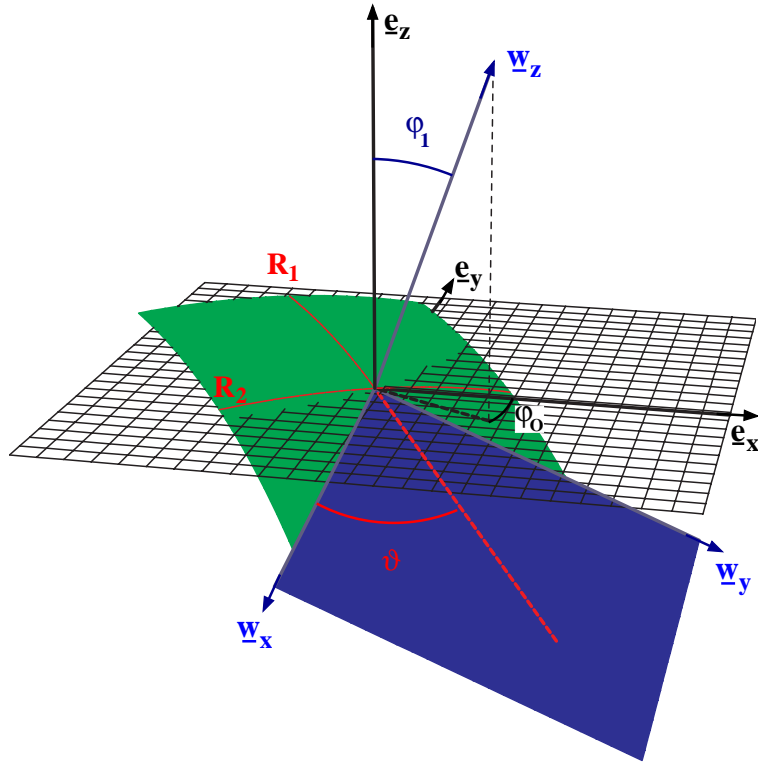
Figure 5.1: local description of a wavefront. The wavefront along a ray is described by its curvature matrix. Its eigenvalues are the principal curvatures $1/R_1$ and $1/R_2$ ($1/R_1, 1/R_2 > 0$ in the shown case); its eigenvectors determine the principal axes. The angle between the first (second) principal axis and $\underline{\mathbf{w_x}}$ ($\underline{\mathbf{w_y}}$) is denoted by ϑ.

The maximum and minimum values of the normal curvature are the so-called principal curvatures. The elements $\hat{a}_{ij}$ of the matrix $\mathbf{A}$ can be related to the principal curvatures (k_1, k_2) of the wavefront and an orientation angle ϑ (Figure 5.1):

$$\hat{\mathbf{A}} = \begin{pmatrix} \hat{a}_{00} & \hat{a}_{01} \\ \hat{a}_{01} & \hat{a}_{11} \end{pmatrix} = \begin{pmatrix} k_1 \cos^2 \vartheta + k_2 \sin^2 \vartheta & \cos \vartheta \sin \vartheta \, (k_1 - k_2) \\ \cos \vartheta \sin \vartheta \, (k_1 - k_2) & k_1 \sin^2 \vartheta + k_2 \cos^2 \vartheta \end{pmatrix}. \tag{5.29}$$

The orientation angle ϑ with respect to the $\underline{\mathbf{w_x}}$-axis in the $x - y$ plane of the ray-centered system

has the following meaning: the first principal curvature k_1 is the normal curvature of the wavefront surface in direction of the vector $\hat{\mathbf{u}} = \left(\begin{smallmatrix} \cos \vartheta \\ \sin \vartheta \end{smallmatrix} \right)$. Only one orientation angle is needed because the orientation angle for k_2 is given by $\vartheta + \pi/2$. The principal radii of curvature are given by $R_1 = 1/k_1$ and $R_2 = 1/k_2$.

Equation (5.29) can be derived by means of a rotation matrix $\mathbf{D_z}(\vartheta)$ that transform the $\underline{\mathbf{w_x}}$ and $\underline{\mathbf{w_y}}$ to the principal axes where the matrix $\hat{\mathbf{A}}$ is given by $\bar{\mathbf{A}} = \hat{\mathbf{A}}(\vartheta = 0)$. In principal axes eq. (5.29) becomes

$$\hat{z} = -\frac{1}{2}\bar{\mathbf{x}}^{\mathbf{T}}\bar{\mathbf{A}}\,\bar{\mathbf{x}} \quad \text{with} \quad \bar{\mathbf{A}} = \begin{pmatrix} k_1 & 0 \\ 0 & k_2 \end{pmatrix}. \tag{5.30}$$

As shown by eq. (5.24), a vector $\hat{\mathbf{x}}$ is represented by $\bar{\mathbf{x}} = \mathbf{D^T}\hat{\mathbf{x}}(\vartheta)$ in the principal axes system. This yields

$$\hat{z} = -\frac{1}{2}\hat{\mathbf{x}}^{\mathbf{T}}\mathbf{D_z}(\vartheta)\bar{\mathbf{A}}\,\mathbf{D_z^T}(\vartheta)\hat{\mathbf{x}}, \quad \text{hence} \quad \hat{\mathbf{A}} = \mathbf{D_z}(\vartheta)\bar{\mathbf{A}}\,\mathbf{D_z^T}(\vartheta) \tag{5.31}$$

in agreement with eq. (5.27). The determination of the principal curvatures and the orientation angle ϑ from the matrix $\hat{\mathbf{A}}$ is shown in appendix E.

Chapter 6

Coordinate systems for traveltime formulae

The wavefront curvature matrix described in section 5.3 is defined in a ray-centered coordinate system. This chapter explains a ray-centered system and a local observation system, as well as the associated transformation between them. The local observation system has the measurement surface as $x - y$ plane. For the sake of simplicity I assume that it has the same orientation than the global system, such that it can easily be obtained by a translation.

The necessary conditions for the **local observation system** and the considered **ray-centered systems** are:

- both systems are right-handed Cartesian coordinate systems.

- the local observation system has the measurement surface as $x - y$ plane.

- the origins of both systems coincide at the observation point X_0.

- the z-axis of a ray-centered system points in the direction of propagation of the wavefronts at the measurement surface, i. e. in direction of the central ray at the measurement surface.

Figure 6.1 shows two ray-centered systems $[\underline{\mathbf{v}}_{\mathbf{x}}, \underline{\mathbf{v}}_{\mathbf{y}}, \underline{\mathbf{w}}_{\mathbf{z}}]$ and $[\underline{\mathbf{w}}_{\mathbf{x}}, \underline{\mathbf{w}}_{\mathbf{y}}, \underline{\mathbf{w}}_{\mathbf{z}}]$, respectively, as well as the local observation system $[\underline{\mathbf{e}}_{\mathbf{x}}, \underline{\mathbf{e}}_{\mathbf{y}}, \underline{\mathbf{e}}_{\mathbf{z}}]$. As explained above, both ray-centered systems have the same z-axis that can can be represented by a unit vector in terms of the azimuth and polar angle:

$$\underline{\mathbf{w}}_{\mathbf{z}} = \begin{pmatrix} \cos \varphi_0 \sin \varphi_1 \\ \sin \varphi_0 \sin \varphi_1 \\ \cos \varphi_1 \end{pmatrix}. \tag{6.1}$$

6.1 Ray-centered system $\left[\underline{\mathbf{v}}_{\mathbf{x}}, \underline{\mathbf{v}}_{\mathbf{y}}, \underline{\mathbf{w}}_{\mathbf{z}}\right]$

6.1.1 Transformation by means of rotation matrices

The vector $\underline{\mathbf{w}}_{\mathbf{z}}$ can also be obtained by applying two rotations to the z-axis of the local observation system defined by $\underline{\mathbf{e}}_{\mathbf{z}}$:

$$\underline{\mathbf{w}}_{\mathbf{z}} = \underline{\mathbf{D}}_{\mathbf{z}}\left(\varphi_0\right) \underline{\mathbf{D}}_{\mathbf{y}}\left(\varphi_1\right) \underline{\mathbf{e}}_{\mathbf{z}}. \tag{6.2}$$

Submitting the $\underline{\mathbf{e}}_{\mathbf{x}}$ and the $\underline{\mathbf{e}}_{\mathbf{y}}$ vector to the same rotations yields the x- and the y-axis of the ray-centered system $\left[\underline{\mathbf{v}}_{\mathbf{x}}, \underline{\mathbf{v}}_{\mathbf{y}}, \underline{\mathbf{w}}_{\mathbf{z}}\right]$:

$$\underline{\mathbf{v}}_{\mathbf{i}} = \underline{\mathbf{D}}_{\mathbf{z}}\left(\varphi_0\right) \underline{\mathbf{D}}_{\mathbf{y}}\left(\varphi_1\right) \underline{\mathbf{e}}_{\mathbf{i}} \quad (\text{i=x,y}) \tag{6.3}$$

The transformation from the local observation system to this ray-centered system is therefore given by:

$$\underline{\mathbf{T}}_{\mathbf{IV}} = \underline{\mathbf{D}}_{\mathbf{zy}} = \underline{\mathbf{D}}_{\mathbf{z}}\left(\varphi_0\right) \underline{\mathbf{D}}_{\mathbf{y}}\left(\varphi_1\right) \tag{6.4}$$

6.1.2 Transformation by base matrix

One can observe that the y-axis $\underline{\mathbf{v}}_{\mathbf{y}}$ of this system lies in the measurement surface plane, i. e. in the $x-y$ plane of the local observation system. Furthermore, the angle between the y-axes of the local observation system and the ray-centered system is given by φ_0. Therefore, this system can also be determined by:

$$\underline{\mathbf{w}}_{\mathbf{z}} \quad \text{unit direction of central ray} \tag{6.5}$$

$$\underline{\mathbf{v}}_{\mathbf{y}} = \begin{pmatrix} -\sin\varphi_0 \\ \cos\varphi_0 \\ 0 \end{pmatrix} \tag{6.6}$$

$$\underline{\mathbf{v}}_{\mathbf{x}} = \underline{\mathbf{v}}_{\mathbf{y}} \times \underline{\mathbf{v}}_{\mathbf{z}} \tag{6.7}$$

As explained in section 5.2 the corresponding base matrix $\underline{\mathbf{V}} = \left(\underline{\mathbf{v}}_{\mathbf{x}} \, \underline{\mathbf{v}}_{\mathbf{y}} \, \underline{\mathbf{w}}_{\mathbf{z}}\right)$ defines the transformation matrix from the standard base, i. e. $\underline{\mathbf{T}}_{\mathbf{IV}} = \underline{\mathbf{V}}$. It is orthogonal since $\|\underline{\mathbf{v}}_{\mathbf{i}}\| = 1$, with i=x,y,z.

6.2 Ray-centered system $\left[\underline{\mathbf{w}}_{\mathbf{x}}, \underline{\mathbf{w}}_{\mathbf{y}}, \underline{\mathbf{w}}_{\mathbf{z}}\right]$

The ray-centered system $\left[\underline{\mathbf{v}}_{\mathbf{x}}, \underline{\mathbf{v}}_{\mathbf{y}}, \underline{\mathbf{v}}_{\mathbf{z}}\right]$ is solely based on the polar representation of the direction vector $\underline{\mathbf{v}}_{\mathbf{z}}$. Therefore, it does not allow to specify the x- or y-axis of the ray-centered system. My aim is now to construct a ray-centered system where the x- or the y-axis can be chosen. Let me first introduce what I will subsequently call the reference plane.
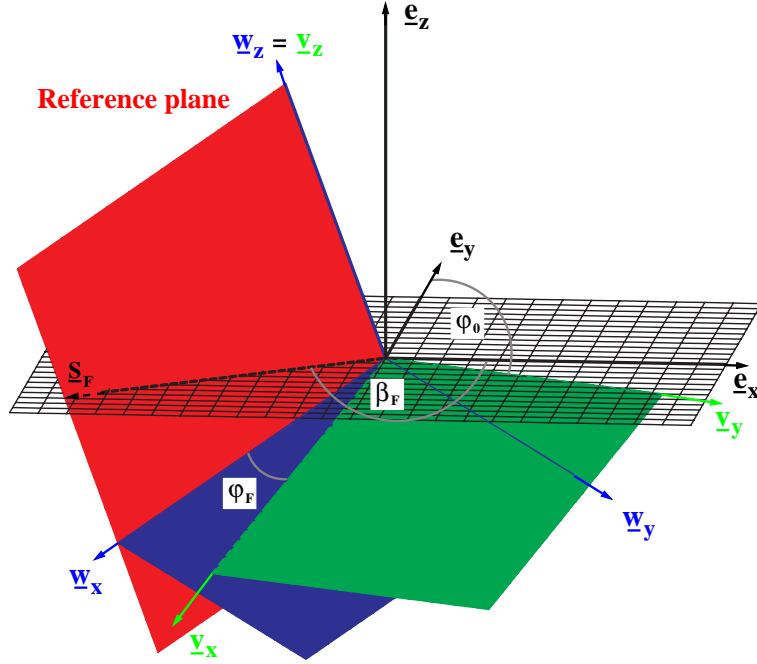
Figure 6.1: local observation and ray-centered coordinate systems. The ray-centered coordinate system with the green base plane is obtained by two rotations whereas the ray-centered system with the blue base plane requires an additional third rotation.

6.2.1 Reference plane

I define the reference plane by a plane that contains a (chosen) unit vector on the measurement surface $\underline{\mathbf{s}}_{\mathbf{F}}$ and the direction vector $\underline{\mathbf{w}}_{\mathbf{z}}$ of the central ray (Figure 6.1). In local observation coordinates this plane is given by:

$$p_F := \underline{\mathbf{n}}_{\mathbf{F}} \cdot \underline{\mathbf{x}} = 0 \quad \text{with} \quad \underline{\mathbf{n}}_{\mathbf{F}} = \underline{\mathbf{w}}_{\mathbf{z}} \times \underline{\mathbf{s}}_{\mathbf{F}}, \quad \underline{\mathbf{s}}_{\mathbf{F}} = \begin{pmatrix} \cos \beta_F \\ \sin \beta_F \\ 0 \end{pmatrix} \quad (-\pi < \beta_F \le \pi). \tag{6.8}$$

Note that $\underline{\mathbf{n}}_{\mathbf{F}} \cdot \underline{\mathbf{x}} = 0$ because the origin lies in the reference plane.

6.2.2 Transformation by means of rotation matrices

To specify the x-axis defined by $\underline{\mathbf{w}}_{\mathbf{x}}$ of this ray-centered coordinate system I demand that it falls into the reference plane (Figure 6.1), i. e

$$\underline{\mathbf{n}}_{\mathbf{F}} \cdot \underline{\mathbf{w}}_{\mathbf{x}} = 0. \tag{6.9}$$

The ray-centered $[\underline{\mathbf{w}}_\mathbf{x}, \underline{\mathbf{w}}_\mathbf{y}, \underline{\mathbf{w}}_\mathbf{z}]$ system can be computed by:

$$\underline{\mathbf{w}}_\mathbf{i} = \underline{\mathbf{D}}_\mathbf{z}\left(\varphi_0\right) \underline{\mathbf{D}}_\mathbf{y}\left(\varphi_1\right) \underline{\mathbf{D}}_\mathbf{z}\left(\varphi_F\right) \underline{\mathbf{e}}_\mathbf{i} \quad (\mathrm{i} = x, y, z) \tag{6.10a}$$

$$\text{with} \quad \begin{pmatrix} \cos\varphi_F \\ \sin\varphi_F \end{pmatrix} = \frac{\mathbf{D}_\mathbf{y}^\mathbf{T}\left(\varphi_1\right) \mathbf{D}_\mathbf{z}^\mathbf{T}\left(\varphi_0\right) \mathbf{s}_\mathbf{F}}{\sqrt{1 - \left(\mathbf{w}_\mathbf{z} \cdot \mathbf{s}_\mathbf{F}\right)^2}} \quad \text{and} \quad \mathbf{s}_\mathbf{F} = \begin{pmatrix} \cos\beta_F \\ \sin\beta_F \end{pmatrix}. \tag{6.10b}$$

The angle φ_F is determined by means of appendix D. The transformation from the local observation system to the $[\underline{\mathbf{w}}_\mathbf{x}, \underline{\mathbf{w}}_\mathbf{y}, \underline{\mathbf{w}}_\mathbf{z}]$ system is given by:

$$\underline{\mathbf{T}}_\mathbf{IW} = \underline{\mathbf{D}}_\mathbf{zyz} = \underline{\mathbf{D}}_\mathbf{z}\left(\varphi_0\right) \underline{\mathbf{D}}_\mathbf{y}\left(\varphi_1\right) \underline{\mathbf{D}}_\mathbf{z}\left(\varphi_F\right) \tag{6.11}$$

6.2.3 Transformation by base matrix

The ray-centered system $[\underline{\mathbf{w}}_\mathbf{x}, \underline{\mathbf{w}}_\mathbf{y}, \underline{\mathbf{w}}_\mathbf{z}]$ is given by the unit base vectors:

$$\mathbf{w}_\mathbf{z} \quad \text{direction vector of ray} \tag{6.12a}$$

$$\underline{\mathbf{w}}_\mathbf{y} = \frac{\underline{\mathbf{w}}_\mathbf{z} \times \underline{\mathbf{s}}_\mathbf{F}}{\|\underline{\mathbf{w}}_\mathbf{z} \times \underline{\mathbf{s}}_\mathbf{F}\|} = \frac{\mathbf{n}_\mathbf{F}}{\|\underline{\mathbf{n}}_\mathbf{F}\|} \tag{6.12b}$$

$$\underline{\mathbf{w}}_\mathbf{x} = \underline{\mathbf{w}}_\mathbf{y} \times \underline{\mathbf{w}}_\mathbf{z} \tag{6.12c}$$

The according base matrix $\underline{\mathbf{W}}$ with unit vectors defines the orthogonal transformation:

$$\underline{\mathbf{T}}_\mathbf{IW} = \underline{\mathbf{D}}_\mathbf{zyz} = \underline{\mathbf{W}} = \left(\underline{\mathbf{w}}_\mathbf{x}, \underline{\mathbf{w}}_\mathbf{y}, \underline{\mathbf{w}}_\mathbf{z}\right). \tag{6.13}$$

6.2.4 Relationship to the system $[\underline{\mathbf{v}}_\mathbf{x}, \underline{\mathbf{v}}_\mathbf{y}, \underline{\mathbf{v}}_\mathbf{z}]$

The $[\underline{\mathbf{w}}_\mathbf{x}, \underline{\mathbf{w}}_\mathbf{y}, \underline{\mathbf{w}}_\mathbf{z}]$ system is a generalization of the $[\underline{\mathbf{v}}_\mathbf{x}, \underline{\mathbf{v}}_\mathbf{y}, \underline{\mathbf{v}}_\mathbf{z}]$ system, i. e. the latter is a special case of the former. The $[\underline{\mathbf{v}}_\mathbf{x}, \underline{\mathbf{v}}_\mathbf{y}, \underline{\mathbf{v}}_\mathbf{z}]$ system can be obtained by setting $\beta_F = \varphi_0$ which implies $\varphi_F = 0$, hence $\underline{\mathbf{D}}_\mathbf{z}(\varphi_F) = \underline{\mathbf{I}}$.

6.3 Considered transformation

In the following I denote the transformation to a ray-centered system simply by $\underline{\mathbf{T}}$. This could be the transformation $\underline{\mathbf{T}}_\mathbf{IV}$ or $\underline{\mathbf{T}}_\mathbf{IW}$ but has in any case to fulfill the conditions mentioned at the beginning of this chapter. Although the transformation $\underline{\mathbf{T}}_\mathbf{IW}$ covers all possible cases that meet the conditions, the shown constructions of it are exemplarily. In any case one has to be aware that the used transformation defines the ray-centered coordinate system to which the curvature matrix of the wavefront refers to. This will be mentioned repeatedly.

6.4   Local construction of a wavefront

The local description of a wavefront can now be expressed in local observation coordinates. Therefore, I first construct the vector

$$\underline{\mathbf{x}} = \begin{pmatrix} x \\ y \\ z \end{pmatrix} \quad \text{with} \quad z = -\frac{1}{2}\mathbf{x}^{\mathrm{T}}\hat{\mathbf{A}}\mathbf{x} \quad \text{and} \quad \mathbf{x} = \begin{pmatrix} x \\ y \end{pmatrix}$$

in local observation coordinates.

This vector transformed by eqs. (6.10) to the ray-centered coordinate system, i. e.

$$\underline{\mathbf{x}}_{\mathbf{w}} = \underline{\mathbf{T}}\,\underline{\mathbf{x}},$$

expresses the wavefront in terms of local observation coordinates.

Chapter 7

Relationships of the 2D and the 3D case

Let us consider a wavefront emerging at the measurement surface as shown in Figure 7.1. The direction of propagation of the wavefront is indicated by the central ray. Let us further specify a seismic line on the measurement surface by an azimuth angle β, which yields the following unit direction vectors of the seismic line:

$$
\underline{s_i} = \begin{pmatrix} \cos\beta_i \\ \sin\beta_i \\ 0 \end{pmatrix}, \quad s_i = \begin{pmatrix} \cos\beta_i \\ \sin\beta_i \end{pmatrix} \quad \text{with } -\pi < \beta_i \le \pi. \tag{7.1}
$$

7.1 Observation plane

An observation plane is defined in the same manner than the reference plane (eq. (6.8)) with the difference that an observation plane contains the direction vector $\underline{s_i}$ of a seismic line:

$$
p_i := \underline{n_i} \cdot \underline{x} = 0 \quad \text{with} \quad \underline{n_i} = \underline{w_z} \times \underline{s_i}. \tag{7.2}
$$

The observation plane p_i is important with respect to the 2D case: the wavefront attributes that are observed at the current emergence location of the wavefront in direction of the seismic line $\underline{s_i}$ describe the wavefront surface within the observation plane (Figures 7.1 and 7.2). This is based on the fact that, along a seismic line, one measures the influence of the wavefront in propagation direction. Note that the observation plane is a normal section plane defined by $\underline{w_z}$ and $\underline{s_i}$.

7.2 Relationship of angles

The incidence angle α_i observed in the 2D case is the angle between the propagation vector (central ray) of the wavefront surface and the normal to the seismic line in the observation plane. It is
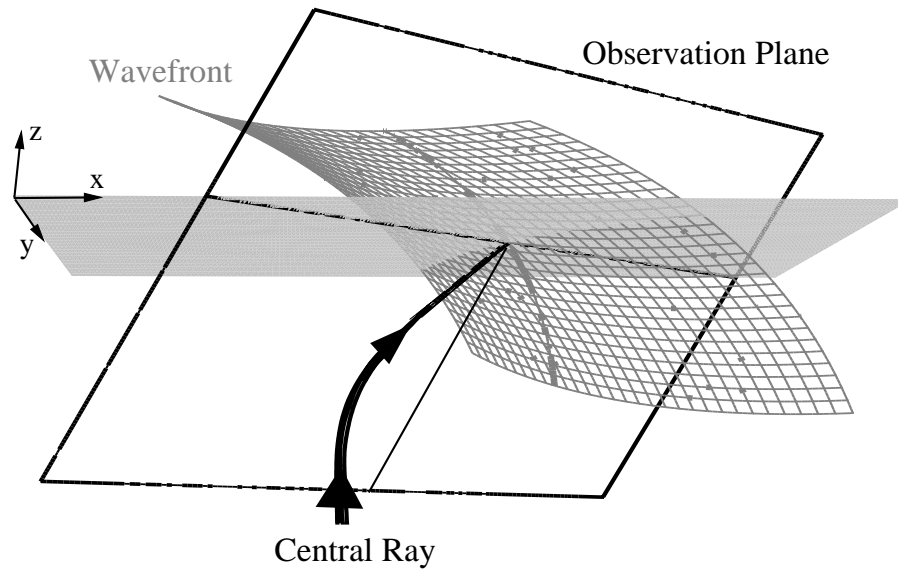
Figure 7.1: a wavefront (gray) emerging at the measurement surface. The seismic line (black line on the measurement surface) and the direction of the central ray (black) at the measurement surface define the observation plane. The intersection of the wavefront with the observation plane yields the bold gray curve.
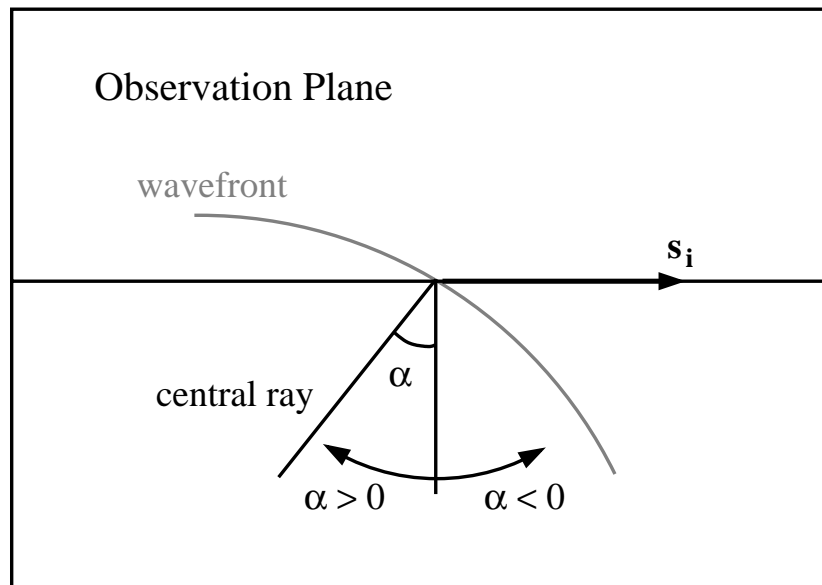
Figure 7.2: observation plane. the parameters observed in the 2D case describe the 3D wavefront in the observation plane.
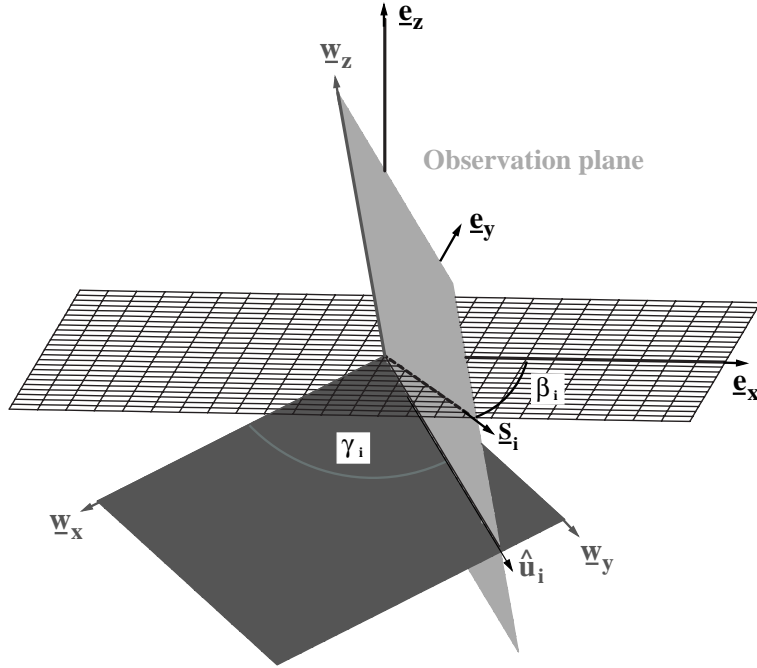
Figure 7.3: observation plane in the 3D space. An observation plane contains the vector $\underline{\mathbf{w}}_\mathbf{z}$ as well as a seismic line specified by the unit vector $\underline{\mathbf{s}}_\mathbf{i}$. Note that the *x*- and the *y*-axis of the ray-centered system could also be $\underline{\mathbf{v}}_\mathbf{x}$ and $\underline{\mathbf{v}}_\mathbf{y}$.

related to the 3D case by one of the following equations:

$$\boxed{\sin \alpha_i = \mathbf{w_z} \cdot \mathbf{s_i} \quad \text{or} \quad \cos \alpha_i = \sqrt[+]{1 - \left(\mathbf{w_z} \cdot \mathbf{s_i}\right)^2}} \tag{7.3}$$

where α is defined in the range $-\pi/2 < \alpha < \pi/2$.

7.3 Relationship of curvatures

The wavefront curvature observed in the 2D case is the curvature of the wavefront surface in the observation plane. As mentioned in section 5.3, it is given by a directional derivative in direction of the unit vector $\underline{\hat{\mathbf{u}}}_\mathbf{i}$:

$$\boxed{\frac{1}{R_i} = \hat{\mathbf{u}}_\mathbf{i}^\mathbf{T} \hat{\mathbf{A}} \hat{\mathbf{u}}_\mathbf{i}} \tag{7.4a}$$

To determine $\hat{\underline{u}}_i$ by means of $\underline{s}_i$, the vector $\underline{s}_i$ is expressed in ray-centered coordinates, projected to the $x - y$ plane of the ray-centered system, and finally normalized (see appendix D):

$$\hat{\mathbf{u}}_{\mathbf{i}} = \begin{pmatrix} \cos \gamma_i \\ \sin \gamma_i \end{pmatrix} = \frac{\mathbf{T}^{\mathbf{T}} \mathbf{s}_{\mathbf{i}}}{\sqrt{1 - (\mathbf{w}_{\mathbf{z}} \cdot \mathbf{s}_{\mathbf{i}})^2}} . \qquad (7.4b)$$

$\mathbf{T}$ is the upper left 2×2 submatrix of the transformation $\underline{\mathbf{T}}$ to the ray-centered coordinate system in which the curvature matrix $\hat{\underline{\mathbf{A}}}$ is expressed (see section 6.3).

Chapter 8

Traveltime formulae

In this chapter, I present two second-order approximations of the traveltimes for 3D media: the so-called parabolic and a hyperbolic formulae. A possibility is to use the following second-order approximations of the CRS stack formulae for 2D:

$$t_{par}(x_m, h) = t_0 + \frac{2 \sin \alpha}{v_0} (x_m - x_0) + \frac{\cos^2 \alpha}{v_0} \left(\frac{(x_m - x_0)^2}{R_N} + \frac{h^2}{R_{NIP}} \right), \tag{8.1a}$$

$$t_{hyp}^2(x_m, h) = \left(t_0 + \frac{2 \sin \alpha}{v_0} \right)^2 + 2 \frac{t_0 \cos^2 \alpha}{v_0} \left(\frac{(x_m - x_0)^2}{R_N} + \frac{h^2}{R_{NIP}} \right). \tag{8.1b}$$

Here, h denotes the half-offset, x_m the midpoint between shot and receiver. The location x_0 is the observation point on the seismic line. The attributes α, R_{NIP}, and R_N describe the wavefronts in the observation plane.

By means of the relationships established in chapter 7 one obtains

$$t_{par} = t_0 + \frac{2}{v_0} \mathbf{w_z} \cdot \mathbf{m} + \frac{1}{v_0} \mathbf{m^T} \mathbf{T} \hat{\mathbf{N}} \mathbf{T^T} \mathbf{m} + \frac{1}{v_0} \mathbf{h^T} \mathbf{T} \hat{\mathbf{M}} \mathbf{T^T} \mathbf{h}, \tag{8.2a}$$

$$t_{hyp}^2 = \left(t_0 + \frac{2}{v_0} \mathbf{w_z} \cdot \mathbf{m} \right)^2 + \frac{2t_0}{v_0} \mathbf{m^T} \mathbf{T} \hat{\mathbf{N}} \mathbf{T^T} \mathbf{m} + \frac{2t_0}{v_0} \mathbf{h^T} \mathbf{T} \hat{\mathbf{M}} \mathbf{T^T} \mathbf{h}, \tag{8.2b}$$

where

- $\mathbf{T}$ is the upper left 2×2 submatrix of the transformation $\underline{\mathbf{T}}$ to a ray-centered coordinate system as explained in section 6.3.

- $\hat{\mathbf{M}}$ and $\hat{\mathbf{N}}$ denote the curvature matrices of the NIP and normal wave, respectively, that are expressed with respect to the ray-centered system defined by the transformation $\underline{\mathbf{T}}$.

- $\mathbf{m}$ denotes the midpoint vector with respect to the observation point X_0; $\mathbf{h}$ denotes the half-offset vector between shot and receiver. If the shot and the receiver are specified with respect to the

observation point X_0 by $\mathbf{s}$ and $\mathbf{g}$, respectively, these vectors are connected by:

$$\underline{\mathbf{h}} = \frac{1}{2}\left(\underline{\mathbf{g}} - \underline{\mathbf{s}}\right), \quad \underline{\mathbf{m}} = \frac{1}{2}\left(\underline{\mathbf{g}} + \underline{\mathbf{s}}\right) = \underline{\mathbf{s}} + \underline{\mathbf{h}}.$$

- v_0 denotes, as in the 2D case, the near surface velocity.

Now, I have to consider the validation of these formulae, since their derivation is based on the 2D case. A 2D (observation) plane is a subset of the 3D space and with respect to the variables $(\mathbf{m}, \mathbf{h})$ of the formulae one can state that this derivation is based on parallel midpoint and half-offset vectors, i.e., $\mathbf{m} \| \mathbf{h}$. Therefore, appendix G provides an alternative derivation using Hamilton's equation that leads to the same result. Appendix H compares eqs. (8.2) to the paraxial traveltime approximations formulated by Schleicher et al. (1993).

Chapter 9

Determination of wavefront parameters

9.1 Required parameters

In chapter 5.3 I have shown that I use 5 parameters to describe a wavefront in 3D. Because the CRS stack is based on two hypothetical wavefronts, one would have to determine 10 parameters. However, the wavefronts are considered along the same central ray. Therefore, the angles φ_0 and φ_1 of the direction vector $\underline{\mathbf{w_z}}$ are common to both wavefronts. This reduces the number of the searched-for parameters to the following 8.

searched-for parameters	involved in
$\varphi_0,\ \varphi_1$	direction vector $\underline{\mathbf{w_z}}$ of central ray
$\hat{m}_{00},\ \hat{m}_{11},\ \hat{m}_{01}$	curvature matrix $\hat{\mathbf{M}}$ of the NIP wavefront
$\hat{n}_{00},\ \hat{n}_{11},\ \hat{n}_{01}$	curvature matrix $\hat{\mathbf{N}}$ of the normal wavefront

9.2 Determination by a 3D CRS stack

Let me in the following use the hyperbolic traveltime formula given by eq. (8.2b), which gave in the 2D case an empirical proof to be a better approximation than its parabolic counterpart. To determine the parameters for a point P_0 in the ZO section one would first rewrite eq. (8.2b) as

$$t_{hyp}^2 = \left(t_0 + \frac{2}{v_0}\,\mathbf{w_z}\cdot\mathbf{m}\right)^2 + \frac{2t_0}{v_0}\,\mathbf{m^T A\,m} + \frac{2t_0}{v_0}\,\mathbf{h^T B\,h} \tag{9.1}$$

and fit this hypersurface to to the reflection events.[1] In order to save computation time in the practical application it is recommended to determine the parameters in successive steps. Since

---

[1]The matrices $\mathbf{A}$ and $\mathbf{B}$ should not be confused with the submatrices of the surface-to-surface ray propagator explained in appendix H.

formula (9.1) has the same structure as its 2D counterpart a similar strategy than in the 2D case (Mann et al., 1999) is possible. Note that, although $\mathbf{T}$ is not symmetric, $\mathbf{A} = \mathbf{T}\hat{\mathbf{N}}\mathbf{T}^{\mathbf{T}}$ and $\mathbf{B} = \mathbf{T}\hat{\mathbf{M}}\mathbf{T}^{\mathbf{T}}$ are symmetric. Having determined $\mathbf{w_z}$, $\mathbf{A}$ and $\mathbf{B}$ the first step is to compute the angles φ_0 and φ_1 from $\mathbf{w_z}$:

$$\cos \varphi_0 = \frac{w_{z0}}{\sigma}, \quad \sin \varphi_0 = \frac{w_{z1}}{\sigma}, \quad \cos \varphi_1 = w_{z2}, \quad \sin \varphi_1 = \sigma \quad \text{with} \quad \sigma = \sqrt[+]{w_{z0}^2 + w_{z1}^2}. \quad (9.2)$$

By means of this angles the 2×2 upper left matrix $\mathbf{T}$ of the transformation matrix $\underline{\mathbf{T}}$ can be constructed by e. g. eq. (6.4) or eq. (6.11). Then, the curvature matrices of the NIP and normal wavefront are simply given by

$$\hat{\mathbf{N}} = \mathbf{T}^{\mathbf{T}}\mathbf{A}\mathbf{T} \tag{9.3}$$

$$\text{and} \quad \hat{\mathbf{M}} = \mathbf{T}^{\mathbf{T}}\mathbf{B}\mathbf{T}. \tag{9.4}$$

The curvature matrices are defined in the ray-centered coordinates that are associated with the used transformation, i. e., for instance, in the $[\underline{\mathbf{v_x}}, \underline{\mathbf{v_y}}, \underline{\mathbf{w_z}}]$ system if $\mathbf{T} = \mathbf{T_{IV}}$, or in the $[\underline{\mathbf{w_x}}, \underline{\mathbf{w_y}}, \underline{\mathbf{w_z}}]$ system if $\mathbf{T} = \mathbf{T_{IW}}$ (see chapter 6).

9.3 Determination by the 2D CRS stack

In this section I make use of the relationship of the 2D and the 3D case to determine these parameters. Figure 9.1 shows a ZO sample P_0 for which the wavefronts have to be determined. If one performs the CRS stack for 2D for point P_0 with the multicoverage data sets of three different seismic lines that pass through X_0, one can obtain the following 8 parameters:

detected parameters	obtained by
α_0, $R_{NIP,0}$, $R_{N,0}$	seismic line $\underline{\mathbf{s_0}}$
α_1, $R_{NIP,1}$, $R_{N,1}$	seismic line $\underline{\mathbf{s_1}}$
$R_{NIP,2}$, $R_{N,2}$	seismic line $\underline{\mathbf{s_2}}$

The inversion of the detected parameters to the searched for parameters is shown in the following. The dependencies are

- $\underline{\mathbf{w_z}} = \underline{\mathbf{w_z}}(\alpha_0, \alpha_1)$

- $\hat{\mathbf{M}} = \hat{\mathbf{M}}(\alpha_0, \alpha_1, R_{NIP,0}, R_{NIP,1}, R_{NIP,2})$

- $\hat{\mathbf{N}} = \hat{\mathbf{N}}(\alpha_0, \alpha_1, R_{N,0}, R_{N,1}, R_{N,2})$

The inversion procedure starts with the determination of the direction vector $\underline{\mathbf{w_z}}$. Thereafter, I will show the determination of a curvature matrix. Because the matrices $\hat{\mathbf{M}}$ and $\hat{\mathbf{N}}$ are independent of each other and the inversion formulae for them are the same, I will show the inversion for the matrix $\hat{\mathbf{A}} = \hat{\mathbf{A}}(\alpha_0, \alpha_1, R_0, R_1, R_2)$.
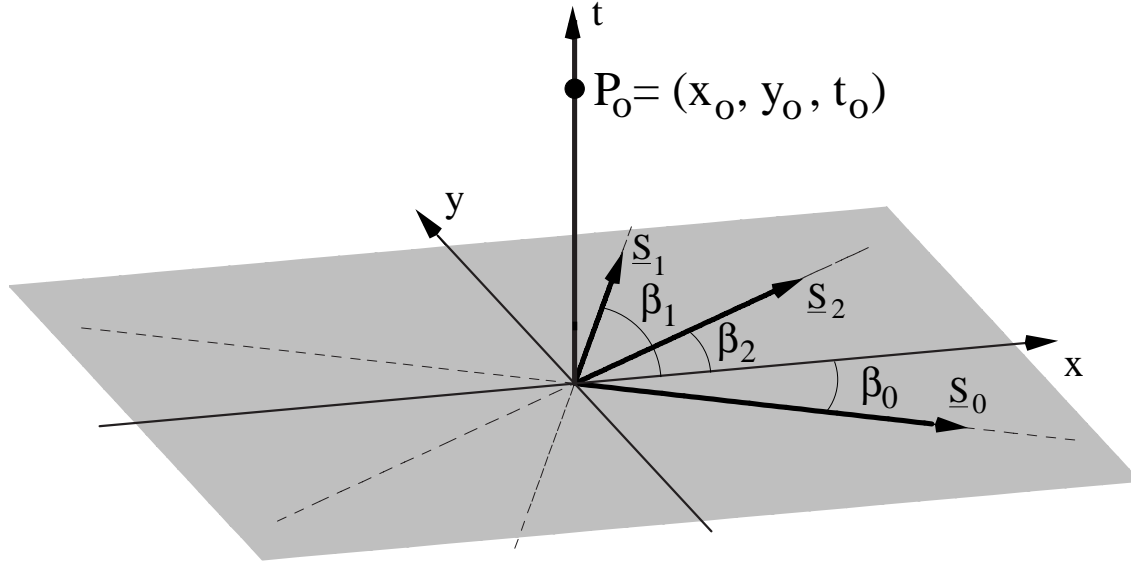
Figure 9.1: seismic lines on the measurement surface. This figure indicates that three different seismic lines (specified by the unit vectors $\underline{\mathbf{s}}_0$, $\underline{\mathbf{s}}_1$, $\underline{\mathbf{s}}_2$) are involved in the determination of the wavefront parameters for point P_0. Note that the direction of a seismic line has to be chosen in dependency on the sign of α_i as shown in Figure 7.2.

9.3.1   Relationship of the angles

To compute the direction vector $\underline{\mathbf{w}}_{\mathbf{z}}$ I make use of the relationship given by eq. (7.3). To determine the two elements of $\underline{\mathbf{w}}_{\mathbf{z}}$ one requires the two emergence angles in the observation planes of two different seismic lines. To increase the stability it is recommended to use the two seismic lines which directions are the closest to orthogonality, i. e. which yield the minimum of $\lfloor \underline{\mathbf{s}}_{\mathbf{i}} \cdot \underline{\mathbf{s}}_{\mathbf{j}} \rfloor$ $(i \neq j)$. In Figure 9.1 this is the case for $\underline{\mathbf{s}}_0$ and $\underline{\mathbf{s}}_1$. The corresponding incidence angles α_1 and α_0 allow to determine the projected vector $\mathbf{w}_{\mathbf{z}}$ of the direction vector $\underline{\mathbf{w}}_{\mathbf{z}}$ onto the measurement surface (appendix F.1):

$$
w_{z0} = \cos\varphi_0 \sin\varphi_1 = \frac{\sin\beta_1 \sin\alpha_0 - \sin\beta_0 \sin\alpha_1}{\cos\beta_0 \sin\beta_1 - \sin\beta_0 \cos\beta_1} = \frac{\sin\beta_1 \sin\alpha_0 - \sin\beta_0 \sin\alpha_1}{\det \mathbf{S}^{\mathbf{T}}},
$$

$$
w_{z1} = \sin\varphi_0 \sin\varphi_1 = \frac{\cos\beta_0 \sin\alpha_1 - \cos\beta_1 \sin\alpha_0}{\cos\beta_0 \sin\beta_1 - \sin\beta_0 \cos\beta_1} = \frac{\cos\beta_0 \sin\alpha_1 - \cos\beta_1 \sin\alpha_0}{\det \mathbf{S}^{\mathbf{T}}},
$$

$$
\text{where} \quad \det \mathbf{S}^{\mathbf{T}} = \begin{vmatrix} \cos\beta_0 & \sin\beta_0 \\ \cos\beta_1 & \sin\beta_1 \end{vmatrix}. \tag{9.5a}
$$

With eqs. (9.2) this yields the angles φ_0 and φ_1 and thereby the direction of the central ray $\underline{\mathbf{w}}_{\mathbf{z}}$ at the measurement surface as well as the required transformation matrix $\underline{\mathbf{T}}$ to a ray-centered coordinate system. Note that the incidence angles have the range $-\frac{\pi}{2} < \alpha_0, \alpha_1 < \frac{\pi}{2}$. Important in this respect is that the direction of a seismic line $\underline{\mathbf{s}}_{\mathbf{i}}$ has to be chosen in agreement with the sign of α_i as shown in Figure 7.2.

9.3.2 Relationship of the radii of curvature

As explained in chapter 7, a radius of curvature R_i detected by the CRS stack for 2D media is the radius of curvature of a wavefront in the observation plane. The basic relationship between the curvature matrix $\hat{\mathbf{A}}$ of the wavefront and a curvature in the observation plane is given by eqs. (7.4). To determine the three elements of the symmetric curvature matrix $\hat{\mathbf{A}}$, I use directional derivatives of the second-order of $\hat{\mathbf{A}}$. The whole derivation is shown in appendix F.2.

First one has to compute the normalized direction vectors $\hat{\mathbf{u}}_i$ in the ray-centered $x - y$ plane for the three seismic lines $\hat{\mathbf{s}}_i$ by means of equation (7.4b).

Relating the directional derivatives of second-order of the wavefront surface in the three different directions $\hat{\mathbf{u}}_i$ to the respective detected curvatures k_i one can compute the elements $\hat{a}_{ij}$ of the matrix $\hat{\mathbf{A}}$ (appendix F.2.2):

$$\hat{a}_{00} = \frac{1}{\det \underline{\mathbf{B}}} \begin{pmatrix} 2\cos\gamma_2 \sin\gamma_2 \sin^2\gamma_1 - 2\cos\gamma_1 \sin\gamma_1 \sin^2\gamma_2 \\ 2\cos\gamma_0 \sin\gamma_0 \sin^2\gamma_2 - 2\cos\gamma_2 \sin\gamma_2 \sin^2\gamma_0 \\ 2\cos\gamma_1 \sin\gamma_1 \sin^2\gamma_0 - 2\cos\gamma_0 \sin\gamma_0 \sin^2\gamma_1 \end{pmatrix} \cdot \underline{\mathbf{k}} \,, \tag{9.6a}$$

$$\hat{a}_{11} = \frac{1}{\det \underline{\mathbf{B}}} \begin{pmatrix} 2\cos\gamma_1 \sin\gamma_1 \cos^2\gamma_2 - 2\cos\gamma_2 \sin\gamma_2 \cos^2\gamma_1 \\ 2\cos\gamma_2 \sin\gamma_2 \cos^2\gamma_0 - 2\cos\gamma_0 \sin\gamma_0 \cos^2\gamma_2 \\ 2\cos\gamma_0 \sin\gamma_0 \cos^2\gamma_1 - 2\cos\gamma_1 \sin\gamma_1 \cos^2\gamma_0 \end{pmatrix} \cdot \underline{\mathbf{k}} \,, \tag{9.6b}$$

$$\hat{a}_{01} = \frac{1}{\det \underline{\mathbf{B}}} \begin{pmatrix} \cos^2\gamma_1 - \cos^2\gamma_2 \\ \cos^2\gamma_2 - \cos^2\gamma_0 \\ \cos^2\gamma_0 - \cos^2\gamma_1 \end{pmatrix} \cdot \underline{\mathbf{k}} \tag{9.6c}$$

$$\text{with} \quad \underline{\mathbf{k}} = \begin{pmatrix} k_0 \\ k_1 \\ k_2 \end{pmatrix} = \begin{pmatrix} 1/R_0 \\ 1/R_1 \\ 1/R_2 \end{pmatrix}, \quad \det \underline{\mathbf{B}} = \begin{vmatrix} \cos^2\gamma_0 & \sin^2\gamma_0 & 2\cos\gamma_0 \sin\gamma_0 \\ \cos^2\gamma_1 & \sin^2\gamma_1 & 2\cos\gamma_1 \sin\gamma_1 \\ \cos^2\gamma_2 & \sin^2\gamma_2 & 2\cos\gamma_2 \sin\gamma_2 \end{vmatrix} .$$

Note that the transformation of which the submatrix is used in (7.4b) defines the ray-centered system to which the curvature matrix $\hat{\mathbf{A}}$ refers to.

Chapter 10

Wavefront curvatures in layered media

In the framework of this thesis, I implemented an interactive code that computes and visualizes the curvatures of a wavefront along a ray for media with iso-velocity layers (or blocks). An interface has to be continuous up to the second-order which advises the use of cubic splines to connect the interface points. The underlying theory is described in detail in Hubral and Krey (1980). Here, I describe its application in practice. This involves the determination of the different coordinate systems and transformations as well as how to obtain the curvature matrices of a wavefront and an interface.

10.1   Coordinate transformation

In chapter 6, I explained the coordinate transformation from a local observation system to a ray-centered system that is required for a local description of the wavefront at the measurement surface. In the following, the wavefront curvatures are determined along a specific moving ray-centered coordinate system and a local description of the interface is required in a specific interface coordinate system.

Consider two right-handed Cartesian local coordinate system: a local system and a Y-system $[\underline{\mathbf{y}}_\mathbf{x}, \underline{\mathbf{y}}_\mathbf{y}, \underline{\mathbf{y}}_\mathbf{z}]$. The local system is simply obtained by translating the global system to the origin of the $[\underline{\mathbf{y}}_\mathbf{x}, \underline{\mathbf{y}}_\mathbf{y}, \underline{\mathbf{y}}_\mathbf{z}]$ system. The bases of these systems are given by $\underline{\mathbf{I}} = (\underline{\mathbf{e}}_\mathbf{x}, \underline{\mathbf{e}}_\mathbf{y}, \underline{\mathbf{e}}_\mathbf{z})$ and $\underline{\mathbf{Y}} = (\underline{\mathbf{y}}_\mathbf{x}, \underline{\mathbf{y}}_\mathbf{y}, \underline{\mathbf{y}}_\mathbf{z})$, respectively. The translation of the global system to the local system will play no role in the following; only the orientation of different coordinate systems will enter in the determination of the wavefront curvatures. As explained in section 5.2, the transformation from the local system to the $[\underline{\mathbf{y}}_\mathbf{x}, \underline{\mathbf{y}}_\mathbf{y}, \underline{\mathbf{y}}_\mathbf{z}]$ system,

$$\underline{\mathbf{y}}_\mathbf{i} = \underline{\mathbf{T}}_{\mathbf{IY}} \underline{\mathbf{e}}_\mathbf{i} \quad (\text{i=x,y,z}), \tag{10.1}$$

is given by:

$$\underline{\mathbf{T}}_{\mathbf{IY}} = \underline{\mathbf{Y}}. \tag{10.2}$$

67

Note that $\|\underline{\mathbf{y}}_{\mathbf{i}}\| = 1$ (i=x,y,z) is required in order to build an orthogonal transformation $\underline{\mathbf{T}}_{\mathbf{IY}}$.

An alternative solution is given by means of rotation matrices:

$$\underline{\mathbf{T}}_{\mathbf{IY}} = \underline{\mathbf{D}}_{\mathbf{z}}\left(\phi_0\right)\underline{\mathbf{D}}_{\mathbf{y}}\left(\phi_1\right)\underline{\mathbf{D}}_{\mathbf{z}}\left(\phi_2\right), \tag{10.3a}$$

$$\text{with} \quad \cos\phi_0 = \frac{y_{z0}}{\sigma}, \quad \sin\phi_0 = \frac{y_{z1}}{\sigma}, \quad \cos\phi_1 = \frac{y_{z2}}{r}, \quad \sin\phi_1 = \mathrm{sgn}\left(y_{z2}\right)\frac{\sigma}{r}, \tag{10.3b}$$

$$\sigma = \sqrt[+]{y_{z0}^2 + y_{z1}^2}, \quad r = \|\underline{\mathbf{y}}_{\mathbf{z}}\| = \sqrt[+]{y_{z0}^2 + y_{z1}^2 + y_{z2}^2} = 1,$$

$$\begin{pmatrix}\cos\phi_2 \\ \sin\phi_2\end{pmatrix} = \frac{\tilde{\mathbf{t}}}{\|\tilde{\mathbf{t}}\|}, \quad \tilde{\mathbf{t}} = \mathbf{D}_{\mathbf{z}}\left(\phi_0\right)\mathbf{D}_{\mathbf{y}}\left(\phi_1\right)\begin{pmatrix}y_{x0} \\ y_{x1}\end{pmatrix} - \begin{pmatrix}y_{x2}\sin\varphi_1 \\ 0\end{pmatrix}. \tag{10.3c}$$

The angles are defined in the following range: $-\pi < \phi_0, \phi_1, \phi_2 \leq \pi$. The angles ϕ_0, ϕ_1 are determined by expressing $\underline{\mathbf{y}}_{\mathbf{z}}$ in polar coordinates (r, ϕ_0, ϕ_1). The angle ϕ_2 is determined by means of appendix D. The associated additional rotation $\underline{\mathbf{D}}_{\mathbf{z}}(\phi_2)$ matrix assures that $\underline{\mathbf{y}}_{\mathbf{x}}$ lies in the incident plane that will be explained below. The upper left 2×2 submatrix $\mathbf{T}_{\mathbf{IY}}$ of $\underline{\mathbf{T}}_{\mathbf{IY}}$ can also be computed by:

$$\mathbf{T}_{\mathbf{IY}} = \mathbf{D}_{\mathbf{z}}\left(\phi_0\right)\mathbf{D}_{\mathbf{y}}\left(\phi_1\right)\mathbf{D}_{\mathbf{z}}\left(\phi_2\right). \tag{10.4}$$

I recommend, however, to determine the transformation by means of eq. (10.2), i. e. by means of the base matrix.

10.2   Ray segments

To determine the curvature of a wavefront along a ray, I split a ray into segments, where each ray segment describes the direction of propagation in a constant velocity environment. Therefore, each ray segment builds a straight line. The direction of the ray segment is described by the unit vector $\underline{\mathbf{w}}_{\mathbf{z}}$. The discontinuities of the velocity distribution are analytical given by the spline interpolation of the interfaces. Hence, in this case, a ray segment connects two points of the interfaces and lies in a constant velocity layer: the ray segment starts at the intersection point Q_{-1} and ends at the intersection point Q_i. The ordering of these points are defined by the ray direction. Denoting by $\underline{\mathbf{r}}_{\mathbf{i-1}}$ and $\underline{\mathbf{r}}_{\mathbf{i}}$ the location vectors to the points Q_{i-1} and Q_i, respectively, the following relation holds for a ray segment:

$$\underline{\mathbf{r}}_{\mathbf{i}} = \underline{\mathbf{r}}_{\mathbf{i-1}} + d\,\underline{\mathbf{w}}_{\mathbf{z}} \quad (d > 0), \tag{10.5}$$

where the d is the distance between Q_{i-1} and Q_i, i. e. the length of the ray segment. Note that in the following I assume that $\underline{\mathbf{w}}_{\mathbf{z}}$ is simply given by

$$\underline{\mathbf{w}}_{\mathbf{z}} = \begin{pmatrix}w_{z0} \\ w_{z1} \\ w_{z2}\end{pmatrix} \quad \text{with} \quad \|\underline{\mathbf{w}}_{\mathbf{z}}\| = 1. \tag{10.6}$$

10.3   Incident plane

The incident plane is constructed by means of the direction of a ray segment $\underline{\mathbf{w}}_\mathbf{z}$ and the interface normal $\underline{\mathbf{q}}_\mathbf{z}$. I define the normal to the incident plane by:

$$\underline{\mathbf{n}}_\mathbf{Inc} = \underline{\mathbf{q}}_\mathbf{z} \times \underline{\mathbf{w}}_\mathbf{z} \tag{10.7}$$

It is used to define the moving ray-centered coordinate system explained below.

10.4   Moving ray-centered coordinate system

To propagate the wavefront I use a moving ray-centered coordinate system. Within a layer the orientation of the moving ray-centered system is fixed. To define it consider the associated ray segment and its intersection point Q_i with the next interface (in ray direction). The z-axis is defined by the direction vector $\underline{\mathbf{w}}_\mathbf{z}$ of the ray segment. The x- and the y-axis are defined as follows: by means of the interface normal $\underline{\mathbf{q}}_\mathbf{z}$ at Q_i and the ray direction $\underline{\mathbf{w}}_\mathbf{z}$ I compute the incident plane, which contains both vectors. The x- and the y-axis are specified by this plane: the x-axis $\underline{\mathbf{w}}_\mathbf{x}$ lies in the incident plane; the y-axis $\underline{\mathbf{w}}_\mathbf{y}$ is normal to the incident plane:

$$\underline{\mathbf{w}}_\mathbf{z} \quad \text{unit ray direction vector,} \tag{10.8a}$$

$$\underline{\mathbf{w}}_\mathbf{y} = \frac{\underline{\mathbf{q}}_\mathbf{z} \times \underline{\mathbf{w}}_\mathbf{z}}{\|\underline{\mathbf{q}}_\mathbf{z} \times \underline{\mathbf{w}}_\mathbf{z}\|} = \frac{\underline{\mathbf{n}}_\mathbf{Inc}}{\|\underline{\mathbf{q}}_\mathbf{z} \times \underline{\mathbf{w}}_\mathbf{z}\|}, \tag{10.8b}$$

$$\underline{\mathbf{w}}_\mathbf{x} = \underline{\mathbf{w}}_\mathbf{y} \times \underline{\mathbf{w}}_\mathbf{z}, \tag{10.8c}$$

$$\text{where } \underline{\mathbf{q}}_\mathbf{z} \text{ is the interface normal}$$

$$\text{and} \quad \underline{\mathbf{q}}_\mathbf{z} \cdot \underline{\mathbf{w}}_\mathbf{z} > 0, \quad \|\underline{\mathbf{q}}_\mathbf{z}\| = 1.$$

The direction of the interface normal $\underline{\mathbf{q}}_\mathbf{z}$ is defined by the direction of the ray segment $\underline{\mathbf{w}}_\mathbf{z}$ such that the interface normal points away from the incident wavefront. From $\|\underline{\mathbf{w}}_\mathbf{z}\| = \|\underline{\mathbf{w}}_\mathbf{y}\| = 1$ and $\underline{\mathbf{w}}_\mathbf{y} \cdot \underline{\mathbf{w}}_\mathbf{z} = 0$, follows $\|\underline{\mathbf{w}}_\mathbf{x}\| = 1$. Therefore, an orthogonal base matrix is given by

$$\underline{\mathbf{W}} = \left(\underline{\mathbf{w}}_\mathbf{x}\underline{\mathbf{w}}_\mathbf{y}\underline{\mathbf{w}}_\mathbf{z}\right) . \tag{10.8d}$$

10.4.1   Transformation to ray-centered coordinate system

The orthogonal transformation matrix from a local (translated global) to the ray-centered system is given by the base matrix defined by eqs. (10.8):

$$\underline{\mathbf{T}}_\mathbf{IW} = \underline{\mathbf{W}} \tag{10.9}$$

or can be determined by eqs. (10.3) with $[\underline{\mathbf{y}}_\mathbf{x}, \underline{\mathbf{y}}_\mathbf{y}, \underline{\mathbf{y}}_\mathbf{z}]$ given by $[\underline{\mathbf{w}}_\mathbf{x}, \underline{\mathbf{w}}_\mathbf{y}, \underline{\mathbf{w}}_\mathbf{z}]$.

10.5 Local description of an interface

For the propagation law, no information about the interface is required. However, as explained above, the ray-centered coordinate system is defined by means of a local first order description of the interface that determines the interface normal. To compute the curvature change along a ray due to the transmission or reflection of the wave at an interface, a local second-order description of the interface is required. Furthermore, the curvature matrix of the interface has to be expressed in a specific interface coordinate system. The following explains the interface coordinate system and the determination of the interface curvature matrix in this system, since, in general the interface is expressed in global coordinates.

Consider a local coordinate system that is simply obtained by translation of the global coordinate system to the intersection point Q_i. Here, a local second-order description of the interface is given by

$$z = \frac{1}{2}\mathbf{x}^T\mathbf{C}\mathbf{x} + \mathbf{b}^T\mathbf{x} \tag{10.10}$$

$$\text{with} \quad \mathbf{C} = \begin{pmatrix} c_{00} & c_{01} \\ c_{01} & c_{11} \end{pmatrix}, \ \mathbf{b} = \begin{pmatrix} b_0 \\ b_1 \end{pmatrix}, \ \mathbf{x} = \begin{pmatrix} x \\ y \end{pmatrix}, \tag{10.11}$$

$$\text{and} \quad c_{00} = \frac{d^2z}{dx^2}, \ c_{01} = c_{10} = \frac{d^2z}{dxdy}, \ c_{11} = \frac{d^2z}{dy^2}, \tag{10.12}$$

$$b_0 = \frac{dz}{dx}, \ b_1 = \frac{dz}{dy}. \tag{10.13}$$

10.5.1 Interface coordinate system

For the transmission and reflection law one has to express the matrix $\mathbf{C}$ in the interface coordinate system

$$\underline{\mathbf{q}}_{\mathbf{z}} = \frac{\text{sgn}\left(w_{z2}\right)}{\sqrt{b_0^2 + b_1^2 + 1}} \begin{pmatrix} -b_0 \\ -b_1 \\ 1 \end{pmatrix}, \tag{10.14a}$$

$$\underline{\mathbf{q}}_{\mathbf{y}} = \frac{\underline{\mathbf{q}}_{\mathbf{z}} \times \underline{\mathbf{w}}_{\mathbf{z}}}{\|\underline{\mathbf{q}}_{\mathbf{z}} \times \underline{\mathbf{w}}_{\mathbf{z}}\|} = \underline{\mathbf{w}}_{\mathbf{y}}, \tag{10.14b}$$

$$\underline{\mathbf{q}}_{\mathbf{x}} = \underline{\mathbf{q}}_{\mathbf{y}} \times \underline{\mathbf{q}}_{\mathbf{z}}, \tag{10.14c}$$

with the base matrix

$$\underline{\mathbf{Q}} = (\underline{\mathbf{q}}_{\mathbf{x}}\, \underline{\mathbf{q}}_{\mathbf{y}}\, \underline{\mathbf{q}}_{\mathbf{z}}). \tag{10.14d}$$

The normalization of $\underline{\mathbf{q}}_{\mathbf{z}}$ and $\underline{\mathbf{q}}_{\mathbf{y}}$ is required to build an orthogonal base matrix $\underline{\mathbf{Q}}$: with $\|\underline{\mathbf{q}}_{\mathbf{y}}\| = \|\underline{\mathbf{q}}_{\mathbf{z}}\| = 1$ and $\underline{\mathbf{q}}_{\mathbf{y}} \cdot \underline{\mathbf{q}}_{\mathbf{z}} = 0$ follows $\|\underline{\mathbf{q}}_{\mathbf{x}}\| = 1$. Note that for this definition the ray direction $\underline{\mathbf{w}}_{\mathbf{z}}$ is the ray direction of the incident ray segment. The z-axis $\underline{\mathbf{q}}_{\mathbf{z}}$ is the interface normal that points

in propagation direction of the incident wave. The x-axis $\underline{\mathbf{q}}_{\mathbf{x}}$ lies in the incident plane, the y-axis $\underline{\mathbf{q}}_{\mathbf{y}}$ is normal to the incident plane. Therefore, the y-axis coincides with the y-axis of the incident ray-centered coordinate system. Variables with respect to the interface coordinate system are in the following indicated by the symbol "$\sim$".

10.5.2 Transformation to interface coordinate system

The orthogonal transformation matrix from a local (translated global) to the interface system is given the base matrix defined by eqs. (10.14)

$$\underline{\mathbf{T}}_{\mathbf{IQ}} = \underline{\mathbf{Q}} \tag{10.15}$$

or by eqs. (10.3) with $[\underline{\mathbf{y}}_{\mathbf{x}}, \underline{\mathbf{y}}_{\mathbf{y}}, \underline{\mathbf{y}}_{\mathbf{z}}] = [\underline{\mathbf{q}}_{\mathbf{x}}, \underline{\mathbf{q}}_{\mathbf{y}}, \underline{\mathbf{q}}_{\mathbf{z}}]$. The upper left 2×2 submatrix is in the following denoted by $\mathbf{Q}$.

10.5.3 Interface curvature matrix

The curvature matrix $\tilde{\mathbf{B}}$ in the interface system is given by (see appendix I):

$$\tilde{\mathbf{B}} = \frac{1}{\sqrt{b_0^2 + b_1^2 + 1}} \mathbf{Q}_{\mathbf{zyz}}^{\mathbf{T}} \, \mathbf{C} \, \mathbf{Q}_{\mathbf{zyz}} \tag{10.16}$$

10.6 Propagation law of curvature

This law is used to compute the change of the curvature along a single ray segment due to the propagation of the wavefront in a constant velocity layer. Therefore, let me consider an arbitrary point $P_1 = (x_1, y_1, z_1)$ and an initial point $P_0 = (x_0, y_0, z_0)$ of the ray segment. To compute the curvature at P_1 one requires the curvature matrix $\hat{\mathbf{A}}_{\mathbf{0}}$ at P_0 and the distance from P_0 to P_1. The latter is given by $v\Delta t$, where v is the velocity and Δt the time that the wavefront travels from P_0 to P_1.

$$\hat{\mathbf{R}}_{\mathbf{1}} = \hat{\mathbf{R}}_{\mathbf{0}} + v\Delta t \, \mathbf{I}, \tag{10.17}$$
$$\text{with} \quad \hat{\mathbf{R}}_{\mathbf{i}} = \hat{\mathbf{A}}_{\mathbf{i}}^{-1} \quad (i = 0, 1)$$
$$\text{and} \quad \Delta t = t_1 - t_0.$$

The matrix $\hat{\mathbf{R}}_{\mathbf{i}}$ denotes the radius matrix at a Point P_i and is given by the inverse of the curvature matrix $\hat{\mathbf{A}}_{\mathbf{i}}$. The matrix $\mathbf{I}$ is the identity matrix. Note that one does not have to transform the curvature matrix to the principal axes. However, to handle also the cases when the curvature matrix is singular, this transformation is recommended. One possibility is to apply the following steps:

1. compute the angle ϑ to the principal axes (appendix E):

$$\tan \hat{\vartheta} = \left(\hat{a}_{11} - \hat{a}_{00} + b \right) / \left(2 \hat{a}_{01} \right) \quad \text{with} \quad b = \sqrt[+]{\left(\hat{a}_{00} - \hat{a}_{11} \right)^2 + 4 \hat{a}_{01}^2},$$

where $\hat{a}_{ij}$ are the elements of $\mathbf{A_0}$.

2. express $\hat{\mathbf{A}}_0$ in the principal axes system: $\quad \bar{\mathbf{A}}_0 = \mathbf{D}_{\mathbf{z}}^{\mathbf{T}}(\vartheta) \hat{\mathbf{A}}_0 \mathbf{D}_{\mathbf{z}}(\vartheta)$.

3. invert $\bar{\mathbf{A}}_0$: $\quad \bar{\mathbf{R}}_0 = \bar{\mathbf{A}}_0^{-1} = \begin{pmatrix} 1/\bar{a}_{00} & 0 \\ 0 & 1/\bar{a}_{11} \end{pmatrix}$, where $\bar{a}_{ii}$ are the elements of $\bar{\mathbf{A}}_0$.

4. propagate to P_1: $\quad \bar{\mathbf{R}}_1 = \bar{\mathbf{R}}_0 + v\Delta t\, \mathbf{I}$.

5. invert $\bar{\mathbf{R}}_1$: $\quad \bar{\mathbf{A}}_1 = \bar{\mathbf{R}}_1^{-1} = \begin{pmatrix} 1/\bar{r}_{00} & 0 \\ 0 & 1/\bar{r}_{11} \end{pmatrix}$, where $\bar{r}_{ii}$ are the elements of $\bar{\mathbf{R}}_1$.

6. express $\bar{\mathbf{A}}_1$ in the moving ray-centered system: $\quad \hat{\mathbf{A}}_1 = \mathbf{D}_{\mathbf{z}}(\vartheta) \bar{\mathbf{A}}_1 \mathbf{D}_{\mathbf{z}}^{\mathbf{T}}(\vartheta)$.

If the curvature matrix $\hat{\mathbf{A}}_0$ is already expressed in principal axes (and this has to be checked due to the division by $\hat{a}_{01}$ in step 1), i.e. $\hat{a}_{01} = 0$, $\bar{\mathbf{A}}_i = \hat{\mathbf{A}}_i$ and steps 1, 2 and 6 are omitted.

10.7 Transmission and reflection laws for wavefront curvatures

Let me in the following denote the point, where the ray and the interface intersect each other, by Q_i. The direction of the incident ray segment is denoted by $\underline{\mathbf{w}}_{\mathbf{Iz}}$; the direction of the subsequent ray segment that is due to either transmission or reflection of the ray at Q_i is denoted by $\underline{\mathbf{w}}_{\mathbf{Tz}}$. The subsequent intersection point of the ray with the next encountered interface is denoted by Q_{i+1}. Further is the interface normal at Q_i denoted by $\underline{\mathbf{q}}_{\mathbf{Iz}}$; the interface normal at Q_{i+1} by $\underline{\mathbf{q}}_{\mathbf{Tz}}$. Different coordinate systems are involved in order to compute the transmitted or reflected wavefront curvature matrix at Q_i:

- $[\underline{\mathbf{w}}_{\mathbf{Ix}}, \underline{\mathbf{w}}_{\mathbf{Iy}}, \underline{\mathbf{w}}_{\mathbf{Iz}}]$: ray-centered system that is valid between Q_{i-1} and Q_i and constructed by means of eqs. (10.8) with $\underline{\mathbf{w}}_{\mathbf{Iz}}$ and $\underline{\mathbf{q}}_{\mathbf{Iz}}$. The incident curvature matrix $\hat{\mathbf{A}}_{\mathbf{I}}$ refers to this system.

- $[\underline{\mathbf{q}}_{\mathbf{Ix}}, \underline{\mathbf{q}}_{\mathbf{Iy}}, \underline{\mathbf{q}}_{\mathbf{Iz}}]$: interface system constructed by means of eqs. (10.14) with $\underline{\mathbf{w}}_{\mathbf{Iz}}$ and $\underline{\mathbf{q}}_{\mathbf{Iz}}$. The interface curvature matrix $\tilde{\mathbf{B}}$ refers to this system.

- $[\underline{\mathbf{w}}_{\mathbf{Tx}}, \underline{\mathbf{w}}_{\mathbf{Ty}}, \underline{\mathbf{w}}_{\mathbf{Tz}}]$: ray-centered system that is valid between Q_i and Q_{i+1} and constructed by means of eqs. (10.8) with $\underline{\mathbf{w}}_{\mathbf{Tz}}$ and $\underline{\mathbf{q}}_{\mathbf{Tz}}$. The transmitted or reflected curvature matrix $\hat{\mathbf{A}}_{\mathbf{T}}$ refers to this system.

- $[\underline{\mathbf{w}}_{\mathbf{Hx}}, \underline{\mathbf{w}}_{\mathbf{Hy}}, \underline{\mathbf{w}}_{\mathbf{Hz}}]$: intermediate system constructed by means of eqs. (10.8) with $\underline{\mathbf{w}}_{\mathbf{Tz}}$ and $\underline{\mathbf{q}}_{\mathbf{Iz}}$.

Transformation from the intermediate to the transmitted system

The intermediate system is a ray-centered system that, however, is not part of the moving ray-centered system. The z-axis $\underline{\mathbf{w}}_{\mathbf{Tz}}$ of the intermediate system coincides with the z-axis of transmitted system, but, the x-axis of the intermediate system lies in the incident plane constructed at Q_i whereas the x-axis of the transmitted system lies in the incident plane constructed for Q_{i+1}. Therefore, the transformation between the intermediate and the transmitted system is a rotation around $\underline{\mathbf{w}}_{\mathbf{Tz}}$. It is required to express the transmitted or reflected curvature matrix in the transmitted system rather than in the intermediate system as can be seen by the formulae for transmission and reflection presented below.

The transformation from the intermediate system to the transmitted system is given by (see eq. (5.8) in section 5.2.1):

$$\bar{\underline{\mathbf{T}}}_{\mathbf{W_H W_T}} = \underline{\mathbf{W}}_{\mathbf{H}}^{\mathbf{T}} \underline{\mathbf{W}}_{\mathbf{T}} . \tag{10.18}$$

As pointed out above this transformation is a rotation around the z-axis $\underline{\mathbf{w}}_{\mathbf{Tz}}$ by an angle γ. Required is only its upper left 2×2 submatrix, to which I refer to as $\mathbf{D}_{\mathbf{z}}(\gamma)$:

$$\mathbf{D}_{\mathbf{z}}(\gamma) = \bar{\mathbf{T}}_{\mathbf{W_H W_T}} . \tag{10.19}$$

An alternative solution to construct the matrix $\mathbf{D}_{\mathbf{z}}(\gamma)$ is to use the rotation matrices. Therefore, I firstly determine the transformation matrix $\underline{\mathbf{T}}_{\mathbf{IW_H}}$ to this system by means of eqs. (10.3) with $\underline{\mathbf{y}}_{\mathbf{i}}$ given by $\underline{\mathbf{w}}_{\mathbf{Hi}}$ (i=x,y,z). The upper left 2×2 submatrix is referred to as $\mathbf{T_{IW}}$; the associated angles ϕ_0, ϕ_1, ϕ_2 are denoted by $\phi_{H0}, \phi_{H2}, \phi_{H2}$. By means of this transformation I can proceed as in appendix D: the x-axis $\underline{\mathbf{w}}_{\mathbf{Tx}}$ of the ray-centered coordinate system for the next ray segment is expressed in the intermediate system, projected to the $x-y$ plane of the intermediate system, and finally normalized to get the angle γ:

$$\begin{pmatrix} \cos\gamma \\ \sin\gamma \end{pmatrix} = \frac{\tilde{\mathbf{t}}}{\|\tilde{\mathbf{t}}\|}, \quad \tilde{\mathbf{t}} = \mathbf{D}_{\mathbf{z}}\left(\phi_{H0}\right) \mathbf{D}_{\mathbf{y}}\left(\phi_{H1}\right) \mathbf{D}_{\mathbf{z}}\left(\phi_{HF}\right) \begin{pmatrix} w_{Tx0} \\ w_{Tx1} \end{pmatrix} + \begin{pmatrix} -w_{Tx2}\sin\phi_{H1}\cos\phi_{H2} \\ w_{Tx2}\sin\phi_{H1}\sin\phi_{H2} \end{pmatrix} . \tag{10.20}$$

Cosines of angles and auxiliary matrices

Required are only the cosines of the incidence angle ε_I and transmission or reflection angle ε_T

$$\cos\varepsilon_I = \underline{\mathbf{w}}_{\mathbf{Iz}} \cdot \underline{\mathbf{q}}_{\mathbf{Iz}}, \quad \cos\varepsilon_T = \underline{\mathbf{w}}_{\mathbf{Tz}} \cdot \underline{\mathbf{q}}_{\mathbf{Tz}}, \tag{10.21}$$

that are independent of the sign of ε_I, ε_T, respectively. Further I define the auxiliary matrices:

$$\mathbf{S} = \begin{pmatrix} \cos\varepsilon_I/\cos\varepsilon_T & 0 \\ 0 & 1 \end{pmatrix}, \quad \mathbf{S}_{\mathbf{T}}^{-1} = \begin{pmatrix} 1/\cos\varepsilon_T & 0 \\ 0 & 1 \end{pmatrix} .$$

10.7.1 Transmission and reflection law

$$\hat{\mathbf{A}}_{\mathbf{T}} = \mathbf{D}_{\mathbf{z}}^{\mathbf{T}}(\gamma) \left(\frac{v_T}{v_I} \mathbf{S} \, \hat{\mathbf{A}}_{\mathbf{I}} \, \mathbf{S} + \rho \, \mathbf{S}_{\mathbf{T}}^{-1} \, \tilde{\mathbf{B}} \, \mathbf{S}_{\mathbf{T}}^{-1} \right) \mathbf{D}_{\mathbf{z}}(\gamma) , \tag{10.22}$$

with $\quad \rho = \dfrac{v_T}{v_I} \cos \varepsilon_I - \cos \varepsilon_T \quad$ for transmission

and $\quad \rho = \dfrac{v_T}{v_I} \cos \varepsilon_I + \cos \varepsilon_T \quad$ for reflection.

10.8   Remarks

The ray-centered coordinate systems defined here and in chapter 6 are closely related: for an upcoming wavefront that emerges on a planar measurement surface the $[\underline{\mathbf{w}}_{\mathbf{x}} \, \underline{\mathbf{w}}_{\mathbf{y}}, \underline{\mathbf{w}}_{\mathbf{z}}]$ system defined by eqs. (10.8) coincides with the $[\underline{\mathbf{w}}_{\mathbf{x}}, \underline{\mathbf{w}}_{\mathbf{y}}, \underline{\mathbf{w}}_{\mathbf{z}}]$ defined in section 6.2 for $\varphi_F = 0$, i. e. with the $[\underline{\mathbf{v}}_{\mathbf{x}}, \underline{\mathbf{v}}_{\mathbf{y}}, \underline{\mathbf{w}}_{\mathbf{z}}]$ system (section 6.1).[1] This should be clear since the vector $\underline{\mathbf{v}}_{\mathbf{y}}$ is always contained in the measurement surface plane. Likewise, the y-axis defined by eqs. (10.8) lies in the measurement surface plane since the measurement surface normal is given by $\underline{\mathbf{e}}_{\mathbf{z}}$.

---

[1]Although the global system may be arbitrarily chosen in this chapter, this relationship is only valid if the global system is chosen like in chapter 6, i. e. the measurement surface is parallel to $x - y$ plane of the global system.

Chapter 11

Comparisons

In this chapter I compare the approximated traveltimes given by eq. (8.2b) to the traveltimes computed by means of a ray-tracer for the model shown in Figure 11.1. The model consists of three iso-velocity layers with velocities of 1.5, 2.5 and 4.0 km/s from top (light gray plane in Figure 11.1) to bottom. The traveltimes and the central ray (black line segments) were computed by a ray-tracer. To determine the approximated traveltimes (eq. (8.2b)), I had to compute the NIP and normal wavefront. This was done by means of the visualization program that has been developed in the framework of this thesis.

Figure 11.1 also shows the NIP and normal wavefronts in dark gray and medium gray, respectively, at different instants of time for a specified observation point $X_0 = (3.7 \text{ km}, 4.6 \text{ km}, 0 \text{ km})$ on the measurement surface. Figure 11.2a is a close up of Figure 11.1 and shows the wavefronts emerging at X_0. Figures 11.3a and 11.4a display the traveltimes for ZO and CS, respectively. The traveltimes computed with the ray-tracer are shown in black, the hyperbolic approximation (equation (8.2b)) is shown in gray. P_0 is given by X_0 and the ZO traveltime t_0=2.625 s.

Figures 11.2a,b also display the observation plane for a seismic line specified by an azimuth of $\beta = -75°$. The corresponding ZO and CS traveltimes are shown in Figures 11.3a,b and 11.4a,b. The same illustrations are given by Figures 11.5-11.7 for a seismic line with an azimuth of $\beta = 58°$. In the 2D traveltime plots P_0 is located at (0 km, t_0).

For the seismic line with an azimuth of $-75°$ (Figures 11.2-11.4) the moveout of the traveltime can be well fitted by a second-order approximation. In the case of the seismic line with an azimuth of $58°$ (Figures 11.5-11.7) the true traveltime surface has an inflection point near P_0. Therefore the range of a good approximation by a hyperbola is smaller than in the former case. However, such a case cannot be well approximated with a second-order approach.

Figures 11.8 and 11.9 show the common-shot traveltimes for a shot location at X_S=(4.3 km, 5.9 km, 0 km). The distance is $\sqrt{2}/10$ km to the observation point X_0=(4.4 km, 6.0 km, 0 km). As expected the approximation gets worse. This is due to the second-order approximation that is valid at X_0 which does not coincide with X_S in this case. Nevertheless, also in this case some signal will constructively contribute to the stack due to the pulse length of the wavelet.
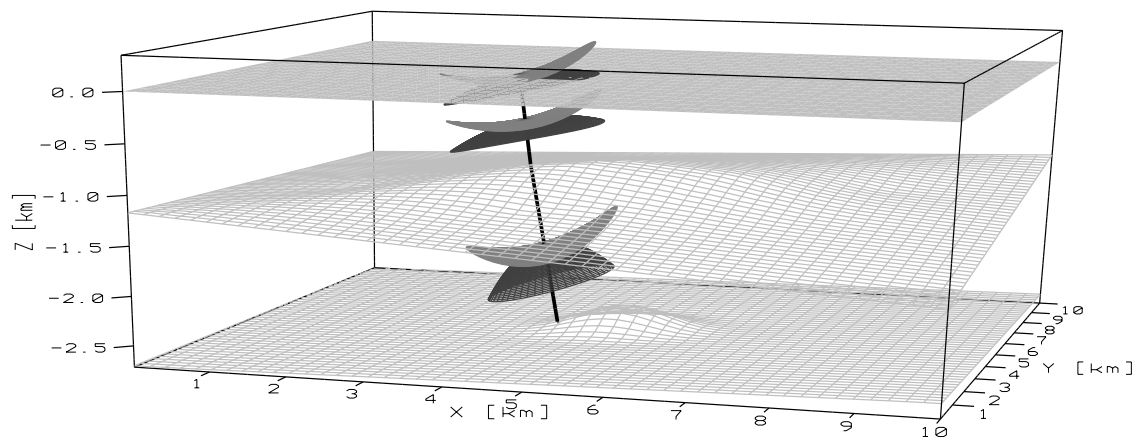
Figure 11.1: Model consisting of three iso-velocity layers. The interfaces are plotted in light gray; the light gray plane on top forms the measurement surface. The central ray is plotted in black and describes the direction of propagation of the NIP and the normal wavefronts. The NIP and the normal wavefronts are shown at different instants of time in dark and medium gray, respectively.
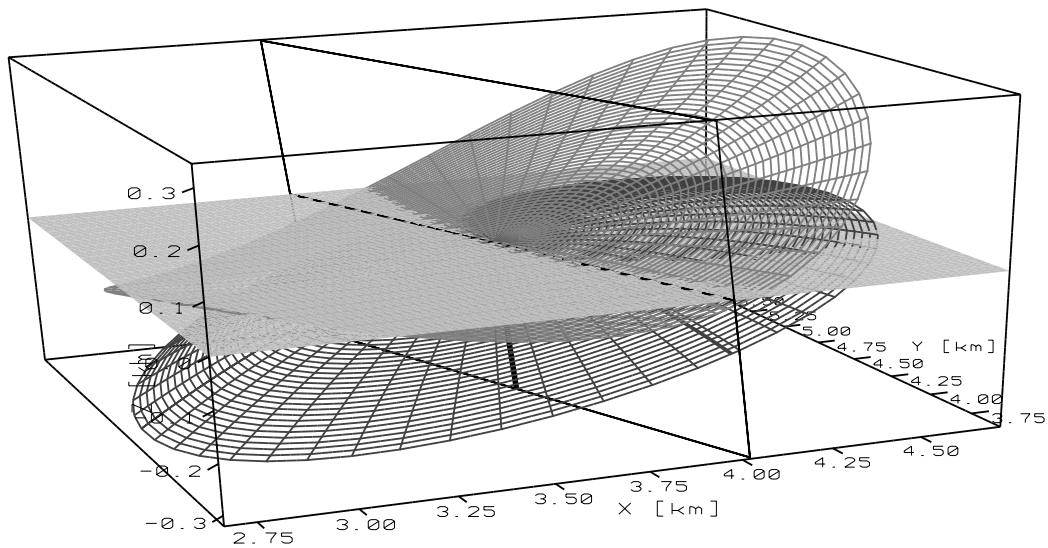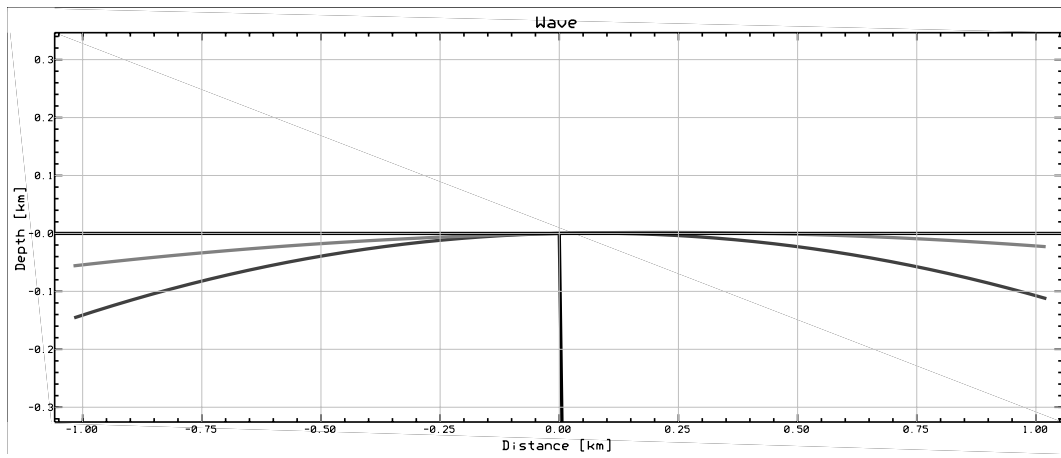
Figure 11.2:
a) NIP (dark gray) and normal (medium gray) wavefronts emerging at the measurement surface. The plane indicated by the black rectangle is the observation plane for a seismic line (black line on the measurement surface) with an azimuth of $\beta = -75°$.
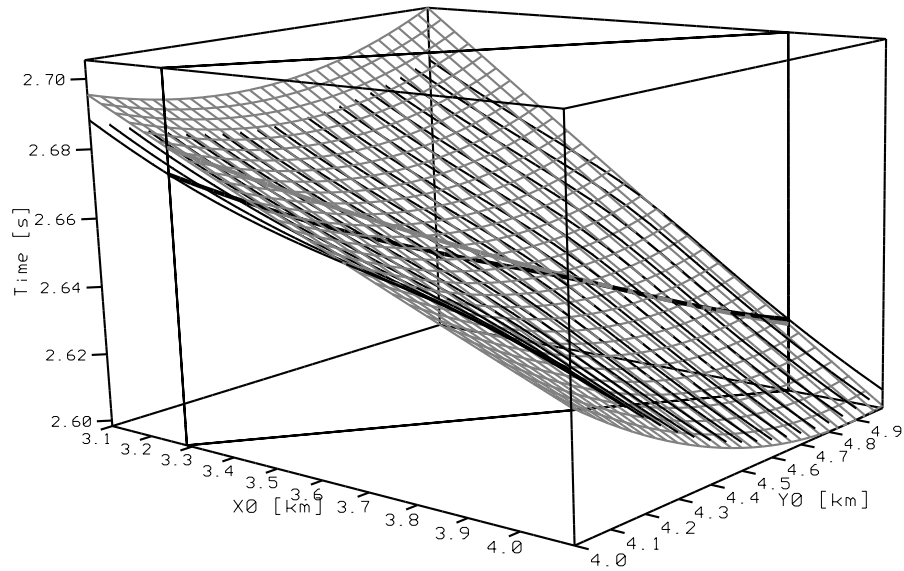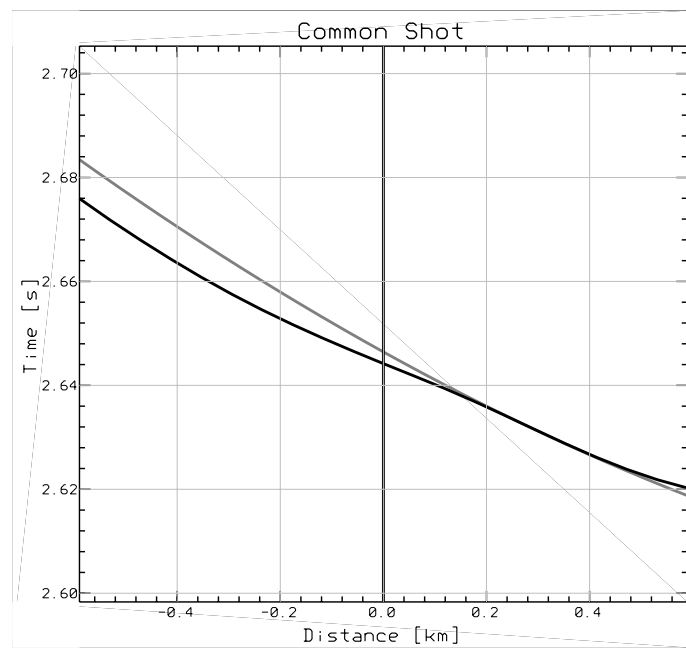b) NIP and normal wavefronts in the observation plane of Fig. 11.2a.
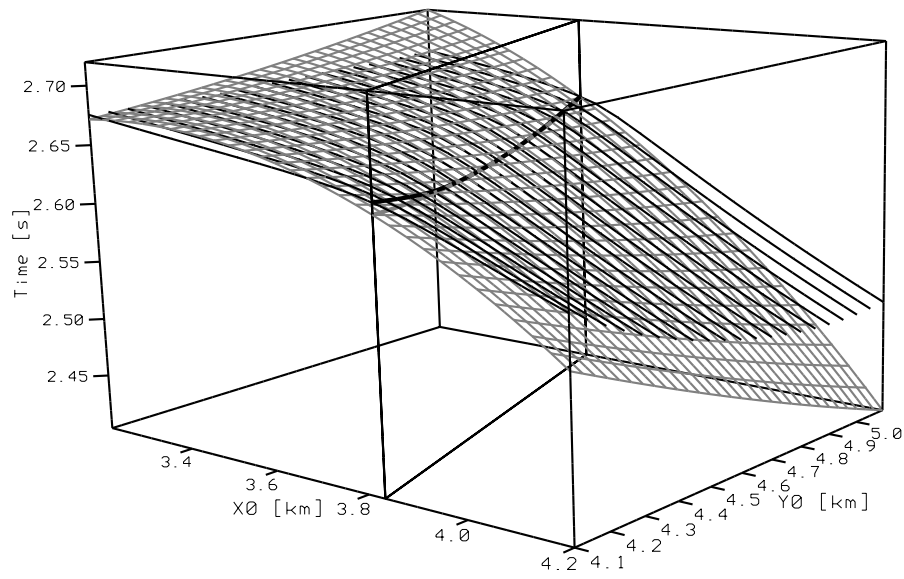
a)
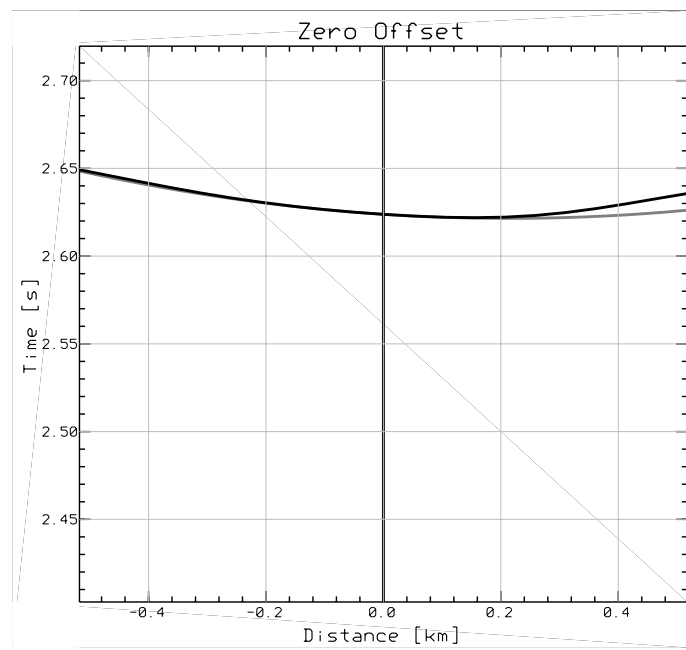
b)

Figure 11.3:
a) ZO traveltimes computed by a ray tracer (black) and approximative ZO traveltimes (gray) determined by the attributes of the normal wavefront. The black rectangle indicates the ZO section for the seismic line in Fig. 11.2a.
b) 2D display of the ZO section indicated by the black rectangle in Fig. 11.3a.

a)

b)
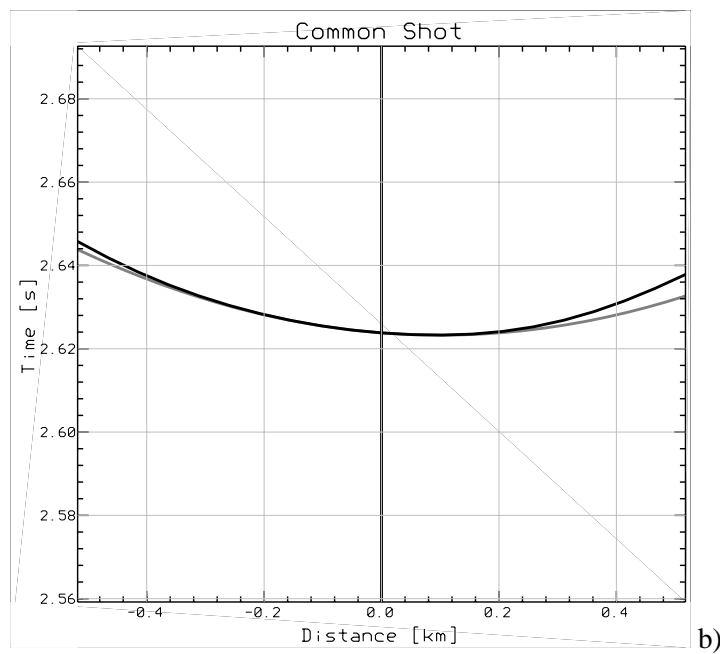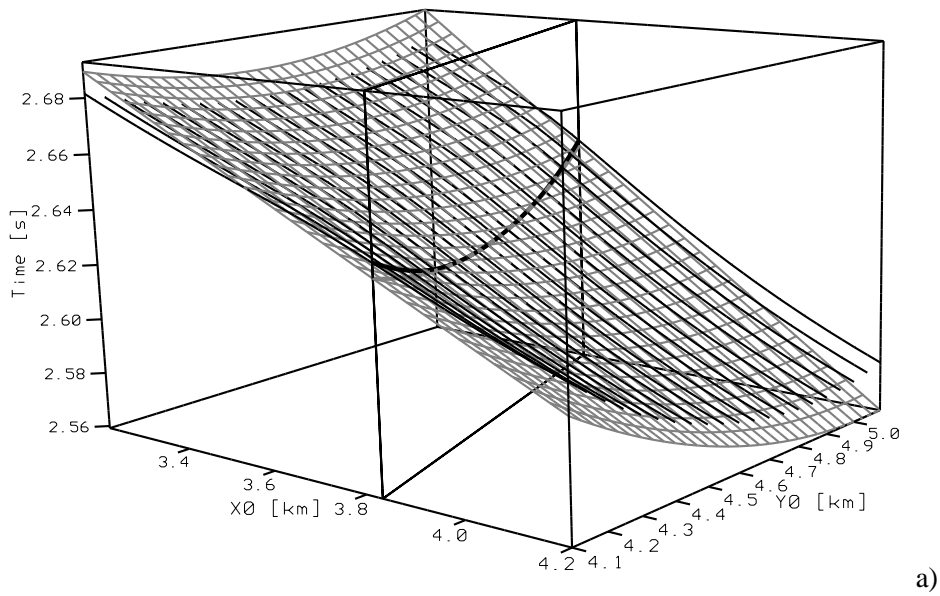
Figure 11.4:
a) CS traveltimes computed by a ray tracer (black) and approximative CS traveltimes (gray) determined by the attributes of the normal wavefront. The location of the shot coincides with the observation point X_0. The black rectangle indicates the CS section for the seismic line in Fig. 11.2a.
b) 2D display of the CS section indicated by the black rectangle in Fig. 11.4a.
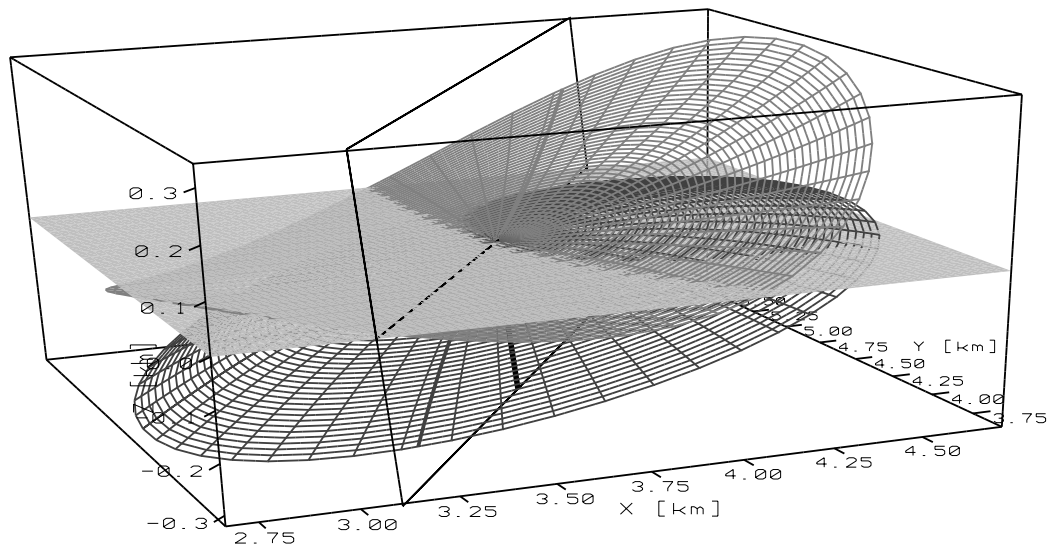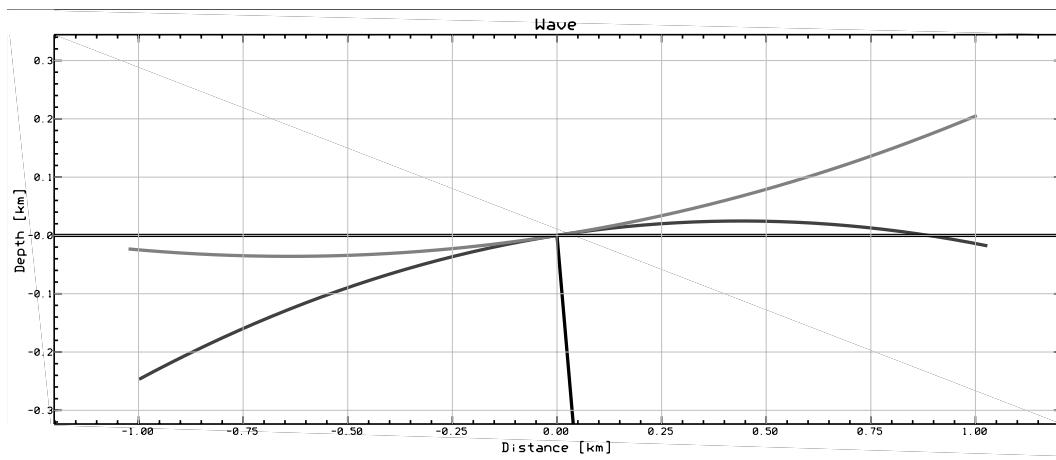
Figure 11.5:
a) NIP (dark gray) and normal (medium gray) wavefronts emerging at the measurement surface. The plane indicated by the black rectangle is the observation plane for a seismic line (black line on the measurement surface) with an azimuth of $\beta = 58°$.
b) NIP and normal wavefronts in the observation plane of Fig. 11.5a.
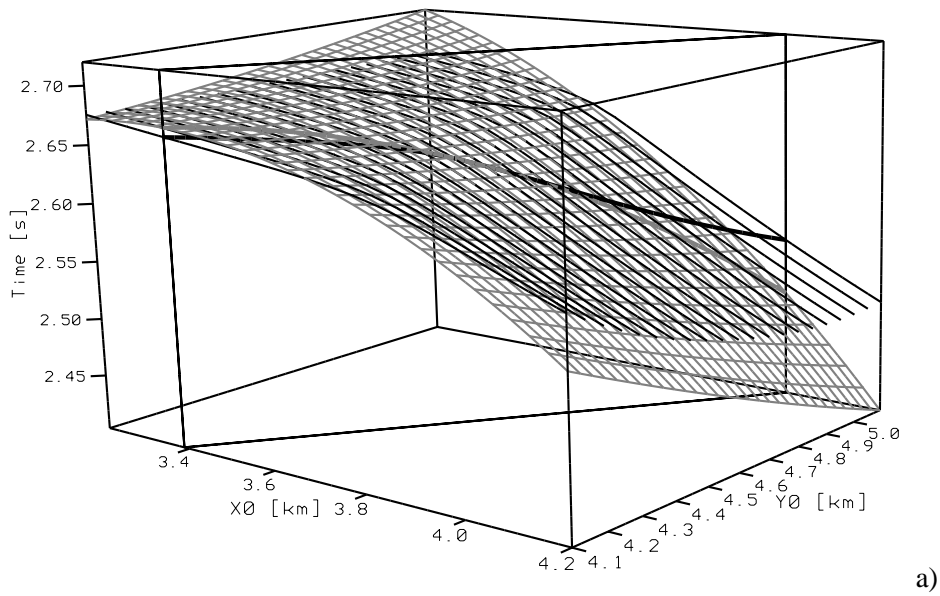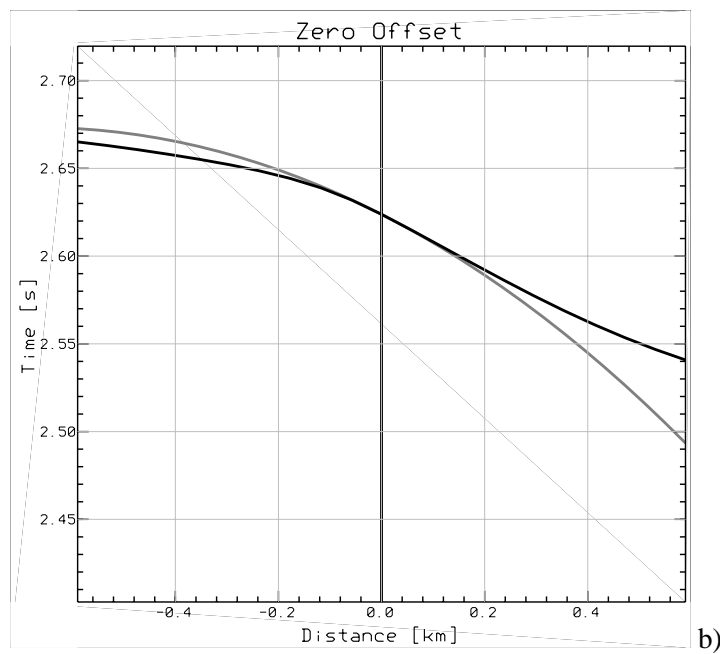
Figure 11.6:
a) ZO traveltimes computed by a ray tracer (black) and approximative ZO traveltimes (gray) determined by the attributes of the normal wavefront. The black rectangle indicates the ZO section for the seismic line in Fig. 11.5a.
b) 2D display of the ZO section indicated by the black rectangle in Fig. 11.6a.

a)

b)
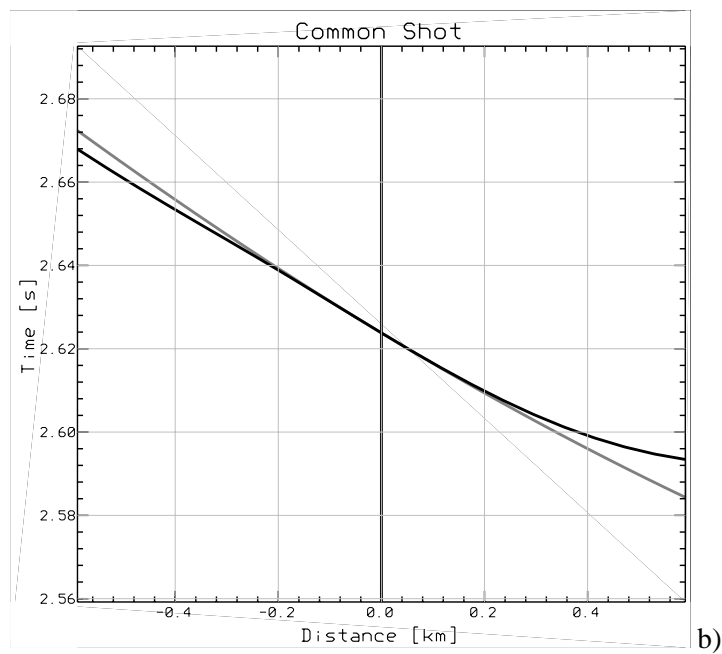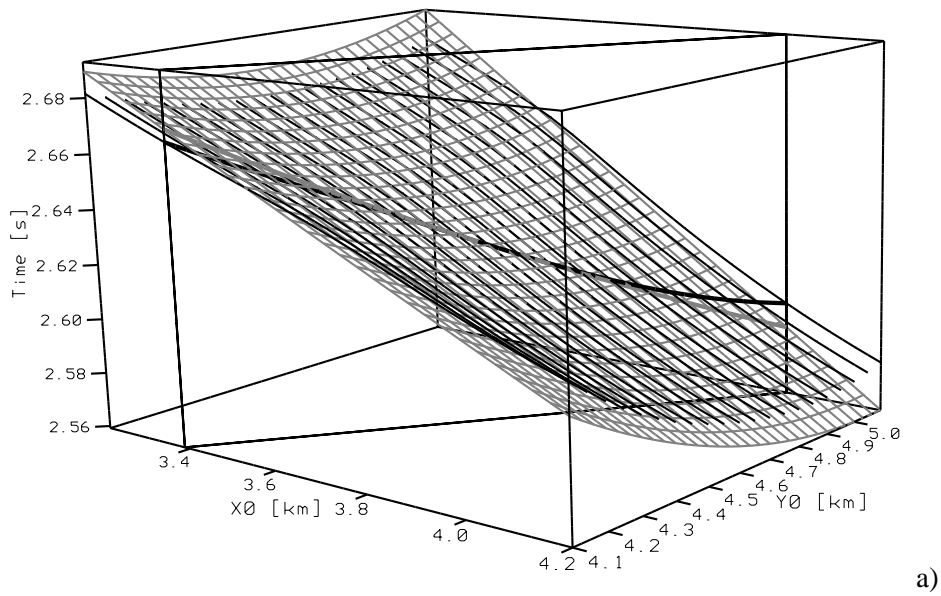
Figure 11.7:
a) CS traveltimes computed by a ray tracer (black) and approximative CS traveltimes (gray) deter-
mined by the attributes of the normal wavefront. The location of the shot coincides with the ob-
servation point X_0. The black rectangle indicates the CS section for the seismic line in Fig. 11.5a.
b) 2D display of the CS section indicated by the black rectangle in Fig. 11.7a.
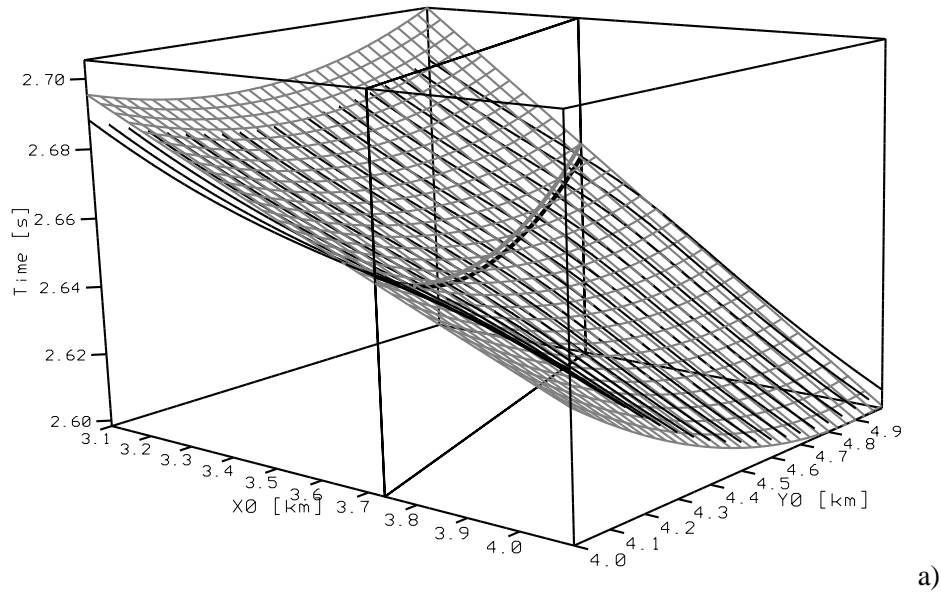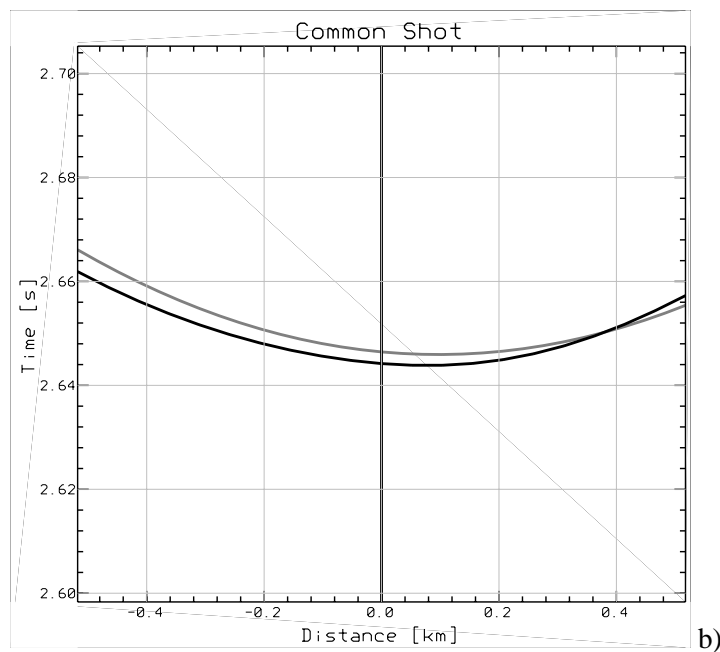
Figure 11.8:

a) CS traveltimes computed by a ray tracer (black) and approximative CS traveltimes (gray) determined by the attributes of the normal wavefront. The location of the shot is $X_S=(4.3, 5.9)$ with a distance of $0.1\sqrt{2}$ km to the observation point $X_0=(4.4, 6.0)$. The black rectangle indicates the CS section for a seismic line with an azimuth of $75°$.

b) 2D display of the CS section indicated by the black rectangle in Fig. 11.8a.

a)

b)

Figure 11.9:

a) CS traveltimes computed by a ray tracer (black) and approximative CS traveltimes (gray) determined by the attributes of the normal wavefront. The location of the shot is $X_S=(4.3, 5.9)$ with a distance of $0.1\sqrt{2}$ km to the observation point $X_0=(4.4, 6.0)$. The black rectangle indicates the CS section for a seismic line with an azimuth of $58°$.

b) 2D display of the CS section indicated by the black rectangle in Fig. 11.9a.

84

Chapter 12

Conclusions

The eight parameters involved in the CRS stack for 3D acquisitions locally describe two important hypothetical wavefronts at the measurement surface. These parameters serve for different applications in seismic reflection imaging as presented in the 2D case by Vieth (2001) and Majer (2000). The theory for the application of the parameters in 3D seismic imaging is already established with respect to the computation of geometrical spreading factors and projected Fresnel zones (Hubral et al., 1992a,b). Closer investigations have to be performed in order to determine a 3D velocity model by means of the parameters. Such a velocity model estimation delivers models with constant velocity layers or blocks. The presented method for the computation of the wavefront curvatures along a ray are involved in such a procedure. Other hints and formulae in this respect are given by Hubral and Krey (1980).

The determination of eight parameters is, of course, expensive, but, considering the profit that has been gathered in the 2D case, worthwhile. Furthermore, an accurate parameter estimation depends strongly on the acquisition geometry. Roughly speaking, the sparser the acquisition the less it is possible to determine the parameters in successive steps. The 3D CRS formulae are of the same structure than its 2D counterparts. This fact makes it possible to use the strategies established for the 2D case, i.e. to search for the parameters in subsets of the data and intermediate stacking results. Another possibility is to use the CRS stack for 2D acquisitions since the latter already accounts for 3D media. Other strategies are and will be subject to further investigations.

The comparisons for a model with iso-velocity layers and curved interfaces confirmed the demanded second-order fit of the 3D CRS formulae. This approves that the first- and second-order coefficients of the formulae can be accurately determined. Difficulties occur in cases when the traveltime surface has an inflection point near the expansion point of the formulae. Such situations can, however, not be well approximated by a second-order fit.

Appendix D

Transformation angles

In this appendix, I determine the angle γ between two specific planes. This angle often serves to perform rotations. Therefore, the correct sign of γ is required. The computation of γ by means of the normal to the plane is not appropriate, since this yields only the cosine of γ and would therefore require to distinguish between two different cases. Let me use the two coordinate systems $[\underline{e}_x, \underline{e}_y, \underline{e}_y]$ and $[\underline{y}_x, \underline{y}_y, \underline{y}_y]$ with the base matrices $\underline{I}$ and $\underline{Y} = (\underline{y}_x \underline{y}_y \underline{y}_y)$, respectively. The two considered planes are specified by the conditions:

- both planes contain the vector $\underline{y}_z$,

- the first plane contains the vector $\underline{y}_x$, i. e. $\underline{y}_y$ is a normal to this plane.

- the second plane contains a vector $\underline{x}$. The vector $\underline{x}$ is denoted by $\underline{s}$ if it falls into the $x - y$ plane of the $[\underline{e}_x, \underline{e}_y, \underline{e}_y]$ system.

If the transformation from the $[\underline{e}_x, \underline{e}_y, \underline{e}_y]$ to $[\underline{y}_x, \underline{y}_y, \underline{y}_y]$ system is given by

$$\underline{y}_i = \underline{\underline{T}}\underline{e}_i \quad (i=x,y,z), \quad \text{with} \quad \underline{\underline{T}} = \begin{pmatrix} t_{00} & t_{01} & t_{02} \\ t_{10} & t_{11} & t_{12} \\ t_{20} & t_{21} & t_{22} \end{pmatrix}. \tag{D.1}$$

The vector $\underline{x}$ expressed in the Y system is

$$\hat{\underline{x}} = \underline{\underline{T}}^{\mathrm{T}}\underline{x}. \tag{D.2}$$

One can now simply project the vector $\hat{\underline{x}}$ in direction of $\underline{y}_z$ to the base plane $x - y$ of the Y system by setting the third element $\hat{x}_2$ of $\hat{\underline{x}}$ to 0. This projected vector is given by

$$\hat{\mathbf{x}}_{\mathbf{p}} = \begin{pmatrix} \hat{x}_0 \\ \hat{x}_1 \end{pmatrix} = \underline{\underline{T}}_{23}^{\mathbf{T}} \begin{pmatrix} x_0 \\ x_1 \\ x_2 \end{pmatrix} \quad \text{where} \quad \underline{\underline{T}}_{23}^{\mathbf{T}} = \begin{pmatrix} t_{00} & t_{10} & t_{20} \\ t_{01} & t_{11} & t_{21} \end{pmatrix} \tag{D.3}$$

is the 2×3 submatrix of $\underline{\mathbf{T}}^{\mathbf{T}}$. By simple geometrical considerations in the plane that contains $\underline{\mathbf{x}}$ the modulus of $\hat{\mathbf{x}}_{\mathbf{p}}$ can also be obtained by

$$\|\hat{\mathbf{x}}_{\mathbf{p}}\| = \|\underline{\mathbf{x}}\| \, \|\sin\alpha_x\| = \|\underline{\mathbf{x}}\| \sqrt[+]{1 - \left(\frac{\underline{\mathbf{y}}_{\mathbf{z}} \cdot \underline{\mathbf{x}}}{\|\underline{\mathbf{y}}_{\mathbf{z}}\|\|\underline{\mathbf{x}}\|}\right)^2}\,, \tag{D.4}$$

where α_x is the angle between $\underline{\mathbf{y}}_{\mathbf{z}}$ and $\underline{\mathbf{x}}$.

The normalized vector $\hat{\mathbf{u}}$ of $\hat{\mathbf{x}}_{\mathbf{p}}$ then expresses the cosine and sine of the searched-for angle:

$$\hat{\mathbf{u}} = \begin{pmatrix} \cos\gamma \\ \sin\gamma \end{pmatrix} = \frac{\hat{\mathbf{x}}_{\mathbf{p}}}{\|\hat{\mathbf{x}}_{\mathbf{p}}\|}\,. \tag{D.5}$$

If $\underline{\mathbf{x}} = \underline{\mathbf{s}}$, where $\underline{\mathbf{s}}$ lies in the $x-y$ plane of the $[\underline{\mathbf{e}}_{\mathbf{x}}, \underline{\mathbf{e}}_{\mathbf{y}}, \underline{\mathbf{e}}_{\mathbf{y}}]$ system, i.e. $x_2 = 0$, the projected vector $\mathbf{x}_{\mathbf{p}}$ is given by

$$\hat{\mathbf{x}}_{\mathbf{p}} = \mathbf{T}^{\mathbf{T}}\mathbf{s}, \quad \text{where} \quad \mathbf{T}^{\mathbf{T}} = \begin{pmatrix} t_{00} & t_{10} \\ t_{01} & t_{11} \end{pmatrix} \tag{D.6}$$

is the 2×2 submatrix of $\underline{\mathbf{T}}^{\mathbf{T}}$.
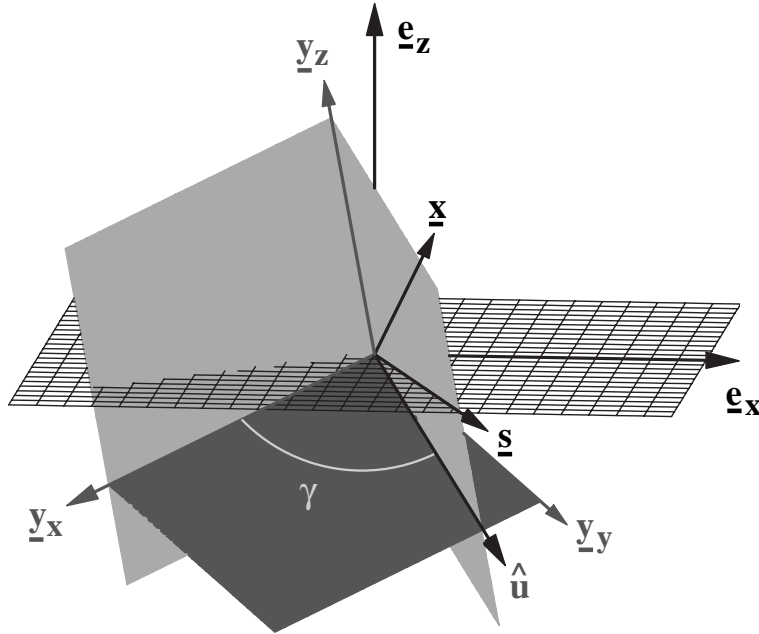
Figure D.1: determination of the angle between two planes. The angle γ can be obtained by the projection of the vector $\underline{\mathbf{x}}$ or $\underline{\mathbf{s}}$ to the dark gray plane and subsequent normalization.

Appendix E

Curvature matrix in principal axes

To express the curvature matrix in coordinates of the principal axes one has to compute the principal curvatures k_1, k_2 and the angle ϑ needed to rotate the x- and the y-axis to the principal axes (see eq. (5.31)).

A possible solution is to determine the eigenvalues and eigenvectors: the eigenvalues are the principal curvatures; the angle between the x-axis and the eigenvector associated with k_1 defines the angle ϑ to the principal axes coordinates. However, a simpler solution is provided by eq. (5.29). Rewriting this equation by expressing $\sin \vartheta$ and $\cos \vartheta$ by $\tan \vartheta$ yields

$$\begin{pmatrix} \hat{a}_{00} & \hat{a}_{01} \\ \hat{a}_{01} & \hat{a}_{11} \end{pmatrix} = \frac{1}{1 + \tan^2 \vartheta} \begin{pmatrix} k_1 + k_2 \tan^2 \vartheta & \tan \vartheta \, (k_1 - k_2) \\ \tan \vartheta \, (k_1 - k_2) & k_1 \tan^2 \vartheta + k_2 \end{pmatrix}. \tag{E.1}$$

Solving this equation for k_1, k_2 and $\tan \vartheta$ yields[1]

$$k_1 = \frac{1}{2} \left(\hat{a}_{00} + \hat{a}_{11} + b \right), \tag{E.2}$$

$$k_2 = \frac{1}{2} \left(\hat{a}_{00} + \hat{a}_{11} - b \right), \tag{E.3}$$

$$\tan \vartheta = \begin{cases} \left(\hat{a}_{11} - \hat{a}_{00} + b \right) / \left(2 \hat{a}_{01} \right) & \text{for} \quad \hat{a}_{01} \neq 0 \\ 0 & \text{for} \quad \hat{a}_{01} = 0 \end{cases} \tag{E.4}$$

$$\text{with} \quad b = \sqrt[+]{\left(\hat{a}_{00} - \hat{a}_{11} \right)^2 + 4 \hat{a}_{01}^2}. \tag{E.5}$$

Note that the second case $\hat{a}_{01} = 0$ for $\tan \vartheta$ only states that the curvature matrix is already expressed in a principal axes system. Then k_1 and k_2 reduce to $\hat{a}_{00}$ and $\hat{a}_{11}$, respectively.

---

[1]Actually, two solutions are determined. Both can be used; the second solution interchanges k_1 and k_2 of the first solution and provides an angle ϑ that is $\vartheta + 90°$ of the first solution. According to eq. (5.29), I use the solution where $R_0 = \hat{a}_{00}$ and $k_1 = \hat{a}_{11}$ for $\vartheta = 0$.

Appendix F

Relationships of 2D and 3D attributes

F.1   Relationship of angles

Let me specify the seismic lines by

$$\underline{\mathbf{s_0}} = \begin{pmatrix} \cos\beta_0 \\ \sin\beta_0 \\ 0 \end{pmatrix}, \ \underline{\mathbf{s_1}} = \begin{pmatrix} \cos\beta_1 \\ \sin\beta_1 \\ 0 \end{pmatrix}. \tag{F.1}$$

and the vectors

$$\mathbf{s_0} = \begin{pmatrix} \cos\beta_0 \\ \sin\beta_0 \end{pmatrix}, \ \mathbf{s_1} = \begin{pmatrix} \cos\beta_1 \\ \sin\beta_1 \end{pmatrix} \text{ and } \mathbf{w_z} = \begin{pmatrix} w_0 \\ w_1 \end{pmatrix} = \begin{pmatrix} \cos\varphi_0 \sin\varphi_1 \\ \sin\varphi_0 \sin\varphi_1 \end{pmatrix}. \tag{F.2}$$

on the measurement surface.

An angle α_i detected by the CRS stack for 2D is the angle between the vector $\underline{\mathbf{w_z}}$ and the normal to the seismic line in the corresponding observation plane (eq. (7.1)). Therefore, the relationships are given by:

$$\underline{\mathbf{w_z}} \cdot \underline{\mathbf{s_0}} = \cos\left(\frac{\pi}{2} - \alpha_0\right) = \sin\alpha_0, \tag{F.3}$$

$$\underline{\mathbf{w_z}} \cdot \underline{\mathbf{s_1}} = \cos\left(\frac{\pi}{2} - \alpha_1\right) = \sin\alpha_1. \tag{F.4}$$

These equations can be formulated by means of a single matrix equation:

$$\mathbf{a} = \mathbf{S}^{\mathbf{T}}\mathbf{w_z} \quad \text{with} \quad \mathbf{S} = (\mathbf{s_0}\,\mathbf{s_1}) = \begin{pmatrix} \cos\beta_0 & \cos\beta_1 \\ \sin\beta_0 & \sin\beta_1 \end{pmatrix} \quad \text{and} \quad a = \begin{pmatrix} \sin\alpha_0 \\ \sin\alpha_1 \end{pmatrix}. \tag{F.5}$$

Therefore $\mathbf{w_z}$ is given by

$$\mathbf{w_z} = \left(\mathbf{S}^{\mathbf{T}}\right)^{-1}\mathbf{a}, \tag{F.6}$$

$$\begin{pmatrix} w_0 \\ w_1 \end{pmatrix} = \begin{pmatrix} \cos\varphi_0 \sin\varphi_1 \\ \sin\varphi_0 \sin\varphi_1 \end{pmatrix} = \frac{1}{\det \mathbf{S}^{\mathbf{T}}} \begin{pmatrix} \sin\beta_1 & -\sin\beta_0 \\ -\cos\beta_1 & \cos\beta_0 \end{pmatrix} \begin{pmatrix} \sin\alpha_0 \\ \sin\alpha_1 \end{pmatrix}. \tag{F.7}$$

The solutions of eq. (F.7) for φ_0 and φ_1 are given by eqs. (9.5).

F.2   Relationship of radii of curvature

The observation plane for a seismic line is specified by the normal (eq. (7.1)) to the observation plane which contains the direction vector of the seismic line $\underline{\mathbf{s_i}}$ and the direction vector $\underline{\mathbf{w_z}}$ of the central ray (determined by eqs. (9.5)). The unit vectors $\underline{\mathbf{s_i}}$ that specify the three different seismic lines are denoted by:

$$\underline{\mathbf{s_i}} = \begin{pmatrix} \cos\beta_i \\ \sin\beta_i \\ 0 \end{pmatrix} \quad (i = 0, 1, 2). \tag{F.8}$$

The problem to be solved is to determine the symmetric matrix $\mathbf{A}$ which describes the wavefront (eq. (5.29)) in the ray-centered coordinate system. Therefore the three unknowns are $\hat{a}_{00}$, $\hat{a}_{11}$ and $\hat{a}_{01}$. Known are the curvatures of the wavefront in three different observation planes ($k_i = \frac{1}{R_i}, i = 0, 1, 2$). By Euler's equation

$$k_i = k_1 \cos^2\vartheta_i + k_2 \sin^2\vartheta_i \quad (i = 0, 1, 2), \tag{F.9}$$

a curvature k_i in an observation plane is related to the principal curvatures (k_1, k_2) by the angles ϑ_i between the observation plane and the normal section plane of the first principal curvature k_1. Therefore, ϑ_i is given by $\vartheta_i = \gamma_i - \vartheta$, where γ_i is defined by eq. (7.4b) and the angle ϑ to the first principal axes (see chapter 5). Then eqs. (F.9) can be formulated as:

$$k_i = k_1 \cos^2(\gamma_i - \vartheta) + k_2 \sin^2(\gamma_i - \vartheta) \quad (i = 0, 1, 2). \tag{F.10}$$

The three unknowns k_1, k_2 and ϑ could be used to compute the matrix $\mathbf{A}$ (eq. (5.29)). However, the solution of eqs. (F.10) is quite complicated and not suitable for programming purposes.

Therefore, I will use another approach, namely directional derivatives of the second order. The directional derivative of order N of a function $f(x, y)$ in direction $\mathbf{u}$ at (x_0, y_0) is given by

$$D_{\mathbf{u}}^N\{f\}(x_0, y_0) = \sum_{p=0}^{N} \frac{N!}{p!(N-p)!} u_0^p u_1^{N-p} D_x^p D_y^{N-p}\{f\}(x_0, y_0) \quad \text{with} \quad \mathbf{u} = \begin{pmatrix} u_0 \\ u_1 \end{pmatrix}. \tag{F.11}$$

Here, D_ξ^k denotes the kth partial derivative with respect to ξ, i.e. $\frac{\partial^k}{\partial \xi^k}$. In my case the function $f(x, y)$ is given by the local description of the wavefront surface in the ray-centered coordinate system:

$$-\hat{z}(\hat{x}, \hat{y}) = \frac{1}{2}\hat{a}_{00}\hat{x}^2 + \frac{1}{2}\hat{a}_{11}\hat{y}^2 + \hat{a}_{01}\hat{x}\hat{y}. \tag{F.12}$$

To make use of a directional derivative in the ray-centered coordinate system, one first has to determine the angle γ_i between the observation plane and the plane that contains the x- and z-axis of the ray-centered system. This angle allows to compute the direction vector $\hat{\mathbf{u_i}}$ in the $x - y$ plane of the ray-centered system.

F.2.1 Angle to an observation plane

The angle between an observation plane (eq. (7.1)) and the plane that contains the x- and the z-axis of the ray-centered system is given by eq. (7.4b), which states

$$\hat{\mathbf{u}}_{\mathbf{i}} = \begin{pmatrix} \cos \gamma_i \\ \sin \gamma_i \end{pmatrix} = \frac{\mathbf{T}^{\mathsf{T}} \mathbf{s}_{\mathbf{i}}}{\sqrt{1 - \left(\mathbf{w}_{\mathbf{z}} \cdot \mathbf{s}_{\mathbf{i}} \right)^2}} \qquad \mathbf{s}_{\mathbf{i}} = \begin{pmatrix} \cos \beta_i \\ \sin \beta_i \end{pmatrix}.$$

F.2.2 Curvature matrix

Now, the goal is to determine the matrix $\mathbf{A}$ in the ray-centered system. The curvature detected in an observation plane is equal to the directional derivative of the second order in direction of $\hat{\mathbf{u}}_{\mathbf{i}} = \begin{pmatrix} \cos \gamma_i \\ \sin \gamma_i \end{pmatrix}$ where additionally the minus sign defined in eq. (5.28b) has to be taken into account:

$$k_i = -D^2_{\hat{\mathbf{u}}_{\mathbf{i}}} \{\hat{z}\} (0, 0). \tag{F.13}$$

This is based on the fact that the observation plane is a normal section plane spanned by $\hat{\mathbf{u}}_{\mathbf{i}}$ and the z-axis of the ray-centered system. Thus, one can set up the three equations:

$$k_i = \cos^2 \gamma_i a_{00} + \sin^2 \gamma_i a_{11} + 2 \cos \gamma_i \sin \gamma_i \hat{a}_{01} \quad (i = 0, 1, 2). \tag{F.14}$$

In matrix notation:

$$\underline{\mathbf{k}} = \underline{\mathbf{B}} \, \underline{\hat{\mathbf{a}}} \tag{F.15}$$

$$\text{with} \quad \underline{\mathbf{k}} = \begin{pmatrix} k_0 \\ k_1 \\ k_2 \end{pmatrix}, \quad \underline{\mathbf{B}} = \begin{pmatrix} \cos^2 \gamma_0 & \sin^2 \gamma_0 & 2 \cos \gamma_0 \sin \gamma_0 \\ \cos^2 \gamma_1 & \sin^2 \gamma_1 & 2 \cos \gamma_1 \sin \gamma_1 \\ \cos^2 \gamma_2 & \sin^2 \gamma_2 & 2 \cos \gamma_2 \sin \gamma_2 \end{pmatrix}, \quad \underline{\hat{\mathbf{a}}} = \begin{pmatrix} \hat{a}_{00} \\ \hat{a}_{11} \\ \hat{a}_{01} \end{pmatrix}. \tag{F.16}$$

The solutions for the elements $\hat{a}_{ij}$ of the matrix $\hat{\mathbf{A}}$ are given by:

$$\underline{\hat{\mathbf{a}}} = \underline{\mathbf{B}}^{-1} \underline{\mathbf{k}} \tag{F.17}$$

$$\text{with} \quad \underline{\mathbf{B}}^{-1} = \frac{1}{\det \underline{\mathbf{B}}} \begin{pmatrix} \underline{\tilde{\mathbf{b}}}_{\mathbf{0}} & \underline{\tilde{\mathbf{b}}}_{\mathbf{1}} & \underline{\tilde{\mathbf{b}}}_{\mathbf{2}} \end{pmatrix}, \tag{F.18}$$

$$\underline{\tilde{\mathbf{b}}}_{\mathbf{0}} = \begin{pmatrix} 2 \cos \gamma_2 \sin \gamma_2 \sin^2 \gamma_1 - 2 \cos \gamma_1 \sin \gamma_1 \sin^2 \gamma_2 \\ 2 \cos \gamma_1 \sin \gamma_1 \cos^2 \gamma_2 - 2 \cos \gamma_2 \sin \gamma_2 \cos^2 \gamma_1 \\ \cos^2 \gamma_1 - \cos^2 \gamma_2 \end{pmatrix}, \tag{F.19}$$

$$\underline{\tilde{\mathbf{b}}}_{\mathbf{1}} = \begin{pmatrix} 2 \cos \gamma_0 \sin \gamma_0 \sin^2 \gamma_2 - 2 \cos \gamma_2 \sin \gamma_2 \sin^2 \gamma_0 \\ 2 \cos \gamma_2 \sin \gamma_2 \cos^2 \gamma_0 - 2 \cos \gamma_0 \sin \gamma_0 \cos^2 \gamma_2 \\ \cos^2 \gamma_2 - \cos^2 \gamma_0 \end{pmatrix}, \tag{F.20}$$

$$\underline{\tilde{\mathbf{b}}}_{\mathbf{2}} = \begin{pmatrix} 2 \cos \gamma_1 \sin \gamma_1 \sin^2 \gamma_0 - 2 \cos \gamma_0 \sin \gamma_0 \sin^2 \gamma_1 \\ 2 \cos \gamma_0 \sin \gamma_0 \cos^2 \gamma_1 - 2 \cos \gamma_1 \sin \gamma_1 \cos^2 \gamma_0 \\ \cos^2 \gamma_0 - \cos^2 \gamma_1 \end{pmatrix}. \tag{F.21}$$

Appendix G

Proof of traveltime formulae

In chapter 8 I established the new traveltime formulae (8.2) more or less intuitively by transferring the formulae of the 2D to the 3D case. In this chapter I give the mathematical proof of these formulae. Starting point of all is Hamilton's equation for reflected events which describes the traveltime difference between the central ray and a neighboring ray from any shot to any receiver location. The traveltime difference will be tailored up to the first order which implies a second-order traveltime approximation of the neighboring ray. This traveltime approximation is often named the paraxial approximation (Červený, 2001). By using concepts of geometrical optics, which Bortfeld (1989) calls geometrical seismics when applied to seismology, I will relate the first-order coefficients in Hamilton's equation to wavefront curvatures. In this way, wavefront curvatures are introduced in the traveltime formulae. Considering the NIP and normal wave experiments, this finally leads to eqs. (8.2).

G.1   Hamilton's equation

In Figure G.1, a source S and receiver G of a reflected ray are located on a flat measurement surface in the vicinity of the source/receiver position X_0 of the central (ZO) ray. The origin of the in the following used local observation coordinate system is chosen at X_0. For the specification of rays on the measurement surface I use four 3D vectors expressed in the local observation coordinate system (see Figure G.1). They are the location vector $\underline{\mathbf{x}}_\mathbf{s}$ and ray slowness vector $\underline{\mathbf{p}}_\mathbf{s}$ at the source as well as the location vector $\underline{\mathbf{x}}_\mathbf{g}$ and ray slowness vector $\underline{\mathbf{p}}_\mathbf{g}$ at the receiver. I denote the slowness vector at the central receiver at X_0 by $\underline{\mathbf{p}}_\mathbf{0}$ and, consequently, at the coincident source location with $^-\underline{\mathbf{p}}_\mathbf{0}$.

The above described quantities are the ingredients of Hamilton's equation (see, e.g., Bortfeld, 1989)

$$dt = \underline{\mathbf{p}}_\mathbf{g} \cdot d\underline{\mathbf{x}}_\mathbf{g} - \underline{\mathbf{p}}_\mathbf{s} \cdot d\underline{\mathbf{x}}_\mathbf{s} \,, \tag{G.1}$$

where dt describes the traveltime difference between the central ray and the neighboring ray from S to G. Please note, eq. (G.1) is an alternative mathematical formulation of Fermat's principle.
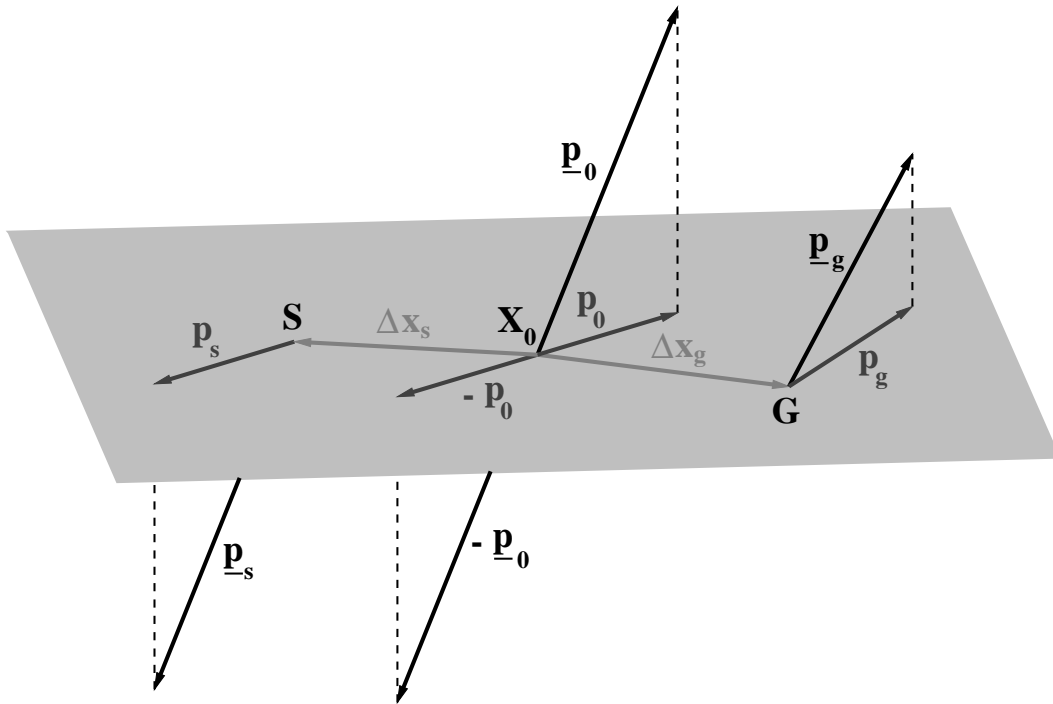
Figure G.1: quantities on the measurement surface describing a paraxial ray from S to G with respect to the central ray at point X_0.
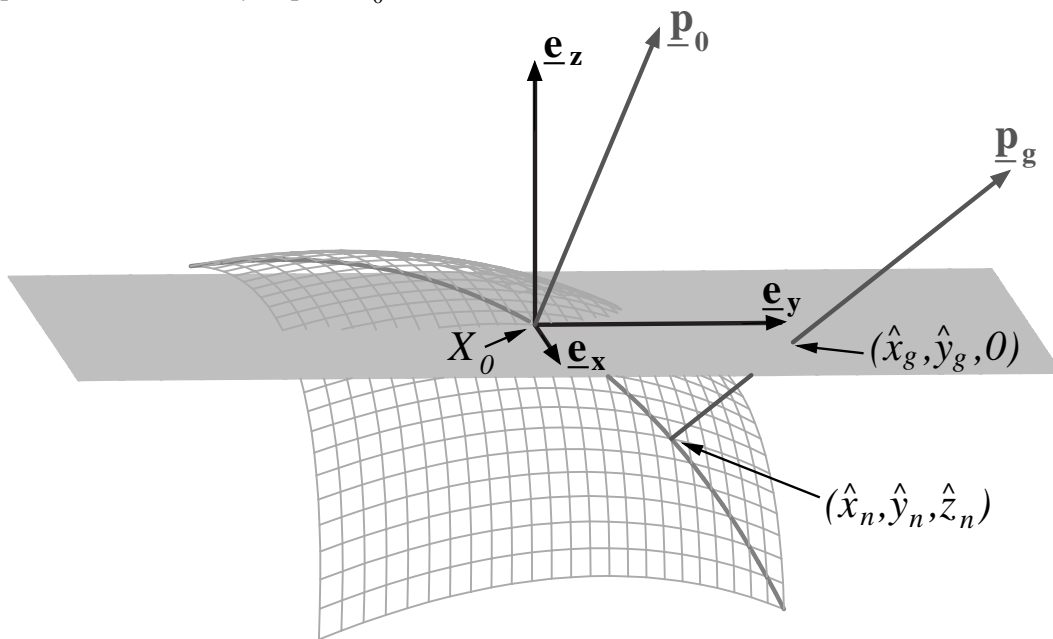

Figure G.2: a wavefront emerging at the central point X_0. Depicted in dark gray are the central slowness vector $\mathbf{p_0}$ and the slowness vector $\mathbf{p_g}$ at G of a neighboring ray.

It states that the first derivative of the traveltime in direction perpendicular to the ray vanishes. Schleicher et al. (2001) showed that eq. (G.1) can be derived via the eikonal equation. Bortfeld (1989) pointed out that proofs of eq. (G.1) exist solely basing on rules for refraction and reflection.

When establishing a second-order approximation of the traveltime in the variables $\underline{\mathbf{x_g}}$ and $\underline{\mathbf{x_s}}$ then terms of powers > 1 in $\underline{\mathbf{x_g}}$ and $\underline{\mathbf{x_s}}$ of eq. (G.1) can be neglected. Bortfeld (1989) showed that the third-component products of the dot product in Hamilton's equation (G.1) are already of second or higher order in $\underline{\mathbf{x_g}}$ and $\underline{\mathbf{x_s}}$. Thus, I neglect these products in eq. (G.1) which yields

$$dt \approx \mathbf{p_g} \cdot d\mathbf{x_g} - \mathbf{p_s} \cdot d\mathbf{x_s} . \tag{G.2}$$

$\mathbf{p_g}$ and $\mathbf{p_s}$ are the projections of $\underline{\mathbf{p_g}}$ and $\underline{\mathbf{p_s}}$ onto the measurement surface in direction of the surface normal. Moreover, I expand $\mathbf{p_s}$ and $\mathbf{p_g}$ in a Taylor series of $\mathbf{x_s}$ and $\mathbf{x_g}$ and take for eq.(G.2) only the terms up to the first-order into account. Please note, the latter statement is in fact nothing else than what the paraxial approximation implies—a linear dependence of the parameters describing a paraxial ray at its source and receiver in the vicinity of the central ray Červený, 2001).

G.2   Ray slowness vectors and wavefront curvatures

In this section I relate the ray slowness vectors at S and G of the ray in the vicinity of the central ray to wavefront curvatures. Thus, these wavefront curvatures are introduced in eq. (G.2). For this purpose all derivations in the following are done in the ray-centered coordinate $[\underline{\mathbf{v_x}} \underline{\mathbf{v_y}}, \underline{\mathbf{w_z}}]$ system defined in section 6. In this way, the considerations are simpler than in the local observation coordinate system .

Let us have a look at Figure G.2 where an up-going wavefront emerging at the central point X_0 is depicted. If the wave propagation velocity in the vicinity of the central point is constant, the slowness vector $\underline{\hat{\mathbf{p}}}_\mathbf{g}$ of any paraxial ray at the receiver can be described by a normalized vector $\underline{\hat{\mathbf{n}}}_\mathbf{0}$ perpendicular to this wavefront:

$$\underline{\hat{\mathbf{p}}}_\mathbf{g} = \frac{1}{v_0}\underline{\hat{\mathbf{n}}}_\mathbf{0} . \tag{G.3}$$

In the following, I assume that the wavefront is a paraboloid. Please note, this is no necessary restriction. The wavefront could have any other representation. In the ray-centered coordinate system the paraboloid is expressed by (see eq. (5.28a))

$$\hat{z} = -\frac{1}{2}\hat{\mathbf{x}}^\mathbf{T}\hat{\mathbf{A}}_\mathbf{g}\hat{\mathbf{x}} , \tag{G.4}$$

where $\hat{\mathbf{A}}_\mathbf{g}$ is the symmetric curvature matrix of the emerging wavefront. Then, the vector $\underline{\hat{\mathbf{n}}}_\mathbf{0}$ perpendicular to the paraboloid at point $(\hat{x}_n, \hat{y}_n, \hat{z}_n)$ on the wavefront is given by

$$\underline{\hat{\mathbf{n}}}_\mathbf{0} = \frac{1}{\sqrt{(\hat{a}_{g,00}\hat{x}_n + \hat{a}_{g,01}\hat{y}_n)^2 + (\hat{a}_{g,01}\hat{x}_n + \hat{a}_{g,1}\hat{y}_n)^2 + 1}} \begin{pmatrix} \hat{\mathbf{A}}_\mathbf{g}\begin{pmatrix}\hat{x}_n\\\hat{y}_n\end{pmatrix} \\ 1 \end{pmatrix} . \tag{G.5}$$

Now, the questions is to which location on the measurement surface the slowness vector $\underline{\hat{\mathbf{p}}}_{\mathbf{g}}$ specified by $\underline{\hat{\mathbf{n}}}_{\mathbf{0}}$ corresponds. Or, in other words, I have $\underline{\hat{\mathbf{p}}}_{\mathbf{g}}$ given in terms of $\hat{x}_n$ and $\hat{y}_n$ but I am looking for an expression of $\underline{\hat{\mathbf{p}}}_{\mathbf{g}}$ in terms of $\hat{x}_g$ and $\hat{y}_g$. Therefore, I calculate the point where the straight line, defined by the direction $\underline{\hat{\mathbf{n}}}_{\mathbf{0}}$ and the point $(\hat{x}_n, \hat{y}_n, \hat{z}_n)$, intersects the measurement surface. This point is the searched-for receiver location on the measurement surface. It is given by

$$\underline{\hat{\mathbf{x}}}_{\mathbf{g}} = \underline{\hat{\mathbf{x}}}_{\mathbf{n}} + s\,\underline{\hat{\mathbf{n}}}_{\mathbf{0}} \qquad \text{with} \qquad s = -\underline{\mathbf{T}}^{\mathbf{T}}\underline{\mathbf{e}}_{\mathbf{z}} \cdot \underline{\hat{\mathbf{x}}}_{\mathbf{n}} / \underline{\mathbf{T}}^{\mathbf{T}}\underline{\mathbf{e}}_{\mathbf{z}} \cdot \underline{\hat{\mathbf{n}}}_{\mathbf{0}} \,, \tag{G.6}$$

where I denote the location vector of the point $(\hat{x}_n, \hat{y}_n, \hat{z}_n)$ by $\underline{\hat{\mathbf{x}}}_{\mathbf{n}}$[1].

As I already stated in the previous section, finding a second-order traveltime approximation of a paraxial ray in the vicinity of the central ray is equivalent with finding a first-order approximation of the paraxial ray slowness vector projected on the measurement surface. Therefore, I project $\underline{\hat{\mathbf{p}}}_{\mathbf{g}}$ in direction of the measurement surface normal $\underline{\mathbf{T}}^{\mathbf{T}}\underline{\mathbf{e}}_{\mathbf{z}}$ onto the measurement surface. The so-obtained vector reads

$$\underline{\hat{\mathbf{p}}}_{\mathbf{g,ms}} = \underline{\hat{\mathbf{p}}}_{\mathbf{g}} - \left(\underline{\mathbf{T}}^{\mathbf{T}}\underline{\mathbf{e}}_{\mathbf{z}} \cdot \underline{\mathbf{p}}_{\mathbf{g}} \right) \underline{\mathbf{T}}^{\mathbf{T}}\underline{\mathbf{e}}_{\mathbf{z}} \,. \tag{G.7}$$

From eqs. (G.3) and (G.5) I see that $\underline{\hat{\mathbf{p}}}_{\mathbf{g,ms}}$ is a function of $\hat{x}_n$ and $\hat{y}_n$ which are—as a result of eq. (G.6)—functions of the first two components of the vector $\underline{\hat{\mathbf{x}}}_{\mathbf{g}} = (\hat{x}_g, \hat{y}_g, \hat{z}_g)^{\mathbf{T}}$. The dependencies of $\underline{\hat{\mathbf{p}}}_{\mathbf{g,ms}}$ are mathematically expressed by

$$\underline{\hat{\mathbf{p}}}_{\mathbf{g,ms}} = \begin{pmatrix} f_1\big(\hat{x}_n(\hat{x}_g, \hat{y}_g), \hat{y}_n(\hat{x}_g, \hat{y}_g)\big) \\ f_2\big(\hat{x}_n(\hat{x}_g, \hat{y}_g), \hat{y}_n(\hat{x}_g, \hat{y}_g)\big) \\ f_3\big(\hat{x}_n(\hat{x}_g, \hat{y}_g), \hat{y}_n(\hat{x}_g, \hat{y}_g)\big) \end{pmatrix} \,. \tag{G.8}$$

Tailoring the components of $\underline{\hat{\mathbf{p}}}_{\mathbf{g,ms}}$ with respect to $\hat{x}_g$ and $\hat{y}_g$ up to the first order at the central point $X_0 = (0,0,0)$ yields

$$\underline{\hat{\mathbf{p}}}_{\mathbf{g,ms}} = \underline{\hat{\mathbf{p}}}_{\mathbf{0,ms}} + \begin{pmatrix} \left[\frac{\partial f_1}{\partial \hat{x}_n}\frac{\partial \hat{x}_n}{\partial \hat{x}_g} + \frac{\partial f_1}{\partial \hat{y}_n}\frac{\partial \hat{y}_n}{\partial \hat{x}_g}\right]\Big|_{(\hat{x}_g=0,\hat{y}_g=0)}\hat{x}_g + \left[\frac{\partial f_1}{\partial \hat{x}_n}\frac{\partial \hat{x}_n}{\partial \hat{y}_g} + \frac{\partial f_1}{\partial \hat{y}_n}\frac{\partial \hat{y}_n}{\partial \hat{y}_g}\right]\Big|_{(\hat{x}_g=0,\hat{y}_g=0)}\hat{y}_g \\ \left[\frac{\partial f_2}{\partial \hat{x}_n}\frac{\partial \hat{x}_n}{\partial \hat{x}_g} + \frac{\partial f_2}{\partial \hat{y}_n}\frac{\partial \hat{y}_n}{\partial \hat{x}_g}\right]\Big|_{(\hat{x}_g=0,\hat{y}_g=0)}\hat{x}_g + \left[\frac{\partial f_2}{\partial \hat{x}_n}\frac{\partial \hat{x}_n}{\partial \hat{y}_g} + \frac{\partial f_2}{\partial \hat{y}_n}\frac{\partial \hat{y}_n}{\partial \hat{y}_g}\right]\Big|_{(\hat{x}_g=0,\hat{y}_g=0)}\hat{y}_g \\ \left[\frac{\partial f_3}{\partial \hat{x}_n}\frac{\partial \hat{x}_n}{\partial \hat{x}_g} + \frac{\partial f_3}{\partial \hat{y}_n}\frac{\partial \hat{y}_n}{\partial \hat{x}_g}\right]\Big|_{(\hat{x}_g=0,\hat{y}_g=0)}\hat{x}_g + \left[\frac{\partial f_3}{\partial \hat{x}_n}\frac{\partial \hat{x}_n}{\partial \hat{y}_g} + \frac{\partial f_3}{\partial \hat{y}_n}\frac{\partial \hat{y}_n}{\partial \hat{y}_g}\right]\Big|_{(\hat{x}_g=0,\hat{y}_g=0)}\hat{y}_g \end{pmatrix} \,, \tag{G.9}$$

where $\underline{\hat{\mathbf{p}}}_{\mathbf{0,ms}}$ corresponds to the projection of the central slowness vector onto the measurement surface in direction of the surface normal. The four derivatives $\frac{\partial \hat{x}_n}{\partial \hat{x}_g}$, $\frac{\partial \hat{y}_n}{\partial \hat{x}_g}$, $\frac{\partial \hat{x}_n}{\partial \hat{y}_g}$, and $\frac{\partial \hat{y}_n}{\partial \hat{y}_g}$ can be calculated by means of the theorem for inverse derivatives for functions of two variables using eq. (G.6). In this way I get the following results summarized in a matrix equation:

$$\begin{pmatrix} \frac{\partial \hat{x}_n}{\partial \hat{x}_g}\Big|_{(\hat{x}_g=0,\hat{y}_g=0)} & \frac{\partial \hat{x}_n}{\partial \hat{y}_g}\Big|_{(\hat{x}_g=0,\hat{y}_g=0)} \\ \frac{\partial \hat{y}_n}{\partial \hat{x}_g}\Big|_{(\hat{x}_g=0,\hat{y}_g=0)} & \frac{\partial \hat{y}_n}{\partial \hat{y}_g}\Big|_{(\hat{x}_g=0,\hat{y}_g=0)} \end{pmatrix} = \mathbf{I} \,, \tag{G.10}$$

---

[1] To derive the receiver location in this way is only possible if I assume a constant wave propagation velocity in the vicinity of X_0

where $\mathbf{I}$ is the 2×2 identity matrix.

Substituting eq. (G.10) into eq. (G.9) and calculating the remaining derivatives in eq. (G.9) yields

$$\underline{\hat{\mathbf{p}}}_{\mathbf{g,ms}} = \underline{\hat{\mathbf{p}}}_{\mathbf{0,ms}} + \frac{1}{v_0} \begin{pmatrix} \hat{a}_{g,00} \sin^2 \varphi_1 - \hat{a}_{g,00} & \hat{a}_{g,01} \sin^2 \varphi_1 - \hat{a}_{g,01} & 0 \\ -\hat{a}_{g,01} & -\hat{a}_{g,11} & 0 \\ -\hat{a}_{g,00} \sin \varphi_1 \cos \varphi_1 & \hat{a}_{g,01} \sin \varphi_1 \cos \varphi_1 & 0 \end{pmatrix} \underline{\hat{\mathbf{x}}}_{\mathbf{g}} . \tag{G.11}$$

Finally, transforming eq. (G.11) to the local observation coordinate system leads to

$$\underline{\mathbf{p}}_{\mathbf{g,ms}} = \frac{1}{v_0} \begin{pmatrix} \cos \varphi_0 \sin \varphi_1 \\ \sin \varphi_0 \sin \varphi_1 \\ 0 \end{pmatrix} + \frac{1}{v_0} \begin{pmatrix} -\mathbf{T} \hat{\mathbf{A}}_{\mathbf{g}} \mathbf{T}^{\mathbf{T}} \\ 0 \end{pmatrix} \underline{\mathbf{x}}_{\mathbf{g}} , \tag{G.12}$$

where I can write for the first two components of $\underline{\mathbf{p}}_{\mathbf{g,ms}}$

$$\mathbf{p}_{\mathbf{g}} = \mathbf{p}_{\mathbf{0}} + \frac{1}{v_0} \mathbf{T} \hat{\mathbf{A}}_{\mathbf{g}} \mathbf{T}^{\mathbf{T}} \mathbf{x}_{\mathbf{g}} . \tag{G.13}$$

Thus, I derived a first-order approximation for the slowness vector projection $\mathbf{p}_{\mathbf{g}}$ in terms of a wavefront curvature matrix. This is one half of what I aimed to at the beginning of this section. For the slowness vector difference $\mathbf{p}_{\mathbf{s}}$ I can follow exactly the same way as for the derivation of $\mathbf{p}_{\mathbf{g}}$. In doing so, I get

$$\mathbf{p}_{\mathbf{s}} = -\mathbf{p}_{\mathbf{0}} + \frac{1}{v_0} \mathbf{T} \hat{\mathbf{A}}_{\mathbf{s}} \mathbf{T}^{\mathbf{T}} \mathbf{x}_{\mathbf{s}} . \tag{G.14}$$

G.3 Traveltime formula with eigenwave matrices

In this section I establish the wavefront curvature matrices of the normal and NIP wave at X_0 in Hamilton's equation and finally perform an integration to obtain the parabolic and hyperbolic traveltime formulae (8.2).

Let me once again have a look at eq. (G.2). This equation could be alternatively written in midpoint and half-offset coordinates which reads

$$dt \approx (\mathbf{p}_{\mathbf{g}} - \mathbf{p}_{\mathbf{s}}) \cdot d\mathbf{m} + (\mathbf{p}_{\mathbf{g}} + \mathbf{p}_{\mathbf{s}}) \cdot d\mathbf{h} . \tag{G.15}$$

By means of eqs. (G.13) and (G.14) I will relate the two coefficients in eq. (G.15) to the wavefront curvature matrices of the normal and NIP wave.

The first experiment I consider is the normal wave experiment which is often also referred to as ZO experiment. All rays of the normal wave experiment are subject to the ZO conditions $\mathbf{h} = \mathbf{0}$ (which is equivalent to $\mathbf{x}_{\mathbf{g}} = \mathbf{x}_{\mathbf{s}}$) and $\mathbf{p}_{\mathbf{g}} = -\mathbf{p}_{\mathbf{s}}$ which immediately yields (see eqs. (G.13) and (G.14)) $\hat{\mathbf{A}}_{\mathbf{g}} = -\hat{\mathbf{A}}_{\mathbf{s}} = \hat{\mathbf{N}}$. Therefore, the coefficients of the midpoint coordinates in eq. (G.15) are given by

$$\mathbf{p}_{\mathbf{g}} - \mathbf{p}_{\mathbf{s}} = 2\mathbf{p}_{\mathbf{0}} + \frac{2}{v_0} \mathbf{T} \hat{\mathbf{N}} \mathbf{T}^{\mathbf{T}} \mathbf{m} . \tag{G.16}$$

The second experiment I want to look at is the NIP wave experiment which is also referred to as CMP experiment. Hubral (1983) showed that the equivalent use of the terms NIP and CMP experiment is justified if I am only interested in a second-order traveltime of rays of the CMP configuration in the vicinity of a ZO central ray. In this case all CMP rays can be viewed as reflecting at NIP (the normal incidence point of the central ray) instead of their actual reflection point. Consequently, the rays of the CMP configuration can approximately be viewed as the orthogonal trajectories to the moving NIP wavefront. This statement is called the NIP wave theorem (Hubral, 1983). All rays of the NIP wave experiment are subject to the CMP condition $\mathbf{m} = \mathbf{0}$ (which is equivalent to $\mathbf{x_g} = -\mathbf{x_s}$). Since the down-going and up-going wavefront at X_0 of the NIP wavefront are identical, I have $\hat{\mathbf{A}}_\mathbf{g} = -\hat{\mathbf{A}}_\mathbf{s} = \hat{\mathbf{M}}$. Therefore, the coefficients of the half-offset coordinates in eq. (G.15) are given by

$$\mathbf{p_g} + \mathbf{p_s} = \frac{2}{v_0}\, \mathbf{T}\, \hat{\mathbf{M}}\, \mathbf{T^T}\, \mathbf{h}\,. \tag{G.17}$$

Substituting eqs. (G.16) and (G.17) into eq. (G.15) and performing subsequently an integration with respect to $\mathbf{m}$ and $\mathbf{h}$ finally yields the parabolic traveltime (8.2a)

$$t_{par} = t_0 + \frac{2}{v_0}\, \mathbf{w_z} \cdot \mathbf{m} + \frac{1}{v_0}\, \mathbf{m^T}\, \mathbf{T}\, \hat{\mathbf{N}}\, \mathbf{T^T}\, \mathbf{m} + \frac{1}{v_0}\, \mathbf{h^T}\, \mathbf{T}\, \hat{\mathbf{M}}\, \mathbf{T^T}\, \mathbf{h}\,, \tag{G.18}$$

where $\frac{1}{v_0}\mathbf{w_z} = \mathbf{p_0}$. If I square eq. (G.18) and retain only its terms up to the second order in $\mathbf{m}$ and $\mathbf{h}$ I obtain the hyperbolic traveltime (8.2b)

$$t_{hyp}^2 = \left(t_0 + \frac{2}{v_0}\, \mathbf{w_z} \cdot \mathbf{m}\right)^2 + \frac{2t_0}{v_0}\, \mathbf{m^T}\, \mathbf{T}\, \hat{\mathbf{N}}\, \mathbf{T^T}\, \mathbf{m} + \frac{2t_0}{v_0}\, \mathbf{h^T}\, \mathbf{T}\, \hat{\mathbf{M}}\, \mathbf{T^T}\, \mathbf{h}\,. \tag{G.19}$$

Appendix H

Eigenwave matrices and ray propagator submatrices

By means of paraxial ray theory Schleicher et al. (1993) formulated a second-order two-point traveltime approximation for rays in the paraxial vicinity of a central ray through an inhomogeneous isotropic 3D medium. In their derivation they used the surface-to-surface propagator matrix concept. With this concept the end point and the direction of the paraxial ray at this point can be described with respect to the central ray for a given start point and direction. That is, as well as a wavefront detected at the measurement surface (or the wavefront curvature matrix) the four 2×2 submatrices of the 4×4 surface-to-surface ray propagator matrix $\underline{\underline{\mathbf{T}}}$ contain the "history" of a wavefront propagating along the central ray. In this chapter the relationships between the eigenwave matrices and the submatrices of the surface-to-surface propagator are presented.

H.1   Hyperbolic traveltime with ray propagator submatrices

In case of a ZO central ray the hyperbolic traveltime approximation for paraxial rays in the vicinity of the central ray can be written as (see, e.g., Schleicher et al., 1993)

$$t_{hyp}^2 = \left(t_0 + 2\,\mathbf{p_0}\cdot\mathbf{m}\right)^2 + 2\,t_0\,\mathbf{m^T}\,\left(\mathbf{B}^{-1}\mathbf{A} - \mathbf{B}^{-1}\right)\,\mathbf{m} + 2\,t_0\,\mathbf{h^T}\,\left(\mathbf{B}^{-1}\mathbf{A} + \mathbf{B}^{-1}\right)\,\mathbf{h}\,. \qquad \text{(H.1)}$$

$\mathbf{p_0}$ is again the slowness vector projection of the up-going central ray onto the measurement surface at the observation point X_0. $\mathbf{A}$ and $\mathbf{B}$ are the 2×2 submatrices of the 4×4 surface-to-surface ray propagator matrix

$$\underline{\underline{\mathbf{T}}} = \begin{pmatrix} \mathbf{A} & \mathbf{B} \\ \mathbf{C} & \mathbf{D} \end{pmatrix}\,. \qquad \text{(H.2)}$$

$\underline{\underline{\mathbf{T}}}$ describes the linear relationship

$$\begin{pmatrix} \mathbf{x_g} \\ \mathbf{p_g} - \mathbf{p_0} \end{pmatrix} = \underline{\underline{\mathbf{T}}} \begin{pmatrix} \mathbf{x_s} \\ \mathbf{p_s} + \mathbf{p_0}\, , \end{pmatrix} \qquad \text{(H.3)}$$

between the quantities specifying the ray at the source and receiver with respect to the central ray. All vectors in eq. (H.3) have the same meaning as shown in Figure G.1. Červený (2001) refers to eq. (H.3) as equation of the paraxial approximation. Please note, the concept of the surface-to-surface propagator matrix is not restricted to the case where all sources and receivers of the paraxial rays are located on the same flat measurement surface in vicinity of a ZO central ray as I use it here. The concept could be, in fact, also used if sources and receivers are located on different curved surfaces where the central ray is no longer a ZO ray (Bortfeld, 1989).

H.2 Comparison of traveltime coefficients

By comparing the coefficients of the hyperbolic traveltime formula of equations (8.2) and equation (H.1) one can easily verify that

$$\mathbf{w_z} = v_0 \, \mathbf{p_0} \tag{H.4}$$

and

$$\frac{1}{v_0} \, \mathbf{T} \, \hat{\mathbf{N}} \, \mathbf{T^T} = \mathbf{B}^{-1} \mathbf{A} - \mathbf{B}^{-1} \tag{H.5a}$$

$$\frac{1}{v_0} \, \mathbf{T} \, \hat{\mathbf{M}} \, \mathbf{T^T} = \mathbf{B}^{-1} \mathbf{A} + \mathbf{B}^{-1}. \tag{H.5b}$$

Solving the quadratic coefficients of equations (H.5) for $\hat{\mathbf{N}}$ and $\hat{\mathbf{M}}$ yields

$$\hat{\mathbf{N}} = v_0 \, \mathbf{T^{-1}} \left(\mathbf{B}^{-1} \mathbf{A} - \mathbf{B}^{-1} \right) \left(\mathbf{T^T} \right)^{-1} \tag{H.6a}$$

$$\hat{\mathbf{M}} = v_0 \, \mathbf{T^{-1}} \left(\mathbf{B}^{-1} \mathbf{A} + \mathbf{B}^{-1} \right) \left(\mathbf{T^T} \right)^{-1}. \tag{H.6b}$$

Vice versa, the four submatrices of the surface-to-surface ray propagator matrix could also be expressed in terms of the curvature matrices of the eigenwaves: summing up eqs. (H.5a) and (H.5b) provides

$$\mathbf{B}^{-1} \mathbf{A} = \frac{1}{2 \, v_0} \, \mathbf{T} \left(\hat{\mathbf{M}} + \hat{\mathbf{N}} \right) \mathbf{T^T} \tag{H.7}$$

and subtracting eqs. (H.5a) from (H.5b) yields

$$\mathbf{B}^{-1} = \frac{1}{2 \, v_0} \, \mathbf{T} \left(\hat{\mathbf{M}} + \hat{\mathbf{N}} \right) \mathbf{T^T}. \tag{H.8}$$

Thus, the submatrices $\mathbf{A}$ and $\mathbf{B}$ are given by

$$\mathbf{A} = \left(\mathbf{T} \left(\hat{\mathbf{M}} - \hat{\mathbf{N}} \right) \mathbf{T^T} \right)^{-1} \mathbf{T} \left(\hat{\mathbf{M}} + \hat{\mathbf{N}} \right) \mathbf{T^T}, \tag{H.9a}$$

$$\mathbf{B} = 2 \, v_0 \left(\mathbf{T} \left(\hat{\mathbf{M}} - \hat{\mathbf{N}} \right) \mathbf{T^T} \right)^{-1}. \tag{H.9b}$$

With eqs. (H.9a) and (H.9b) the matrices $\mathbf{A}$ and $\mathbf{B}$ gain a geometrical meaning which helps to understand why the submatrices are of importance in many seismic applications (Hubral et al., 1992a,b).

Using the symplectic property (Schleicher et al., 1993) of the propagator matrix $\underline{\underline{\mathbf{T}}}$

$$\mathbf{A^T D} - \mathbf{C^T B} = \mathbf{I} \tag{H.10}$$

and the matrix equation (Hubral et al., 1992a)

$$\mathbf{D} = \mathbf{A^T} \tag{H.11}$$

one could also relate the submatrices $\mathbf{C}$ and $\mathbf{D}$ to the wavefront curvature matrices $\hat{\mathbf{M}}$ and $\hat{\mathbf{N}}$. Please note, eq. (H.11) is valid for a ZO central ray only. It is the consequence that source and receiver of the central ray could be interchanged which would not affect the values of the propagator matrix $\underline{\underline{\mathbf{T}}}$.

Appendix I

Interface curvature matrix

Consider a local coordinate system that is simply obtained by translation of the global coordinate system to an interface point. Here, a local second-order description of the interface is given by eq. (10.10), or implicitly by:

$$F = \mathbf{x}^{\mathbf{T}} \underline{\mathbf{C}} \mathbf{x} + 2 \underline{\mathbf{b}}^{\mathbf{T}} \mathbf{x} = 0 \tag{I.1}$$

$$\text{with} \quad \underline{\mathbf{C}} = \begin{pmatrix} c_{00} & c_{01} & 0 \\ c_{01} & c_{11} & 0 \\ 0 & 0 & 0 \end{pmatrix}, \ \underline{\mathbf{b}} = \begin{pmatrix} b_0 \\ b_1 \\ -1 \end{pmatrix}, \ \underline{\mathbf{x}} = \begin{pmatrix} x \\ y \\ z \end{pmatrix}, \tag{I.2}$$

$$\text{and} \quad c_{00} = \frac{d^2 z}{dx^2}, \ c_{01} = c_{10} = \frac{d^2 z}{dxdy}, \ c_{11} = \frac{d^2 z}{dy^2}, \tag{I.3}$$

$$b_0 = \frac{dz}{dx}, \ b_1 = \frac{dz}{dy}. \tag{I.4}$$

The curvature matrix has now to be expressed in the interface system (see section 10.5.1), where the transformation from the local to the interface system is given by $\underline{\mathbf{Q}}$ (see section 10.5.2). Because $\underline{\mathbf{Q}}^{\mathbf{T}} \underline{\mathbf{Q}} = \underline{\mathbf{I}}$, I can write eq. (I.1) as

$$F = \mathbf{x}^{\mathbf{T}} \underline{\mathbf{Q}} \underline{\mathbf{Q}}^{\mathbf{T}} \underline{\mathbf{C}} \underline{\mathbf{Q}} \underline{\mathbf{Q}}^{\mathbf{T}} \mathbf{x} + 2 \underline{\mathbf{b}}^{\mathbf{T}} \underline{\mathbf{Q}} \underline{\mathbf{Q}}^{\mathbf{T}} \mathbf{x} = 0. \tag{I.5}$$

Since the vector $\underline{\mathbf{x}}$ expressed in the interface system is given by $\underline{\tilde{\mathbf{x}}} = \underline{\mathbf{Q}}^{\mathbf{T}} \mathbf{x}$, eq (I.5) becomes

$$F = \tilde{\mathbf{x}}^{\mathbf{T}} \underline{\mathbf{Q}}^{\mathbf{T}} \underline{\mathbf{C}} \underline{\mathbf{Q}} \tilde{\mathbf{x}} + 2 \underline{\mathbf{b}}^{\mathbf{T}} \underline{\mathbf{Q}} \tilde{\mathbf{x}} = 0. \tag{I.6}$$

Therefore, the matrix $\underline{\mathbf{C}}$ and the normal $\underline{\mathbf{b}}$ expressed in the interface system are

$$\underline{\tilde{\mathbf{C}}} = \underline{\mathbf{Q}}^{\mathbf{T}} \underline{\mathbf{C}} \underline{\mathbf{Q}}, \tag{I.7}$$

$$\underline{\tilde{\mathbf{b}}} = \underline{\mathbf{Q}}^{\mathbf{T}} \underline{\mathbf{b}} = \begin{pmatrix} 0 \\ 0 \\ \|\underline{\mathbf{b}}\| \end{pmatrix}. \tag{I.8}$$

However, the matrix $\underline{\tilde{\mathbf{C}}}$ is, in general, not yet a curvature matrix because the transformation introduces non-zero elements $\tilde{c}_{2i}, \tilde{c}_{i2}$ (i=0,1,2). Nevertheless, the curvature matrix can easily be determined by the second-order derivatives of eq. (I.6). The second-order derivatives of

$$F\left(\tilde{x}, \tilde{y}, \tilde{z}\left(\tilde{x}, \tilde{z}\right)\right) = \underline{\tilde{\mathbf{x}}}^{\mathrm{T}} \underline{\tilde{\mathbf{C}}} \underline{\tilde{\mathbf{x}}} + 2 \underline{\tilde{\mathbf{b}}}^{\mathrm{T}} \underline{\tilde{\mathbf{x}}} = 0 \tag{I.9}$$

with respect to $\tilde{x}$ and $\tilde{y}$ yield

$$\frac{d^2 F}{d\tilde{x}^2} = F_{\tilde{x}\tilde{x}} + 2 F_{\tilde{x}\tilde{z}} \tilde{z}_{\tilde{x}} + F_{\tilde{z}\tilde{z}} \tilde{z}_{\tilde{x}}^2 + F_{\tilde{z}} \tilde{z}_{\tilde{x}\tilde{x}} = 0, \tag{I.10}$$

$$\frac{d^2 F}{d\tilde{y}^2} = F_{\tilde{y}\tilde{y}} + 2 F_{\tilde{y}\tilde{z}} \tilde{z}_{\tilde{y}} + F_{\tilde{z}\tilde{z}} \tilde{z}_{\tilde{y}}^2 + F_{\tilde{z}} \tilde{z}_{\tilde{y}\tilde{y}} = 0, \tag{I.11}$$

$$\frac{d^2 F}{d\tilde{x}d\tilde{y}} = \frac{d^2 F}{d\tilde{y}d\tilde{x}} = F_{\tilde{x}\tilde{y}} + F_{\tilde{y}\tilde{z}} \tilde{z}_{\tilde{x}} + F_{\tilde{x}\tilde{z}} \tilde{z}_{\tilde{y}} + F_{\tilde{z}\tilde{z}} \tilde{z}_{\tilde{x}} \tilde{z}_{\tilde{y}} + F_{\tilde{z}} \tilde{z}_{\tilde{x}\tilde{y}} = 0. \tag{I.12}$$

Since $\tilde{z}_{\tilde{x}} = 0$ and $\tilde{z}_{\tilde{y}} = 0$ this simplifies to

$$\frac{d^2 F}{d\tilde{x}^2} = F_{\tilde{x}\tilde{x}} + F_{\tilde{z}} \tilde{z}_{\tilde{x}\tilde{x}} = 0, \tag{I.13}$$

$$\frac{d^2 F}{d\tilde{y}^2} = F_{\tilde{y}\tilde{y}} + F_{\tilde{z}} \tilde{z}_{\tilde{y}\tilde{y}} = 0, \tag{I.14}$$

$$\frac{d^2 F}{d\tilde{x}d\tilde{y}} = \frac{d^2 F}{d\tilde{y}d\tilde{x}} = F_{\tilde{x}\tilde{y}} + F_{\tilde{z}} \tilde{z}_{\tilde{y}\tilde{y}} = 0. \tag{I.15}$$

Therefore, the second-order derivatives in the interface coordinate system are given by

$$\tilde{z}_{\tilde{x}\tilde{x}} = -\frac{F_{\tilde{x}\tilde{x}}}{F_{\tilde{z}}} = \frac{\tilde{c}_{00}}{\underline{\tilde{b}}_2}, \tag{I.16}$$

$$\tilde{z}_{\tilde{y}\tilde{y}} = -\frac{F_{\tilde{y}\tilde{y}}}{F_{\tilde{z}}} = \frac{\tilde{c}_{11}}{\underline{\tilde{b}}_2}, \tag{I.17}$$

$$\tilde{z}_{\tilde{x}\tilde{y}} = \tilde{z}_{\tilde{y}\tilde{x}} = -\frac{F_{\tilde{x}\tilde{y}}}{F_{\tilde{z}}} = \frac{\tilde{c}_{01}}{\underline{\tilde{b}}_2}. \tag{I.18}$$

Finally, this yields the curvature matrix $\tilde{\mathbf{B}}$ in the interface system:

$$\tilde{\mathbf{B}} = \frac{1}{\|\underline{\mathbf{b}}\|} \mathbf{Q}^{\mathrm{T}} \mathbf{C} \mathbf{Q}, \quad \text{where} \quad \mathbf{C} = \begin{pmatrix} c_{00} & c_{01} \\ c_{01} & c_{11} \end{pmatrix}.$$

List of Figures

References

Berkovitch, A., Gelchinsky, B., and Keydar, S. (1994). Basic formulae for multifocusing stack. In *Extended Abstracts*, volume 94. 56th Mtg. Eur. Assoc. Expl. Geophys. Session P140.

Born, M. and Wolf, E. (1959). *Principle of optics*. Pergamon Press Inc.

Bortfeld, R. (1989). Geometrical ray theory: Rays and traveltimes in seismic systems (second-order approximations of the traveltimes). *Geophysics*, 54(3):342–349.

Červený, V. (2001). *Seismic Ray Theory*. Cambridge University Press.

de Bazelaire, E. (1986). Normal moveout revisited – inhomogeneous media and curved interfaces. In *Expanded Abstracts*, volume 86. Soc. Expl. Geophys. Session POS2.4.

de Bazelaire, E. (1988). Normal moveout revisited – inhomogeneous media and curved interfaces. *Geophysics*, 53(2):143–157.

de Bazelaire, E. and Thore, P. (1987). Pattern recognition applied to time and velocity contours. In *Expanded Abstracts*, volume 87. Soc. Expl. Geophys. Session POS2.14.

Fomel, S. and Grechka, V. (1998). On nonhyperbolic reflection moveout in anisotropic media. Technical Report 92, Stanford Exploration Project.

Gelchinsky, B. (1988). The common-reflecting-element (CRE) method. In *Extended Abstracts*, volume 19, pages 71–75. Expl. Geophys.

Höcht, G. (1998). The Common Reflection Surface Stack. Master's thesis, Universität Karlsruhe.

Höcht, G., de Bazelaire, E., Majer, P., and Hubral, P. (1999). Seismics and optics: hyperbolae and curvatures. *J. Appl. Geoph.*, 42(3,4):261–281.

Höcht, G., Perroud, H., and Hubral, P. (1997). Migrating around on hyperbolas and parabolas. *The Leading Edge*, May:473–476.

Hubral, P. (1983). Computing true amplitude reflections in a laterally inhomogeneous earth. *Geophysics*, 48(8):1051–1062.

Hubral, P. and Krey, T. (1980). *Interval velocities from seismic reflection traveltime measurements*. Soc. Expl. Geophys.

Hubral, P., Schleicher, J., and Tygel, M. (1992a). Three–dimensional paraxial ray properties, Part I: Basic relations. *Journal of Seismic Exploration*, 1:265–279.

Hubral, P., Schleicher, J., and Tygel, M. (1992b). Three–dimensional paraxial ray properties, Part II: Applications. *Journal of Seismic Exploration*, 1:347–362.

Jäger, R. (1999). The Common Reflection Surface Stack - Introduction and Application. Master's thesis, Universität Karlsruhe.

Keydar, S., Gelchinsky, B., and Berkovitch, A. (1993). Common source point stacking and imaging. In *Extended Abstracts*. Eur. Assn. of Expl. Geophys. Session:P111.

Keydar, S., Gelchinsky, G., Shtivelman, V., and Berkovitch, A. (1990). Common evolute element (CEE) stack and imaging (zero-offset stack). In *Expanded Abstracts*, pages 1719–1722. Soc. Expl. Geophys.

Majer, P. (2000). Inversion of seismic parameters: Determination of the 2-D iso-velocity layer model. Master's thesis, Universität Karlsruhe.

Mann, J., Jäger, R., Müller, T., Höcht, G., and Hubral, P. (1999). Common-reflection-surface stack - a real data example. *J. Appl. Geoph.*, 42(3,4):301–318.

Müller, T. (1999). *The common reflection surface stack - seismic imaging without explicit knowledge of the velocity model*. Der Andere Verlag, Bad Iburg.

Perroud, H., Hubral, P., and Höcht, G. (1999). Common-reflection-point stacking in laterally inhomogeneous media. *Geophys. Prosp.*, 47(1):1–24.

Perroud, H., Hubral, P., Höcht, G., and de Bazelaire, E. (1997). Migrating around in circles - part III. *The Leading Edge*, June(16):875–883.

Schleicher, J., Tygel, M., and Hubral, P. (1993). Parabolic and hyperbolic paraxial two-point traveltimes in 3D media. *Geophys. Prosp.*, 41(4):495–514.

Schleicher, J., Tygel, M., and Hubral, P. (2001). *Seismic true-amplitude reflection imaging, chapter 4: Surface-to-surface paraxial ray theory*. to be published.

Thore, P. and de Bazelaire, E. (1989). Automatic determination of interval velocities and depth patterns in complex tectonics: General case. In *Soc. Expl. Geophys., Expanded Abstracts*, volume 86. Session:S19.8.

Thore, P. and de Bazelaire, E. (1991). Analysis of the common midpoint gather by decomposition into elementary wavefronts. *Geophys. Prosp.*, 39(4):453–471.

Vieth, K.-U. (2001). *Kinematic wavefield attributes in seismic imaging*. PhD thesis, Universität Karlsruhe.

Danksagung

Lebenslauf

Name   German Höcht

Geburtsdatum/-ort   28.09.1969 in Nürnberg

Nationalität   deutsch

Familienstand   ledig

Schulbildung

09/75 - 08/79	Grundschule Hallstadt
09/79 - 08/81	Gymnasium Bamberg
09/81 - 07/84	Athénnée Royal de Braine l'Alleud (Belgien)
09/84 - 05/89	Gymnasium Landau/Pfalz
05/89	Abitur

Zivildienst

10/89 - 02/91	Mobiler Sozialer Hilfsdienst Südpfalz

Hochschulausbildung

10/91 - 09/92	Studium des Chemieingenieurswesens an der Universität Erlangen-Nürnberg
10/92 - 09/98	Studium der Geophysik an der Universität Karlsruhe
09/98	Abschluss: Diplom-Geophysiker
seit 10/98	Doktorand der Geophysik an der Universität Karlsruhe

Praktika

07/91 - 10/91	Schlosser; Michelin Karlsruhe
08/97 - 10/97	Geophysik; ELF Pau Frankreich